LINEAR AND NONLINEAR DYNAMICS OF DRILLSTRINGS

Shilin CHEN
(B.Sc., M.Sc.)

Thesis submitted in accordance with the requirements for the degree of Doctor of Philosophy

Thèse présentée en vue de l'obtention du titre de Docteur en Sciences Appliquées

Année académique 1994-1995

Faculté des Sciences Appliquées
Université de Liège

ACKNOWLEDGMENTS

First of all, I wish to express my gratitude and appreciation to my academic and thesis advisor, Prof. Michel Géradin, for his helpful insights that lead me to this project, for his enthusiastic and invaluable support and guidance throughout the investigation, for providing me with many opportunities to attend academic conferences and seminars outside Ulg, and for his great personality that made my stay in LTAS (Aerospace Laboratory) of Ulg very fruitful and enjoyable. In fact, his creativity, responsibility and his dedication to the work have made a deep impression on me.

I am greatly indebted to Mr. Etienne Lamine, Manager of R&D Department of Security DBS (Belgium), for his advices and suggestions to the project and the thesis, for his enthusiastic cooperation at every step of the research. Thanks are given to Security DBS (Belgium) for its financial support and for the permission to publish this thesis.

I am very grateful to Dr. Hwa-Shan Ho, external consultant scientist of DBS, with whom I have had many fruitful discussions on practical drillstring dynamics.

Thanks are given to Prof. J.C. Golinval and Mr. D. Rixen, for their criticism and cooperation, and for their review comments of the manuscript. Actually, the work presented in this thesis was partly performed in cooperation with them.

I cannot forget to thank all my other colleagues of LTAS for providing me with the right atmosphere, for their help and friendship during my stay at LTAS, especially Mr. A. Lerusse, Mr. D.B. Doan and Mrs. C. Pregaldien.

My thanks go to my previous supervisors, Prof. Kunquan ZHU, Department of Mechanical Engineering, Wuhan University of Technology, and Prof. Xin SHI, Graduate School at Peking, Wuhan University of Technology, for their encouragement during my stay abroad.

My special thanks are given to my wife, Y. Bai, for her support during the past years.

Finally, I would like to express my sincere appreciation to those persons who are not mentioned here but have ever helped me in different aspects during the period I am far from my motherland and my parents.

ABSTRACT

This thesis may be divided into two parts, namely linear and nonlinear dynamics of drillstrings. For linear drillstrings, an improved dynamic stiffness method (IDSM) is developed. The IDSM is based on the combination of transfer matrix, dynamic stiffness method and finite element method. In the IDSM, the whole structure is first divided into substructures based on the required master degrees of freedom. For each substructure, the global dynamic stiffness matrix (DSM) is obtained directly by rearranging the corresponding global transfer matrix. In this way, the internal degrees of freedom of each substructure are not used in the model. Therefore, the order of the model is greatly reduced. Because the drillstring is one-dimensional structure, the whole system may be modeled only with one or two degrees of freedom depending on the research purpose. The succesful applications of the IDSM to the axial, torsional and lateral vibrations as well as to buckling analysis of drillstrings have demonstrated that the program based on the IDSM can be used as a tool in the drilling fields both to make recommendations for the prevention of drillstring and bit failures and to help in the interpretation of downhole measurements of drillstring dynamics. The IDSM has also been applied to modal analysis for other beam-like structures.

For nonlinear drillstrings, the backward whirl motion due to bit-holewall contact is investigated in detail using both lumped and finite element models. Based on the lumped model, the formula to calculate the whirl speed and whirl radius have been derived in a closed and explicit form. The parameters which influence the backward whirl motion are systematically studied. Because the lumped model may be too simple to completely explain the bit whirl phenomena, finite element model is developed. Effort has been made to modify an existing contact element in order to simulate the dynamic contact phenomenon of the drillstrings. In the contact element, not only the transverse friction forces but also the longitudinal friction forces are taken into account. The element stiffness and damping matrices are derived explicitly. This element is implemented in a general and powerful multi-body dynamic analysis software, namely, Mecano module of Samcef. Therefore, many computational aspects of the Mecano software, for example the nonlinear beam element, the user's element, the implicit time integration method (Hilber-Hughes-Taylor method) as well as the pre- and post-analyzer, can be directly applied. Some observations agree with experimental work performed by other researchers for rotor systems.

Techniques to identify downhole bit whirl motion are developed based on the bit whirl kinematics. All the whirl parameters including whirl speed, whirl amplitude, bit rotation speed can be estimated using either accelerometers or contact sensors.

A List of Acronyms

BHA:	Bottom Hole Assembly
DOF:	Degree Of Freedom
DSM:	Dynamic Stiffness Method
DTIM:	Direct Time Integration Method
FFR:	Forced Frequency Response
FFT:	Fast Fourier Transform
HHT:	Hilber-Hughes-Taylor
IDSM:	Improved Dynamic Stiffness Method
IFFT:	Inverse Fast Fourier Transform
ITMM:	Improved Transfer Matrix Method
FEM:	Finite Element Method
FRF:	Frequency Response Function
MDCM:	Modified Dynamic Condensation Method
MWD:	Measurement While Drilling
MSM:	Modal Superposition Method
PDC:	Polycrystalline Diamond Compact
RPM:	Rotation Per Minute
ROP:	Rate Of Penetration
SCM:	Static Condensation Method
SDOF:	Single Degree Of Freedom
TMM:	Transfer Matrix Method
TOB:	Torque On Bit
WOB:	Weight On Bit

CONTENTS

CHAPTER 1:

GENERAL INTRODUCTION

1.1 DRILLING EQUIPMENT

The equipment for oil-well drilling consists basically of five distinct subsystems: hoisting, circulating, rotating components, well control and power. These five subsystems go together to make a complete drilling system which is located over a wellhead for the sole purpose of making a hole in the ground. Among the five subsystems, the rotating components, or drillstring system, play an important role during drilling.

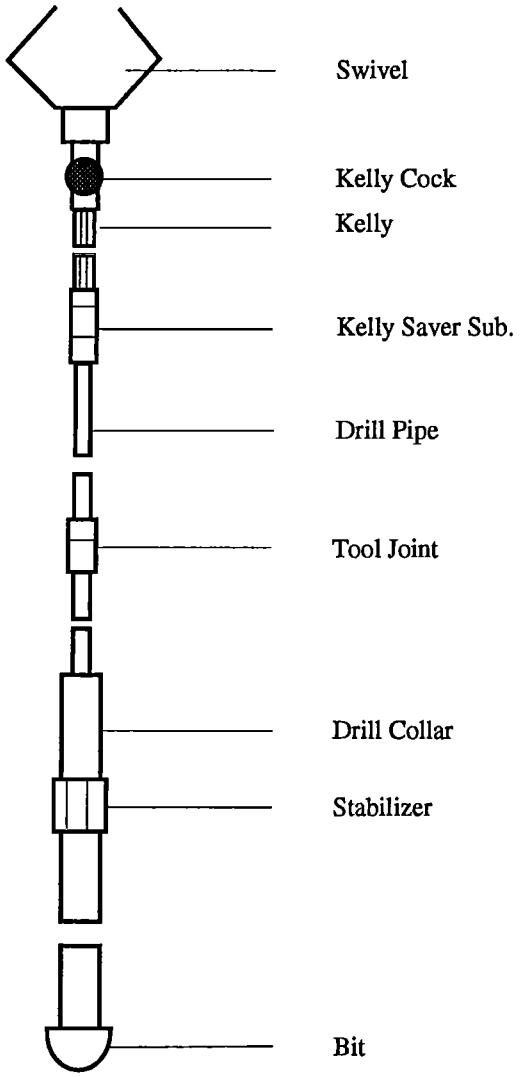

Fig.1.1: Drillstring system

Shown in Fig.1.1 is a typical rotating equipment which consists of the swivel, the kelly, the rotary table, the drill stem and the bit. The drill stem is the assembly of equipment between

the swivel and the bit, including the kelly, drill pipe, and drill collars. The term drillstring system or simply drillstring used in this thesis refers to the drillpipe, drillcollars, stabilizers and bit. Another term BHA (Bottom Hole Assembly) is a section of the drillstring from bit to the top of the drill collar.

Drill collars are heavier than drill pipe and are used on the bottom part of the string to provide weight and torque on the bit. The bit is a rock cutting tool. There are two types of bit which are used very often in the drilling fields: three-cone or roller-cone bit and PDC (Polycrystalline Diamond Compact) bit. The development of PDC bit has had a major impact on drilling practices in medium- to medium-hard formations.

1.2 STATIC AND DYNAMIC PROBLEMS OF DRILLSTRING

1.2.1 Static problems

In order to understand the possible static problems associated with drillstrings, let us first analyze the static forces generated during drilling.

(a) Buoyancy force

The drillstring is usually surrounded by the drilling mud. Therefore the drillstring is subject to buoyancy force which is developed by pressure acting over the cross sectional area of the drill collars at the bottom end. This force is upward.

(b) Gravity force

In vertical hole, the gravity force is generated by the weight of the drillstring itself. The weight of drill collar from the bit to the "neutral point" is used often as the weight on bit (WOB). The gravity force is downward.

(c) External force and moment

At the top end of the drillstring, an external axial force is applied in order to provide an expected axial force on the bit (WOB). For vertical drilling, this force may be upward or downward depending on the expected WOB. Meanwhile, an external moment is applied at the top end of the drillstring in order to rotate the bit.

(d) Reaction forces

The reaction forces include mainly the friction forces due to drillstring and holewall contact, the drilling force and moment due to bit-formation interaction.

These forces are shown in Fig.1.2. Because of these forces, the following issues must be taken into account in the static design of a drillstring:

(a) The state of the stress is varied in the drillstring. The upper part is in tension and the lower part is in compression. Hence the determination of the neutral point becomes very important.

(b) The lower part of the drillstring may be buckled due to the large WOB.

(c) The drilling direction is partly influenced by the static force, especially by the side force. In fact, most of the work about the prediction of drilling direction is based on the static force analysis.

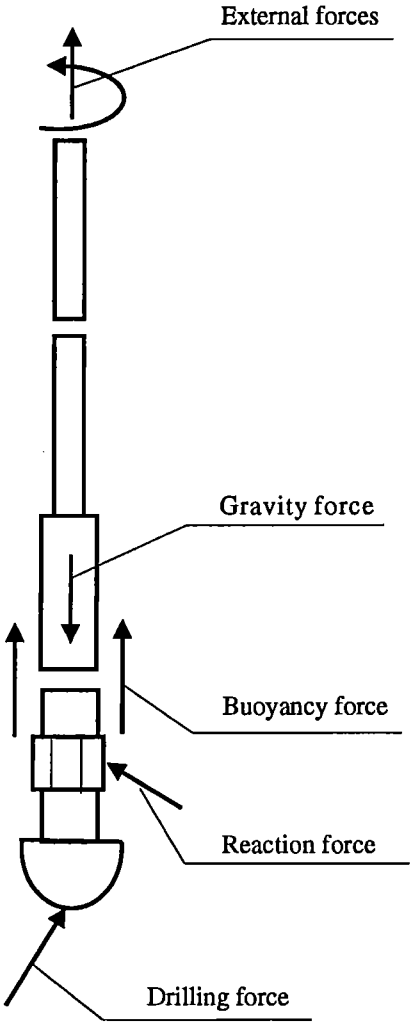

Fig.1.2: Forces acting on drillstring

1.2.2 Dynamic problems

The importance of drillstring and in particular BHA vibration has not arisen at the beginning of the drilling industry development. However, with the requirement of reducing the cost, the drilling equipment works usually in the limit where vibration becomes more than just a side effect. In recent years, vibration was found to be a driving factor not only in directional control but mainly in BHA failure.

The dynamic behavior of drillstrings during drilling operations is very complex because of the multiple excitation sources. The main excitation sources are:

(a) Bit-formation interaction. For roller-cone rock bit, it has been found that the excitation frequency due to bit-formation interaction is three times the rotation speed. However, for PDC bit, the situation is more complex because of the multiple cutters placed on the bit body. Moreover, the bit-formation interaction is one of the coupling mechanisms because of interdependence of the drilling forces on the bit.

(b) Contact between drillstring and holewall. During drilling, not only the stabilizers and the drill collars, but also the drill pipe have all chance to contact with the holewall. Such contact will introduce friction forces and nonlinear restoring forces.

(c) The fluctuations of WOB and TOB, the mass unbalance force, the mud pressure fluctuations are other important excitation sources.

Furthermore, the boundary conditions of the drillstring at both top and bottom ends are very complex.

Because of these excitations and complex boundary conditions, the behavior of drillstring vibration may be very complicated. Basically, the phenomenon is somewhat unpredictable since the drilled formation is generally unknown while drilling. However, understanding the fundamental underlying phenomena is undoubtedly necessary to define adjustable parameters influencing vibration. Particularly for PDC bits, understanding and controlling vibration is of crucial importance because shocks and vibrations are very detrimental to PDC cutters. The dynamic loading is the main reason why PDC bits cannot drill efficiently the hard formations. It is expected that if one can control and reduce the vibration level of the drillstring, the PDC bit could probably supersede rock bit to drill harder formations. This is confirmed by successful use of "low friction pad" or anti-whirl PDC bit.

Although the dynamics of drillstrings has been investigated for some twenty years or so, particularly in recent years, much attention has been paid in this area, some phenomena are still not fully understood. There are also many established models for drillstring dynamics which are mainly either analytical models or FEM (finite element method) based models. The analytical models are usually too simple to predict accurately the dynamic behaviors of drillstring systems. On the other hand, the FEM based models are usually too complicated or too large to use in the drilling fields.

Ideally, the drillstring vibration control must be integrated in the complete economical and technological environment of the drilling process: vibration depending on operation and equipment, an optimum is to be found from a global economical point of view. In order to realize this objective, simple but high accurate dynamic models must be first established. Such models can predict not only the dynamic behavior with high accuracy, but more importantly can be used conveniently in the drilling fields with microcomputers. Developing such a model is one of the purposes of the thesis.

1.3 OUTLINE OF THE THESIS

The thesis is based on part of the work performed during the author's stay at LTAS of University of Liège since February, 1992. It concentrates on the understanding of the vibration behaviors of drillstrings based on both linear and nonlinear models. For the convenience of reading, each chapter is written independently with an introduction and conclusions. However, chapter 2 is the basis of chapter 3 and 4. Chapter 5 and chapter 6 study the backward whirl phenomena by lumped model and FEM model respectively.

Chapter 2 describes the principle of an improved dynamic stiffness method (IDSM) and its application to beam-like systems. The IDSM is based on the combination of the transfer method, the dynamic stiffness method (DSM) and the finite element method (FEM). The procedure of the IDSM is described in detail. It is demonstrated through numerical examples that the IDSM benefit analysis and solution of the eigenvalues, force responses, dynamic force identification problems for beam-like structures.

Chapter 3 applies the IDSM to the axial and torsional vibration analysis of drillstrings. Because the torsional vibration analysis is similar with the axial vibration, only the axial vibration is described in detail. Using the IDSM, the whole drillstring can be reduced exactly either to a SDOF model or to a two DOFs model depending on the research purpose. The model accounts for the frequency-dependent damping. Based on the reduced model, free and forced vibrations are investigated. The procedure of how to estimate the down hole bit axial and torsional forces and motions using surface measurement is described. The design of shock absorber is also discussed.

Chapter 4 describes the application of the IDSM to lateral vibration and buckling analysis of the BHA. The BHA is modeled with the bit displacements as the generalized coordinates. The model takes the effects of WOB, the curvature of the BHA as well as the drilling mud into consideration. It is shown that both the WOB and curvature decrease the bending natural frequencies. The exact bukling loads are also obtained based on the model.

The theory given in chapter 2, 3 and 4 makes it possible in the drilling fields, using only microcomputers, to analyze exactly the axial, torsional and lateral vibrations, to calculate the buckling loads as well as to identify the bit forces and motions by surface measurements. Without doubt, because the simplicity and high efficiency, the model will help both the designer and the driller to control and hence to reduce the vibration levels.

The work presented in the above three chapters (chapter 2,3,4) is mainly based on Chen and Géradin (1992a, 1993c, 1994a $\sim$ h), Géradin and Chen (1994), Chen, Golinval and Géradin (1993, 1994c), Chen, Géradin and Lamine (1993, 1994a,b).

Chapter 5 studies the PDC bit whirl kinematics and backward whirl motion due to bit-holewall contact based on a lumped model. The cutter trajectory, and the overlap condition of cutter path for a whirling bit are given. The relation between the whirl parameters and hole lobes is derived. The bit whirl kinematics is the basis of identification of bit whirl by experiment (described in chapter 7).

The dry friction induced steady-state backward whirl motion is studied both analytically and numerically based on a lumped model. The formula to calculate the whirl speed and the whirl radius have been derived in a closed form. The study presented in this chapter makes it clear that once backward whirl is initiated, the whirl frequency and its amplitude are heavily dependent on the rotation speed, the eigenfrequency, the clearance and the formation stiffness. It also appears that the friction coefficient, which is responsible for the initiation of backward whirl, does not affect the whirl frequency and amplitude. The steady state backward whirl amplitude increases with the rotation speed but the whirl frequency is limited by the eigenfrequency of the joint drillstring-formation system.

This chapter is based on Chen and Géradin (1993d), Chen, Rixen and Géradin (1992, 1994) and Chen, Golinval and Géradin (1994a,b).

Chapter 6 gives a further study of backward whirl due to bit-holewall contact based on FEM model. Effort has been made to modify an existing disk-cylinder contact element in order to simulate the dynamic contact phenomenon of the drillstrings. This element is implemented in a general and powerful multi-body dynamic analysis software, namely, Mecano module of Samcef. Therefore, many computational aspects of the Mecano software, for example the nonlinear beam element, the user's element, the implicit time integration method (Hilber-Hughes-Taylor method) as well as the pre- and post-analyzer, can be directly applied. In the contact element, not only the transverse friction forces but also the longitudinal friction forces are taken into account. The element stiffness and damping matrices are derived explicitly. Using this element, the backward whirl due to bit-holewall contact is further studied. The influences of friction coefficient, the external force, the contact damping and stiffness, and the rotation speed on the backward whirl motion are investigated in detail. It is found that there is a lowest backward whirl speed which is near to but greater than the first bending eigenfrequency of the system. This observation cannot be made in chapter 5 where lumped model is used. The contact-element developed in this chapter may be applied to other contact situations, for example the rotor-stator contact.

This chapter is mainly based on Parisis and Géradin (1990), Chen, Rixen and Géradin (1992,1994), Chen, Géradin and Lamine (1994c).

Chapter 7 develops some techniques of downhole bit whirl identification by experiment. The background of the identification method is the bit whirl kinematics described in chapter 5. Two independent methods are developed: accelerometer-based and contact-sensor based. It is proved that three accelerometers mounted just above the bit are enough to identify all the bit whirl parameters including whirl frequency, whirl amplitude and bit rotation speed. But one cannot directly obtain the bit center trajectory in space coordinate if only accelerometers are used. It is also proved that three contact sensors mounted on the bit gauge are theoretically enough to estimate the bit whirl parameters except the bit rotation speed. Two test data are analyzed in this chapter to demonstrate the principle and the procedure of the methods.

This chapter is based on the work performed by Chen, Géradin and Lamine (1993).

Chapter 8 concludes the results obtained so far in this thesis. Suggestions for future work are also made.

CHAPTER 2:

AN IMPROVED DYNAMIC STIFFNESS METHOD

2.1 INTRODUCTION

2.1.1 State of the Art

A large class of systems occurring in engineering practice consists of one-dimensional beam and beam-like elements. In some cases, the systems contain a number of elements linked together end to end in the form of a chain. A typical example is the oil-well drillstring studied in this thesis.

Various methods for dynamic analysis of beam-like structures have been developed and widely used during the last decades. Among these techniques, the transfer matrix method (TMM), the dynamic stiffness matrix method (DSM) and the finite element method (FEM) are very powerful and very popular.

The transfer matrix method was first proposed by Myklestad (1944, 1945), and later extended by Prohl (1945) to study the critical speeds of a shaft. Holzer (1948) initially applied the transfer matrix method to determine the torsional vibrations of rods. Thomson (1950) applied the method to more general vibration problems. Pestel and Leckie (1963) have studied systematically the theory and the applications of the method. Numerical difficulties were also pointed out. Rubin (1964, 1967) has provided a general treatment for transfer matrices and their relation to other forms of frequency response matrices at element level.

The TMM was used by many researchers during the last decades for different applications. These include Lin (1967), Lin and McDaniel (1969), Mercer and Seavey (1967), Mead (1970, 1971) and McDaniel (1971a, 1971b). Lund (1974), Bansal and Kirk (1975) have applied the transfer matrix method in modal analysis for calculating damped natural frequencies and examining the stability of flexible rotors supported by fluid bearings. In the aforementioned papers, the shaft or the beam is divided into a number of massless segments and the mass is lumped at both ends of each segment. This crude approximation results in considerable error on the predicted natural frequencies. To increase the accuracy, the number of elements used in the analysis must be increased which on one hand, increases the computational effort and, on the other hand, may induce numerical instability due to high number of matrix multiplication.

The most important modification to the transfer matrix method was made by Lund (1967). The transfer matrix of a shaft was represented in a continuous-system sense. Its advantage is that the uniform shaft can be made as long as needed so that the number of elements of the shaft is significantly decreased. As a result, the accuracy is increased and numerical instability may be avoided. Lee et al (1991) have further improved this method by accounting for the effects of rotary inertia and gyroscopic moment in the model and doubling the number of state variables to fit the general orbits of steady-state motion. Later, Chen and Géradin (1993c) and Chen, Golinval and Géradin (1993) further modified this method for the analysis

of the bending vibration of the drillstrings by taking the axial force and the curvature into consideration. The effect of torque has also been included by Lee et al (1993a).

In a more recent study, Lee et al (1993b) extended the transfer matrix method to the rotor mounted on nonlinear bearings. The steady-state analysis of subharmonic, superharmonic and synchronous vibrations was made. However, a great effort is needed to obtain the global transfer matrix of nonlinear systems.

The outstanding advantage of the transfer matrix method is that it requires calculations using matrices of fixed size, independently of the intermediate conditions and the number of degrees of freedom in the problem. This means that the computational complexity is low even when dealing with systems of hundreds of degrees of freedom.

The simplicity, however, gives rise to several numerical difficulties in using the method directly. They can occur first, when calculating higher natural frequencies and secondly, when intermediate geometric compatibility conditions are very stiff (Pestel and Leckie, 1963). In addition, only the natural frequencies, mode shapes and harmonic response are available by this method. The other important dynamic properties such as modal mass, modal stiffness and frequency response function (FRF) of the system as well as transient responses cannot be obtained. In addition, the explicit equations of motion of the structure are lost.

At the current state of dynamics, the finite element method (FEM) has proved to be powerful and versatile for almost all the dynamic problems in engineering. In the FEM, it is well known that one of the basic assumptions usually made is that the displacements throughout a structure are uniquely defined by the displacements at the nodes. This assumption is only valid for static loading, not for dynamic loading when inertia forces are present (Leung, Zhou, 1993). Since the inertia forces are dependent on nodal acceleration, the dynamic element shape functions should be functions of both nodal displacements and nodal accelerations. Dynamic element shape functions should therefore be functions of the frequency of vibration for harmonic motion. Therefore, the FEM is an approximation method and its accuracy depends heavily on the element type and number. Furthermore, many unwanted degrees of freedom are used in the FE model.

The dynamic stiffness matrix method (DSM) represents a powerful matrix technique for exact dynamic analysis. It may be considered as an exact finite element method. This method was developed in the early 1940s by Kolousek (1973). Being different from the FEM, the DSM uses the analytical solutions of the governing equations as shape functions (frequency dependent). Therefore, the obtained dynamic stiffness matrix is exact if the governing equation of the element is exact. These matrices are in general parametric in terms of the vibration frequency and the load factor. This fact enables the infinite number of natural modes to be represented by a finite number of nodal coordinates for continuous structures of beams. For prismatic beam elements, the exact solution can be obtained by using any number of discretized elements.

The DSM has been applied with success to frame structures with uniform members (Johnson and Bishop, 1960; Kolousek, 1973) or non-uniform members (Banerjee and Williams, 1985), straight members (Howson et al, 1983), curved members (Pearson and Wittrick, 1986,

Henrych, 1981), damped beam (Lundon and Akesson, 1983), general variable cross section members (Eisenberger, 1990) and other structures (Leung, 1978, 1979). The DSM has also been applied to response calculation (Leung, 1985,1987). An important progress of enhancing the applicability of the DSM was made through the algorithm of Williams and Wittrick (1970) and Wittrick and Willams (1971) to automatically calculate natural frequencies. A general dynamic stiffness matrix of a Timoshenko beam for transverse vibrations was presented by Y.H. Chen (1987). A coupled bending-torsional dynamic stiffness matrix for Timoshenko beam elements has been derived (Banerjee and Williams, 1992). More recently, this DSM has been applied to flexible multi-body systems for accurate transient response in forced vibrations (Liu and Lin, 1993). Some of the important characteristics of the dynamic stiffness matrix as well as the relationship with modal analysis have been studied recently (Pilkey and Fergusson, 1990, Fergusson and Pilkey, 1992, 1993a). There is a significant number of references describing this method. Fergusson and Pilkey (1991a,b, 1993b,c) have reviewed the relevant literature up to 1992. Most of the literature up to the end of 1992 may be found in their reviews.

One of the most important advantages of the DSM is that the degrees of freedom needed to model a structure is significantly reduced compared to the FEM. This is due to the fact that a uniform shaft, for example, can be taken as long as needed in the DSM. Although the method requires considerable effort to build up the dynamic stiffness matrix describing the basic element in the first instance. Once established, however, the matrix can be used as a standard element as in the case of the FEM.

However, there are some drawbacks associated with the DSM. Firstly, the number of degrees of freedom is still high for large structures. Similarly to the FEM, many unwanted degrees of freedom such as internal and rotational degrees of freedom remain in the model. Secondly, the calculation of modal parameters requires the solution of a highly nonlinear (transcendental) eigenproblem:

$$[D(\omega)]X = 0 \tag{2.1}$$

To this purpose, some special algorithms should be used, such as the algorithms described by Williams and Wittrick (1970) and Richards and Leung (1977). The former algorithm requires calculation of natural frequencies for each individual beam element with fixed ends.

In order to minimize the dynamic degrees of freedom without loss of accuracy, a combination method was first developed by Dokainish (1972) for plate vibration problems in which the element transfer matrix was obtained directly from the element stiffness and mass matrices. In recent years, this combination method has been improved by other researchers (Chiatti and Sestieri, 1979, Ohgh et al, 1983, 1984, 1993, Degen et al, 1985, Subbiah et al, 1988, McDaniel et al, 1977, Sankar and Hoa, 1980) for different applications. In this method, the element or substructure transfer matrix was obtained from the element or substructure stiffness and mass matrices. The eigenfrequencies and mode shapes were then calculated from the global transfer matrix. Therefore, it may be considered as an improved transfer matrix method. However, for beam or shaft systems it seems to be unnecessary to obtain the element transfer matrix from the element stiffness and mass matrices because the exact element transfer matrix may be derived directly from the governing equations (Lund, 1976). Furthermore, because of the nature of the transfer matrix relations used in the method, only eigenfrequencies, mode shapes and harmonic response can be available by this method.

2.1.2 The Work Presented in The Chapter

In this chapter, the principles of the transfer matrix method, the finite element method and the dynamic stiffness method are briefly described. Based on the principles of these three methods, an improved dynamic stiffness method (IDSM) is developed which is based on the combination of transfer, dynamic stiffness matrices and finite element method. In the IDSM, the entire structure is first divided into several substructures according to the required master degrees of freedom and the boundary conditions of the structure. Each substructure may consist of a large number of basic elements. The degrees of freedom for a substructure may be partitioned into two sets. One set is the internal degrees of freedom, and the other set is the boundary degrees of freedom. The transfer matrix of each substructure relates only the boundary degrees of freedom. The dynamic stiffness matrix of the substructure is obtained by rearranging the corresponding transfer matrix. In this way, the internal degrees of freedom are not used. In other words, a substructure is reduced exactly to an equivalent element whose nodal coordinates are the boundary coordinates of the substructure. The dynamic stiffness matrices of equivalent elements become the basic matrices for assembling the global dynamic stiffness matrix for the original structure. The order of the system eigenvalue equation is equal to the number of physical boundary coordinates between substructures. The global matrices are frequency dependent. Because the dynamic stiffness matrices of the basic elements such as beam, lumped mass and stiffness elements are exact, the number of modes predicted by the model is not limited by the number of master degrees of freedom used in the model.

The IDSM is compared with the other three methods through two numerical examples. The advantages and its flexibility in the modelisation of vibrating structures are pointed out. The applications of this method in the area of modal analysis are discussed.

2.2 TRANSFER MATRIX METHOD (TMM)

To demonstrate the transfer matrix procedure, let us consider the beam element shown in Fig.2.1. For node i, we define the state vector:

$$S_i = [X_i, \theta_i, M_i, F_i]^T \tag{2.2}$$

where X_i, θ_i, M_i and F_i corresponds to the lateral displacement, the rotation angle, the moment and the shear force, respectively.

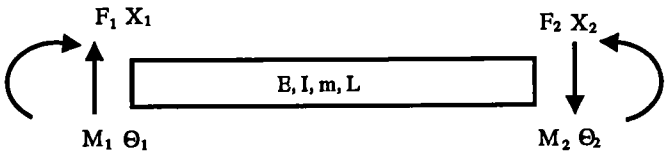

Fig.2.1: Beam element for the transfer matrix method

For this element, a transfer matrix $[T]$ relates the state vectors at station i and station $i+1$ as follows:

$$S_{i+1} = [T]S_i \tag{2.3}$$

If the original structure consists of n elements linked together end to end, then the overall transfer matrix for the whole system is obtained by multiplying all the element transfer matrices. The aim is to relate the state vectors of both ends of the whole structure:

$$S_n = [T]_n[T]_{n-1}.....[T]_1 S_1 = [T_g]S_1 \tag{2.4}$$

where n is the total number of elements, $[T_g]$ is the global transfer matrix.

It is noted that the overall or global transfer matrix $[T_g]$ has the same size as the element transfer matrix.

Applying the boundary conditions at both ends to equation (2.4), a frequency equation can be derived from which the system natural frequencies may be obtained. After the natural frequencies have been found, it becomes easy to calculate the mode shapes from equation (2.4) by taking arbitrarily one boundary displacement or rotational angle as unity. The harmonic responses of the system may also be calculated by expanding the transfer matrix (Pestil and Leckie, 1963).

2.3 FINITE ELEMENT METHOD (FEM)

In the finite element method, the system is divided into n elements. Let us first consider the beam section shown in Fig.2.2.

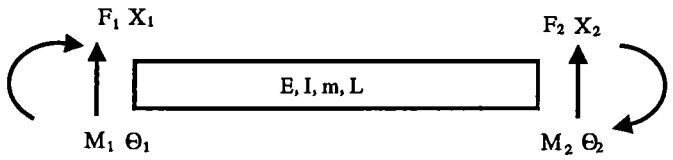

Fig.2.2: Beam element for dynamic stiffness matrix method

Note that the directions of the forces and the moments in Fig.2.2 are different from those in Fig.2.1.

In the FEM, the following steps are usually made:

Step 1:

The mass and the stiffness matrices for the bending vibration of the beam shown in Fig.2.2 may be found in most vibration textbooks (for example, Géradin and Rixen, 1994) and are directly written as (for a Bernoulli-Euler beam):

$$[M^e] = \frac{mL}{420}\begin{pmatrix} 156 & -22L & 54 & 13L \\ -22L & 4L^2 & -13L & -3L^2 \\ 54 & -13L & 156 & 22L \\ 13L & -3L^2 & 22L & 4L^2 \end{pmatrix} \tag{2.5}$$

where m is the mass per unit length, $[M^e]$ is the mass matrix of the beam element.

$$[K^e] = \frac{2EI}{L^3}\begin{pmatrix} 6 & -3L & -6 & -3L \\ -3L & 2L^2 & 3L & L^2 \\ -6 & 3L & 6 & 3L \\ -3L & L^2 & 3L & 2L^2 \end{pmatrix} \tag{2.6}$$

Step 2:

The global mass and stiffness matrices are then obtained by applying compatibility and boundary conditions. This process is achieved by placing the element matrix (after coordinate transformation, if any) at the appropriate location in the global matrix. The assembly process results in the following global differential equation:

$$M\ddot{x} + Kx = f \tag{2.7}$$

where M and K are the global mass and stiffness matrices of dimensions $4(n+1) \times 4(n+1)$ in the case of bending vibration of beam systems, x is the global coordinates vector of dimension $4(n+1)$ and f is the force vector of dimension $4(n+1)$, n is the number of elements.

For harmonic excitation, i.e. $f = Fe^{i\omega t}$ and $x = Xe^{i\omega t}$, equation (2.7) becomes:

$$(K - \omega^2 M)X = D_g^f(\omega)X = F \tag{2.8}$$

where $D_g^f(\omega)$ is global dynamic stiffness matrix with dimension $4(n+1) \times 4(n+1)$.

Step 3:

The eigen-frequencies and eigen-vectors can be obtained by solving the homogeneous equation obtained from (2.8) when F is set to zero. There are various numerical methods to solve this equation (see for example, Géradin and Rixen, 1994).

Note that the mass and stiffness matrices for the beam element (equation (2.5, 2.6)) in the FEM are derived based on static shape functions. Therefore, the global dynamic stiffness matrix $D_g^f(\omega)$ in equation (2.8), although being of high in dimension, is not an exact matrix. Hence, equation (2.7) or (2.8) gives usually approximate results. The only way to increase the accuracy is to refine the mesh which leads to higher dimension.

2.4 DYNAMIC STIFFNESS METHOD (DSM)

In order to demonstrate how the dynamic stiffness method proceeds, let us still consider the beam section shown in Fig.2.2. Similar to the FEM, the DSM takes the following steps.

Step 1:

For the Bernoulli-Euler beam shown in Fig.2.2, the exact dynamic stiffness matrix is obtained directly from the governing equation by Fricker (1983) as follows:

$$\begin{pmatrix} F_1 \\ M_1 \\ F_2 \\ M_2 \end{pmatrix} = B \begin{pmatrix} Z_1 & Z_2 & Z_4 & -Z_5 \\ Z_2 & Z_3 & Z_5 & Z_6 \\ Z_4 & Z_5 & Z_1 & -Z_2 \\ -Z_5 & Z_6 & -Z_2 & Z_3 \end{pmatrix} \begin{pmatrix} X_1 \\ \theta_1 \\ X_2 \\ \theta_2 \end{pmatrix} \tag{2.9}$$

where

$$B = EI/(1 - \cos bL \cosh bL)$$

$$Z_1 = a^3(\cos bL \sinh bL + \sin bL \cosh bL); \quad Z_2 = a^2 \sin bL \sinh bL;$$

$$Z_3 = a(\sin bL \cosh bL - \cos bL \sinh bL); \quad Z_4 = -a^3(\sin bL + \sinh bL);$$

$$Z_5 = a^2(\cos bL - \cosh bL); \quad Z_6 = a(\sinh bL - \sin bL);$$

$$b = (\omega^2 \rho A/EI)^{1/4}$$

with E= Young's modulus, I= area moment, ρ= mass density and A= cross section area.

Note that the elements in the dynamic stiffness matrix are frequency-dependent. Equation (2.9) may be simply written:

$$[D^e(\omega)]X^e = F^e \tag{2.10}$$

where $D^e(\omega)$ is the element dynamic stiffness matrix, ω is angular vibration frequency, $F^e = [F_1, M_1, F_2, M_2]^T$ and $X^e = [X_1, \theta_1, X_2, \theta_2]^T$. It can be easily validated that when $\omega \to 0$, the element dynamic stiffness matrix $[D^e(\omega)]$ in equation (2.10) becomes the static stiffness matrix given by equation (2.6).

Step 2 :

Having the element local matrix, equation (2.10), one next calculates the global dynamic stiffness matrix by assembling all the element matrices as done in the global matrix assembly of the FEM. First, element local equation (2.10) is cast into global form by coordinate transformations. Next, the element global matrices of all elements in the structure are superimposed appropriately to form the unrestrained structure dynamic stiffness matrix. Finally, any restrained displacements at structure boundaries are accounted for by deleting the corresponding rows and columns to form the restrained global dynamic stiffness matrix $[D_g]$. Then the exact structural dynamic equilibrium equation is obtained:

$$[F] = [D_g(\omega)][X] \tag{2.11}$$

Note that the dimension of the global dynamic stiffness matrix $[D_g]$ in equation (2.11) may be much lower than that of $[D_g^f]$ in equation (2.8). It is because a uniform beam element may be as long as necessary without losing accuracy in the DSM.

Step 3:

The eigenfrequencies can be obtained by:

$$det[D_g(\omega_n)] = 0 \tag{2.12}$$

where ω_n is the n order eigenfrequency. Due to the high order of the nonlinear eigenproblem, special algorithms have to be used for large structures (Wittrick and Williams, 1970).

With an ω_n found from equation (2.12), the associated modal vector X_n is calculated from

$$[D_g(\omega_n)]X_n = 0 \tag{2.13}$$

where X_n is the *nth* eigenmode.

Step 4:

The modal mass may be obtained by:

$$m_s = X_n^T[M(\omega_n)]X_n \tag{2.14a}$$

with the mass matrix:

$$[M(\omega)] = -\frac{d[D_g(\omega)]}{d(\omega^2)} \tag{2.14b}$$

If ω_n is sufficiently far from other natural frequencies, the derivatives can be evaluated numerically to any desired accuracy (Richard and Leung, 1977). An exact calculation of the modal mass has also been given by Hallauer and Liu (1982). The stiffness matrix $[K(\omega)]$ for a given frequency is then obtained by

$$[K(\omega)] = \omega^2[M(\omega)] + [D_g(\omega)] \tag{2.14c}$$

Step 5:

The response to harmonic excitation at any frequency ω can be obtained by solving equation (2.11). In fact, $[D_g(\omega)]^{-1}$ is the exact dynamic flexibility or FRF matrix for the given degrees of freedom.

2.5 IMPROVED DYNAMIC STIFFNESS METHOD (IDSM)

In order to show the principle of the IDSM, the bending vibration of beam is chosen as example element.

2.5.1. Derivation of the exact transfer matrix from the dynamic stiffness matrix of an element

Consider the beam as shown in Fig.2.1 and Fig.2.2. Equation (2.10) may be rewritten in submatrix form as follows:

$$\begin{pmatrix} F_l \\ F_r \end{pmatrix} = \begin{pmatrix} D_{11}^e & D_{12}^e \\ D_{21}^e & D_{22}^e \end{pmatrix} \begin{pmatrix} X_l \\ X_r \end{pmatrix} \tag{2.15}$$

where $F_l = [F_1, M_1]^t$, $X_l = [X_1, \theta_1]^t$, $F_r = [F_2, M_2]^t$, $X_r = [X_2, \theta_2]^t$. D^e_{ij} are 2×2 submatrices, $i, j = 1, 2$.

The transfer matrix for the beam element is therefore obtained by:

$$\begin{pmatrix} X_r \\ -F_r \end{pmatrix} = \begin{pmatrix} T^e_{11} & T^e_{12} \\ T^e_{21} & T^e_{22} \end{pmatrix} \begin{pmatrix} X_l \\ F_l \end{pmatrix} \tag{2.16}$$

with $T^e_{11} = -{D^e_{12}}^{-1} D^e_{11}$, $T^e_{12} = {D^e_{12}}^{-1}$

$$T^e_{21} = -D^e_{21} + D^e_{22} {D^e_{12}}^{-1} D^e_{11}, \quad T^e_{22} = -D^e_{22} {D^e_{12}}^{-1}$$

The transfer matrix of a lumped system with stiffness K and damping C or a lumped system with mass M can be found in the book written by Pestel and Leckie (1963). They are also listed in Appendix A for convenience.

2.5.2. Exact transfer matrix of a substructure

Shown in Fig.2.3 is a typical substructure which consists of N_k elastic supports, N_m rigid masses, N_b beam elements and N_d disks.

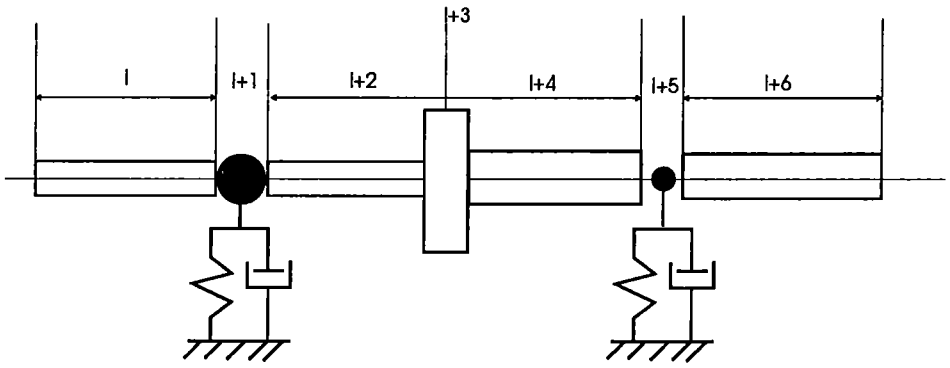

Fig.2.3: A substructure

The global transfer matrix for the substructure is:

$$[T^s] = [T^e_N][T^e_{N-1}].....[T^e_2][T^e_1] \tag{2.17}$$

where $[T^e_i]$, $i = 1, N$, is the transfer matrix of each element, N is the total number of elements of the substructure and $N = N_b + N_k + N_m + N_d$. The superscripts s and e refer respectively to the substructure and the element.

2.5.3. Derivation of the exact dynamic stiffness matrix from the transfer matrix of a substructure

The global transfer matrix $[T^s]$ of a substructure relates the forces and displacements at both ends of the substructure in the following way:

$$\begin{pmatrix} X_r^s \\ -F_r^s \end{pmatrix} = \begin{pmatrix} T_{11}^s & T_{12}^s \\ T_{21}^s & T_{22}^s \end{pmatrix} \begin{pmatrix} X_l^s \\ F_l^s \end{pmatrix} \tag{2.18}$$

where F_l^s and X_l^s are the force and displacement vectors at the left end of the substructure, F_r^s and X_r^s are the same quantities at the right end of the substructure. Equation (2.18) may be rewritten in the dynamic stiffness matrix form:

$$\begin{pmatrix} F_l^s \\ F_r^s \end{pmatrix} = \begin{pmatrix} D_{11}^s & D_{12}^s \\ D_{21}^s & D_{22}^s \end{pmatrix} \begin{pmatrix} X_l^s \\ X_r^s \end{pmatrix} \tag{2.19}$$

with $D_{11}^s = -{T_{12}^s}^{-1} T_{11}^s, \quad D_{12}^s = {T_{12}^s}^{-1}$

$D_{21}^s = -T_{21}^s + T_{22}^s {T_{12}^s}^{-1} T_{11}^s, \quad D_{22}^s = -T_{22}^s {T_{12}^s}^{-1}$

where $[D^s]$ is the global dynamic stiffness matrix of the substructure whose elements are frequency dependent. Note that the global dynamic stiffness matrix of the substructure has the same dimension as the element dynamic stiffness matrix. In other words, the substructure is reduced to an equivalent element whose nodal coordinates are only the boundary coordinates of the substructure.

2.5.4. Exact global dynamic stiffness matrix

The global dynamic stiffness matrix for the entire structure can be assembled using the above dynamic stiffness matrices of all substructures. The assembly process is the same as the one applied in the finite element method. After introducing the boundary conditions, the dimension of the global stiffness matrix can be further decreased. The restrained global dynamic stiffness matrix is denoted by $[D_g(\omega)]$. The unwanted or unobserved degrees of freedom such as rotational dofs can be removed in an exact manner (Leung, 1979). The global equations of motion is therefore:

$$F = [D_g(\omega)]X \tag{2.20}$$

2.5.5. FRF matrix

The frequency response function (FRF) matrix $H(\omega)$ for the selected d.o.f. can be obtained by inverting the above global dynamic stiffness matrix. We have

$$[H(\omega)] = [D_g(\omega)]^{-1} \tag{2.21}$$

The matrix $[D_g]$ is usually very low in dimension because the internal d.o.f.s of all the substructures are not used. Therefore, the inversion of matrix $[D_g]$ is easy to perform. If

the structure consists of only one substructure, the inversion of $[D_g]$ may be avoided by directly rearranging the transfer matrix.

2.5.6. Modal parameter evaluation

Once the global dynamic stiffness matrix $[D_g]$ of the system is obtained, the natural frequencies are the values of ω_n for which

$$[D_g(\omega_n)]X_n = 0 \tag{2.22}$$

where ω_n is the n_{th} eigenfrequency, X_n is the n_{th} eigenmode.

The algorithm developed by Williams and Wittrick (1970) may become tedious if it is directly applied for solving equation (2.22). The reason is that in this algorithm the natural frequencies for each individual beam element with fixed ends should be calculated first. However, in the IDSM, an "element" is a substructure which may consist of a large number of beam elements. Therefore, a newtonian procedure (Simpson, 1984) for solving equation (2.22) is recommended here.

Writing equation (2.22) in a more general form

$$[D_g(\omega)]X = 0 \tag{2.23a}$$

It is obvious that if the assumed frequency ω is not one of the eigenvalues of equation (2.23a), then we have

$$[D_g(\omega)]X = \mathbf{f} \neq 0 \tag{2.23b}$$

Let us partition along the last row and column of $[D_g(\omega)]$ so that

$$\begin{pmatrix} D_g^a & D_g^b \\ D_g^c & D_g^d \end{pmatrix} \begin{pmatrix} X_a \\ x_d \end{pmatrix} = \begin{pmatrix} 0 \\ f \end{pmatrix} \tag{2.24}$$

where the vector $\mathbf{f}$ is replaced by $[0, f]$, and the orders of D_g^a; D_g^b, X_a, D_g^d, x_d are $(n-1 \times n-1)$; $(n-1 \times 1)$ and (1×1), respectively.

The partitioning scheme is flexible in the sense that if, as any eigenvalue is approached, $x_d \rightarrow 0$, a rearrangement of the elements of X and therefore of $[D_g]$ may be performed in order to bring to the x_d position an element that does not vanish. A more detailed partitioning procedure is given by Simpson (1982). The value of x_d, in any case, may be set to unity (Simpson, 1982).

With $x_d = 1$ one has

$$f = X^t[D_g]X = [D_g^d] - [D_g^b]^t[D_g^a]^{-1}[D_g^b] = f(\omega) \tag{2.25}$$

Since the vanishing of $f(\omega)$ implies that $|D_g(\omega)| = 0$, thus an alternative eigenvalue equation is:

$$f(\omega) = 0 \tag{2.26}$$

Differentiation of equation (2.25) yields

$$df(\omega)/d\omega = X^t \frac{d[D_g]}{d\omega} X \tag{2.27}$$

Using equation (2.14b), equation (2.27) may be written alternatively as:

$$df(\omega)/d\omega = -2\omega X^t [M(\omega)] X \tag{2.27a}$$

where $[M(\omega)]$ is the mass matrix.

Since the mass matrix $[M(\omega)]$ is positive definite for all ω, the slope of the $f(\omega)$ is everywhere negative. The roots of $f(\omega)$ are the eigenvalues which must be real (for undamped system) and non-negative. Therefore, from equation (2.25) it is evident that the poles and zeros of $f(\omega)$ are necessarily interlaced.

Suppose that ω_0 is an estimate of an eigenvalue, then the Newtonian improved estimate will be:

$$\omega_n = \omega_0 - f(\omega_0)/X^t(\omega_0)[dD_g(\omega)/d\omega]_{(\omega_0)} X(\omega) \tag{2.28}$$

It is noted that ω_n may not be an improved estimate of ω_0 if it does not lie between the poles of $f(\omega)$ on either side of ω. First, one needs to be sure that ω_0 lies between these poles before the Newtonian process is used. If it does, once ω_n is calculated, one needs to ensure that ω_n also lies between the poles —and should it not, one rejects it. The reader may refer to the work done by Simpson (1982, 1984).

Because $[D_g]$ is very low in dimension, equation (2.21) may be solved by a straightforward procedure of calculating $det[D_g(\omega)]$ by inspection method.

The modal mass for mode n may be obtained by (Richard and Leung, 1977):

$$m_s^n = X_n^T [M(\omega_n)] X_n \tag{2.14a}$$

The frequency-dependent mass and stiffness matrices may be calculated from the dynamic stiffness matrix by equation (2.14).

Based on the reduced IDSM model, all the modal parameters such as natural frequencies, mode shapes and modal masses in a large frequency range can be calculated. The detailed procedures were described by Chen and Géradin (1994a,1994b).

2.5.7. Forced response

There are two main ways to calculate the steady-state response under any type of excitation: modal superposition method (MSM) and direct time integration method (DTIM). However, if the model is established by the IDSM as presented above, both the MSM and the DTIM are not convenient due to the fact that the matrix elements are frequency dependent. Only in the case of harmonic excitation, the DTIM may be applied to the IDSM model after the global mass and stiffness matrices have been obtained using equation (2.14).

In this section, an FFT-based method is proposed.

The response in frequency domain is:

$$X(\omega) = [H(\omega)]F(\omega) \tag{2.29}$$

Theoretically, the FRF matrix obtained in section 2.5.5 is valid not only for harmonic excitation but also for other types of excitation. That is, equation (2.29) still holds for arbitrary excitation in which $X(\omega)$ and $F(\omega)$ are displacement and force vectors in frequency domain. Performing IFFT on equation (2.29), we have:

$$x(t) = ifft[H(\omega)F(\omega)] \tag{2.30}$$

where $x(t)$ is the displacement vector in time domain (assuming zero initial conditions). In Equation (2.30), the FRF matrix $[H(\omega)]$ may be calculated in advance and stored in the computer for a given system because it depends only on the eigenproperties of the system. Therefore, for different types of excitation, it is not necessary to recalculate the FRF matrix.

Both lumped systems and continuous systems were studied using the IDSM and the procedure was described by Chen, Golinval and Géradin (1994c).

2.5.8. Recovery of mode shape and response amplitudes at arbitrary locations

Since the IDSM does not use most of the internal degrees of freedom, and since the size of the dynamic element can be very long compared to the conventional element, the ability to recover the mode shape and to compute the response at some internal nodes and at arbitrary locations within an element is sometimes necessary. This is realized through the following two steps:

Step 1:

The mode shape and response amplitudes can be recovered at the internal dofs within a substructure. Consider the substructure shown in Fig.2.3. The mode shape or response amplitudes at both ends have been obtained by equation (2.21) or equation (2.29). Now we want to calculate the mode shape or response amplitudes at node j within the substructure.

The state vector at node j can be easily obtained by the transfer matrix between node j and the left end node:

$$S_j = [T]_j[T]_{j-1}.....[T]_l S_l \tag{2.31}$$

where S_l is defined by equation (2.2).

Using equation (2.31), the displacement, rotational angle as well as the internal forces at node j can be obtained.

Step 2:

In order to compute the mode shape or the response amplitude at arbitrary locations within an element, it is necessary to obtain first the dynamic shape function. As an example,

consider the bending vibration of a Bernoulli-Euler beam whose dynamic stiffness matrix has been obtained (equation (2.9)). The dynamic shape function is (Liu and Lin, 1993):

$$N_1(x) = \frac{b}{H}(A_1 \sin bx + A_2 \cos bx + A_3 \sinh bx + A_4 \cosh bx) \tag{2.32a}$$

$$N_2(x) = \frac{1}{H}(B_1 \sin bx + B_2 \cos bx + B_3 \sinh bx + B_4 \cosh bx) \tag{2.32b}$$

$$N_3(x) = \frac{b}{H}(C_1 \sin bx + C_2 \cos bx + C_3 \sinh bx + C_4 \cosh bx) \tag{2.32c}$$

$$N_4(x) = \frac{1}{H}(D_1 \sin bx + D_2 \cos bx + D_3 \sinh bx + D_4 \cosh bx) \tag{2.32d}$$

and H, A_i, B_i, C_i and D_i, i=1,2,3,4 in equation (2.32) are

$H = 2b(-1 + \cos bl \cosh bl)$

$A_1 = \cos bl \sinh bl + \sin bl \cosh bl$; $A_2 = -1 - \sin blsinhbl + \cos bl \cosh bl$;

$A_3 = -\cos bl \sinh bl - \sin bl \cosh bl$; $A_4 = -1 + \sin blsinhbl + \cos bl \cosh bl$;

$B_1 = -1 + \cos bl \cosh bl + \sin bl \sinh bl$; $B_2 = \cos blsinhbl - \sin bl \cosh bl$;

$B_3 = -1 + \cos bl \cosh bl - \sin bl \sinh bl$; $B_4 = -\cos bl \sinh bl + \sin bl \cosh bl$;

$C_1 = -\sin bl - \sinh bl$; $C_2 = -\cos bl + \cosh bl$;

$C_3 = \sin bl + \sinh bl$; $C_4 = \cos bl - \cosh bl$;

$D_1 = -\cos bl - \cosh bl$; $D_2 = \sin bl - \sinh bl$;

$D_3 = \cos bl - \cosh bl$; $D_4 = -\sin bl + \sinh bl$;

where $b = (\omega^2 \rho A/EI)^{1/4}$

The displacement function at an arbitrary location x in harmonic vibration can be obtained from:

$$V(x) = [N_1(x) \quad N_2(x) \quad N_3(x) \quad N_4(x)]X \tag{2.33}$$

where X is the nodal displacement vector.

2.5.9. Dynamic force identification

The dynamic force in frequency domain may be directly estimated by equation (2.20). The corresponding time history can be easily obtained by performing IFFT on equation (2.20):

$$f(t) = ifft([D_g(\omega)]X(\omega)) \tag{2.34}$$

It should be noted at this stage that the force identification procedure based on equation (2.34) has the following advantages:

(1.) The global dynamic stiffness matrix in equation (2.34) uses only the coordinates of excitation locations. Therefore, the matrix $[D_g]$ is always a square matrix. In other words, the number of measured responses is the same as the number of excitation forces. This reduces much of the experimental work.

(2.) Using equation (2.34) to estimate the forces is straightforward and does not require the inversion of the global matrix. The ill-conditioning problem associated with the usual force identification algorithms may be avoided.

(3.) The model uses directly the coordinates of the excitation points as the master degrees of freedom, model reduction is not necessary. Although some of the rotational dofs may remain in the model, they can be deleted from equation (2.34) in an exact manner.

(4.) No modal parameter extraction is needed.

2.6 COMPARISON OF THE METHODS VIA NUMERICAL EXAMPLES

Example 1: Free vibration analysis

In order to make a direct comparison of the above described four methods, namely the TMM, the FEM, the DSM and the IDSM, let us study the free vibration of the non-uniform beam shown in Fig.2.4.

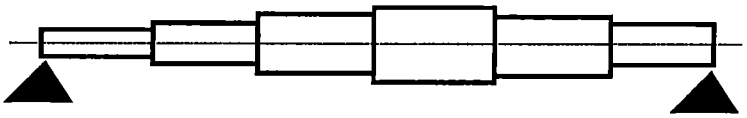

Fig.2.4: A single-span beam with non-uniform cross sections

The first four eigenfrequencies are calculated using the four different methods. It is found that the TMM, the DSM and the IDSM gives exactly the same results since the exact matrices are used in these methods. Therefore, only the results calculated by the FEM (Samcef, 1994) and the IDSM are listed in Table 2.1.

Table 2.1: Natural frequencies (Hz) of example 1

Mode	ω_1	ω_2	ω_3	ω_4
FEM	9.99	48.94	121.86	231.42
IDSM	9.99	48.69	121.83	231.25

In the FEM model, 18 beam elements were used, the corresponding global matrices are 36 x 36 in dimension. In the DSM, only 6 beam elements were needed, the global matrices are therefore 12 x 12. The matrices used in the TMM and in the IDSM are always 4 x 4 in dimension. The restrained global matrix in IDSM is only 2 x 2 in dimension.

From this example, it is seen that both the TMM and IDSM deal with low order matrices and give exact results. In the TMM, however, the equations of motion of the original system are lost. The IDSM keeps the explicit equations of motion (in the case of example 1, the generalized coordinates are the rotational angle at both ends).

Example 2: Modeling of a cantilever beam

The simple cantilever beam shown in Fig.2.5 ($600mm \times 25.5mm \times 6.0mm$) is used as the second example.

This example is taken from the work carried out by Lee and Dobson (1991) where the purpose was to validate a direct measurement method for structural mass, stiffness and damping properties. We choose this as an example because of the availability of the results obtained by other modeling techniques and experiment. The lumped masses on the beam have the purpose to simulate the attached accelerometers.

The purpose here is to build up a model with three degrees of freedom (translation degrees of freedom at node 1,2,3) for the system shown in Fig.2.5. These degrees of freedom were also measured during the experiment. The detailed description of the modeling procedure is given in a previous report (Géradin and Chen, 1994). Only the main results are repeated here.

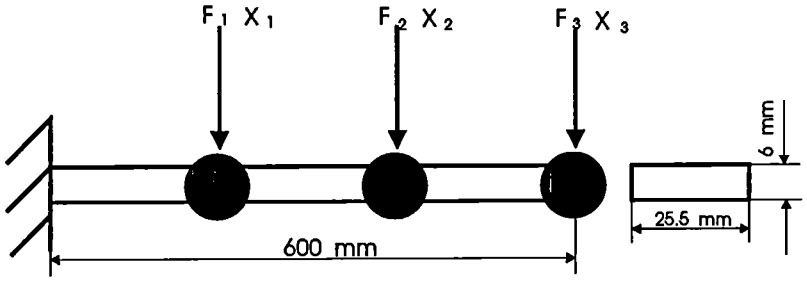

Fig.2.5: A cantilever beam with lumped masses

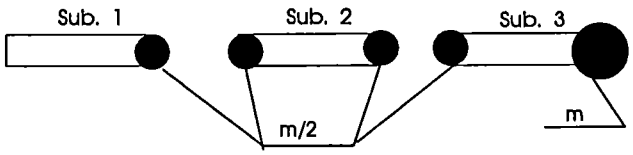

Fig.2.6: Three substructures

Because the internal degrees of freedom, X_1, X_2, X_3, should be kept in the equations of motion, the TMM can not be applied in this case. The difference between the IDSM and the DSM in this case is not obvious, only the IDSM and the FEM are compared.

In the FEM, 24 beam elements are used which leads to 50 degrees of freedom. In order to establish the three degrees of freedom model, 47 degrees must be removed from the FEM

model. Two reduction methods are applied, namely the static condensation (SCM) and the modified dynamic condensation (MDCM) (Lee and Dobson (1991)).

In the IDSM, the beam is divided into three substructures as shown in Fig.2.6. Therefore, according to the principle of the IDSM, the IDSM based model uses only six degrees of freedom, i.e., three translational and three rotational dofs. The three rotational dofs can be further removed in an exact manner (Leung, 1979).

Table 2.2: Eigenfrequencies regenerated by different methods, Hz

Mode	ω_1	ω_2	ω_3	ω_4	ω_5	ω_6
*SCM**	13.52	84.24	236.15	—	—	—
*MDCM***	12.65	83.32	238.73	435.10	674.81	964.20
IDSM	13.48	84.06	233.08	467.63	763.89	1129.24
Full FEM	13.72	85.08	233.99	477.53	771.89	1135.05

*: Static Condensation Method; **: Modified Dynamic Condensation Method.

The eigenfrequencies regenerated by the above models are listed in Table 2.2. It is seen that the model established by the IDSM, which has only three degrees of freedom, can predict all eigenmodes in a large frequency range. The results are comparable with the full FEM results in which 24 elements were used (50 degrees of freedom).

2.7 DISCUSSIONS AND APPLICATIONS OF THE IDSM

The proposed method (IDSM) was originally developed for linear oil-well drillstrings. However, its application to beam-like structures can be done in a straightforward manner. So far the method has been applied to the following dynamic problems:

(1) Modal parameter evaluation

It is well known that the correctly predicted number of eigenvalues based on the FEM model is equal to or less than half the number of degrees of freedom in the model (Géradin and Rixen, 1994). If the frequency range of interest is high the number of degrees of freedom used in the FEM model can be very large.

In contrast, the IDSM can yield exact solutions using any number of elements. The accuracy of the results are not dependent on the refinement of the mesh. The number of exactly predicted eigenmodes may be much higher than the number of degrees of freedom used in the model. Therefore, in the IDSM one can always handle low dimension matrices and save much computational effort in this manner. The mode shape amplitude at the slave nodes

(internal nodes) and arbitrary locations within an element can be recovered using the theory described in section 2.4.8.

(2) Model reduction

One problem occurs when the FEM model and DSM models are compared with the experimental one due to the large difference in the numbers of coordinates involved in both investigations. To solve this problem, model reduction techniques or modal expansion techniques have to be used. That is, the high dimension model is reduced to a lower dimension one in terms of master degrees of freedom. This reduction process may induce additional errors. In order to achieve reasonably accurate results, the master DOFs must be selected with care, otherwise some of the lower frequencies in the eigen-spectrum may even be lost (Mottershead and Friswell,1993). Different sets of masters may be required for different modes because the distributions of energy in the coordinates are different from mode to mode.

However, if the IDSM is used for modeling a structure, the structure may be directly modelled with the measurement coordinates as the global coordinates. In this sense, no reduction procedure may be needed. But it does reach the objective of the model reduction. The application of the IDSM to model reduction was described by Géradin and Chen (1994), Chen, Géradin and Lamine (1994a).

(3) Forced response calculation

Various methods for the determination of transient response of one-dimensional vibration structures such as beam or shaft systems have been developed and widely used during the last decades. Among these techniques, the modal superposition method (MSM), the direct time integration method (DTIM) are widely used (Géradin and Rixen, 1994).

In the finite element method (FEM), the number of degrees of freedom (dof) is usually very large which can lead to matrices [M], [C], [K] of large dimension. The use of the MSM requires to solve first the corresponding free vibration problem in order to get the modal parameters. The Duhamel integration and the decomposition into generalized coordinates and forces are required. The effectiveness of the MSM is remarkable as long as fundamental modes are predominant in the response (Géradin and Rixen, 1994). However, in the opposite case where the frequency spectrum requires to include a high number of modes so as to ensure good convergence, the procedure of calculating the response by this method is often tedious.

The DTIM, which is based on finite time differences, allows to take care of high frequency components in a straightforward manner. It is also a powerful method for nonlinear systems. However, the parameters of the time integration process are to be adjusted correctly according to accuracy and stability requirements. For large structures, this method can become very time consuming.

The IDSM is further extended to the forced response analysis of the one-dimensional structures, such as beam or rotor-bearing systems. The frequency response function (FRF)

matrix between any two points of the structures is obtained by inverting the corresponding dynamic stiffness matrix. Because the dynamic stiffness matrix obtained by the IDSM is usually very low, exact FRF matrix may be obtained. In order to calculate the forced response, the dynamic equations in frequency domain are transformed to time domain by the inverse fast Fourier transform (IFFT). The detail procedure was described by Chen, Golinval and Géradin (1994c).

(4) Dynamic force identification

The identification of exciting forces using the corresponding responses has received considerable attention in recent years. The reason is that in many situations the direct measurement of the excitation can be very difficult in practice or even sometimes impossible. Many techniques for force identification have been developed, for example, among others, the sum of weighted accelerations technique (Gregory et al., 1986, Priddy et al., 1988, Priddy et al 1989, Wang et al, 1987), and the deconvolution technique (Hillary and Ewins, 1984). H.Park and Y.Park (1994) have studied the arbitrary impact force identification, including the location and the time history of the impact force, using the wave propagation theory. Almost all the force identification algorithms require (a) the measurement of the responses (displacement, velocity or acceleration) at several locations on the structure due to the unknown force, and (b) a model of the structure. While the response may be easily obtained by direct measurement using transducers, the establishment of the structure model becomes a key issue in the force identification. There are three types of structure models which may be used in the force identification: spatial model (mass, damping and stiffness matrices), modal model (natural frequencies and mode shapes) and response model (or frequency response function matrix) (Ewins, 1988). If the modal model or the response model is used, the force identification process requires inevitably the inversion of global matrices which tend to be very ill conditioned. That is, very small errors in measurements generate large errors in estimated forces, especially at the frequencies close to resonance and anti-resonance conditions (Starkey and Merrill, 1989). Although efforts have been made to overcome this difficulty, for example the pseudo inverse technique (Fabunmi, 1985) and the singular-value decomposition (Elliott, Juang, Robinson, 1988), no significant progress has been achieved to the author's knowledge.

The use of the spatial model, usually established by finite element method (FEM), may offer significant advantages in some cases because it avoids the necessity to invert matrices (Dobson and Rider, 1990). However, the FEM model makes use of a large number of degrees of freedom (dof), but most of the dofs are not necessarily needed, especially those dofs at which no force is applied and no response is measured. In order to compute the excitations, the FEM model has to be reduced by model reduction technique so that the response needs only to be measured at a limited number of points. The reduction process may introduce errors as pointed out by many researchers (e.g., Leung, 1978, Freed and Flanigan, 1990).

Under the condition of knowing the number of excitations and their locations, it is found that the use of the IDSM for force identification has some advantages. The IDSM technique developed for force identification (Chen and Géradin, 1994d) bypasses the processes of modal parameter extraction, global matrix inversion as well as model reduction and hence

eliminates many of the approximations and errors which may be introduced during these processes.

(5) Rotor-bearing systems and branched beam-like systems

The application of the IDSM to rotor-bearing systems and to branched beam-like systems is straightforward. The principle was described by Chen and Géradin (1994c) and Chen, Golinval and Géradin (1995, to appear).

(6) Plate vibrations

The principle of the IDSM can be easily extended to the case of 2D and 3D plate vibrations. However, the description of the procedures exceeds the scope of the thesis. Details were given by Chen and Géradin (1994e).

2.8 CONCLUSIONS

An improved dynamic stiffness method is proposed in this chapter to model the beam structures directly at the required master degrees of freedom. What makes the present approach so simple and useful is that a substructure, which may consist of a large number of basic elements, can be always reduced exactly to an equivalent element whose nodal coordinates are the boundary coordinates of the substructure. The internal degrees of freedom of the substructure are not used in the model. This leads to an drastic reduction in the required degrees of freedom.

It is obvious that the present approach is different from the transfer matrix method and from the dynamic stiffness matrix method. In the transfer matrix method, the explicit equation of motion of the system has disappeared. Only the boundary conditions are related by the global transfer matrix. In the dynamic stiffness matrix method, on the other hand, the internal degrees of freedom in a substructure have to be used which leads to high order dimension. The present method is also different from the Dokainish combination method. Firstly, the exact stiffness matrix is used in the present method while in Dokainish combination method finite element matrices are used. Secondly, the Dokainish's method is actually an improved transfer matrix method because the eigen-properties are obtained from the global transfer matrix. Only eigenfrequencies, mode shapes and harmonic responses are available in Dokainish's method. In the present method, the explicit equation of motion is obtained and all the modal parameters such as eigenfrequencies, mode shapes, modal masses, modal stiffness, and FRF matrix can be calculated. Therefore, the present method may be considered as an improved dynamic stiffness matrix method.

The present method has also been applied to transient dynamic response analysis, dynamic force identification and to rotor-bearing and branched beam-like systems.

Compared to other methods, the IDSM has the following advantages:

(1) Numerical difficulties present in the usual transfer matrix method may be overcome. This is due to the fact that the number of elements in a substructure is low and the very stiff intermediate condition may be taken as boundary conditions directly in the global matrices.

(2) The system can be modeled exactly with arbitrary degrees of freedom, most of the internal degrees of freedom being automatically avoided. Therefore, the dimension of the global matrices is greatly reduced. This fact is very attractive for engineering applications. For example, the axial vibration model of a 5000 meter length drillstring may have 1000 dofs if the FEM is used, and only 2 dofs if the IDSM is used.

(3) The method handles only small matrices, hence, the computation effort is reduced considerably without loosing any accuracy.

Like any other method, the IDSM has also some disadvantages:

(1) At the current time, the IDSM can be applied only to linear systems.

(2) Although the IDSM may be applied to plate vibrations (Chen and Géradin, 1994e) or more complicated structures, some of the advantages of the IDSM may disappear. For example, when the required master degrees of freedom are randomly distributed over the plate, and the external force are distributed over the plate, then the order cannot be reduced by the IDSM method.

CHAPTER 3:

LINEAR AXIAL AND TORSIONAL VIBRATIONS OF DRILLSTRINGS

3.1 INTRODUCTION

3.1.1. An Overview

The vibration of oil-well drillstring includes axial, torsional and lateral vibrations. In most cases, these three vibrations are coupled through drillstring large deflection and bit formation interaction (Besaisow, 1986, Dunayevskey,1985). However, when dealing only with linear vibration, the coupling effects may be negligible. Therefore, the three kinds of vibration, namely axial, torsional and lateral vibrations may be considered separately.

It is well known that drillstring dynamics plays an important role in the oil well drilling practice. Poor drillstring dynamic behaviors will cause many problems, such as drilling failures, bit damages. In addition, drillstring vibrations affect the rate of penetration (ROP), the reliability of MWD (Measurement While Drilling) systems and the drilling direction. That is probably why so significant efforts are being expanded in the drilling dynamics presently.

The importance of drillstring vibration has not risen at the beginning of the drilling industry development. For a long time, the design of the drillstring was based on the static analysis such as stress distribution and static buckling. However with the increase of power transmission and the increase of rate of penetration, which became possible after the invention of PDC (Polycrystalline Diamont Compact) bit, and with the need of cost reduction by pushing the drilling equipment up to limits, the vibration problem becomes more than just a side effect. Indeed, vibration was found in the drilling field as the main source of BHA (Bottom Hole Assembly) failures.

For PDC bits, understanding and controlling vibration is of crucial importance. That is because the shocks and vibrations are very detrimental to PDC cutters. In some cases, shocks and vibrations can unable PDC bit to drill medium and hard rocks (Rixen, 1992a).

Much of the work about the dynamics of the drillstring has been directed toward the development of analytical and numerical models designed to predict the behavior of rotating and vibrating BHA and drill strings. For linear vibrations, three types of models have been developed in the past, namely analytical models, FEM and transfer matrix models.

A large part of early research work based on analytical model is focused on the buckling, axial and torsional vibrations of drill strings, long vertical pipes, etc. (Dareing and Livesay, 1968, Huang and Dareing, 1968, 1969, Dareing, 1984a,b). Although the model used in their analysis includes all the elements from the bit to rig of a drillstring, it usually considers the drillstring as having a uniform cross section.

Millheim and Apostal (1981a,b) were the first to implement complex three dimensional dynamic models of a rotating BHA to study the BHA dynamics based on the FEM model. More recently, Apostal et al (1990) developed a FEM based, forced-frequency-response

model (FFR model) for linear vibration analysis of drill strings. The FFR model can determine the force frequency response (Harmonic excitation) of a BHA due to imposed load and/or displacement excitations anywhere along the drill string. However, like any other FEM models, the FFR model has some disadvantages as described in Chapter 2. The applications of the FEM based models to drilling fields are therefore limited due to significant computational efforts.

A research team at MIT leaded by Prof. Vandiver developed a model based on transfer matrix method for axial vibration analysis of drill strings and for the design of shock absorbers (Lee, 1991, Vandiver et al, 1993). The model is used also for studying the effects of surface and down hole boundary conditions on the vibration of drill strings (Clayer, Vandiver and Lee, 1990). As pointed out in Chapter 2, the most important advantage of the transfer matrix model is that the dimension of the global matrix is independent on the number of elements. However, the limitation is also obvious, namely, only eigen-properties and harmonic response can be calculated.

3.1.2. Outline of the chapter

The IDSM described in Chapter 2 is applied to linear vibration analysis of drill strings. Axial, torsional vibrations are investigated separately in this chapter. Since the differential equation of motion for a basic element for the axial and torsional vibrations are similar, only axial vibration is described in detail. The same procedures can be followed for torsional vibration.

The whole drillstring (from bit to rig) is reduced exactly either to a SDOF model with the bit displacement as the generalized coordinate for free, forced vibration analysis and for shock absorber design, or to a two DOFs model with the displacements at the bit and surface measurement point as the generalized coordinates for identification of bit forces and motions by surface measurement. Based on the reduced models, the free and forced vibrations are studied. Exact eigen-frequencies are calculated. In the forced vibration analysis, the frequency-dependent damping is taken into account. The principle of estimation of down-hole bit forces and motions using surface measurement is described. Finally, the design of the shock absorber and its influence on the drillstring dynamics are discussed.

3.2 AXIAL VIBRATION ANALYSIS

3.2.1. Mechanical model of drillstring

Fig.3.1 shows a diagram of a typical drill string model. The topside boundary condition is modeled with an equivalent lumped mass-spring-damper system (Clayer, Vandiver and Lee, 1990). The bit is assumed to be free and an equivalent force is applied on it. Other boundary conditions at the bit such as an equivalent spring with damping can also be introduced without any difficulty. The equivalent mass, M_a, is the total mass of travelling block, power swivel and other equipment. The following values are assumed:

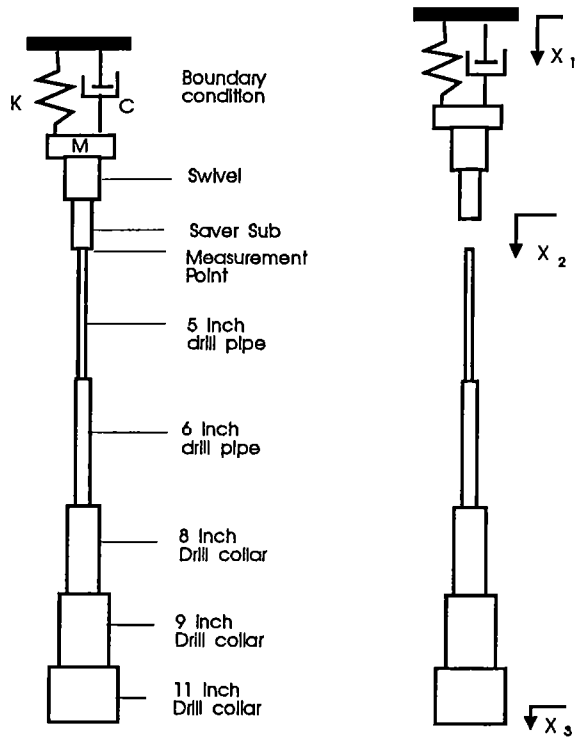

Fig.3.1: Mechanical model of the drillstring

K_a=1.0 $\times 10^7 N/m$, M_a=23765 Kg, C_a=40000 Ns/m

where subscript a denotes the axial vibration parameters. The geometric data of the drillstring are listed in Table 3.1.

Table 3.1: Geometry of the drillstring of Fig.3.1

Section Nr.	**1**	**2**	**3**	**4**	**5**	**6**	**7**
R_i (inch)	1.4	1.4	1.4	1.4	1.4	1.4	1.4
R_o (inch)	6.0	4.0	2.5	3.0	4.0	4.5	5.5
Length (meter)	5	5	200	200	50	40	30

3.2.2. Basic frequency-dependent matrices

From Fig.3.1 it is seen that there are three kinds of basic element for axial vibration: a lumped stiffness element with damping, a lumped mass element and a continuous beam element. Their associated transfer matrices or dynamic stiffness matrices are given below (Pestel and Leckie, 1963, Yang and Pilkey, 1992):

(1) Transfer matrix of a lumped stiffness K_a and damping C_a:

$$[T_a^{kc}] = \begin{pmatrix} 1 & 1/(K_a + i\omega C_a) \\ 0 & 1 \end{pmatrix} \tag{3.1}$$

where the subscripts a denotes the axial vibration.

(2) Transfer matrix of a lumped mass M_a:

$$[T_a^m] = \begin{pmatrix} 1 & 0 \\ -M_a\omega^2 & 1 \end{pmatrix} \tag{3.2}$$

(3) Axial dynamic stiffness matrix $[D_a]$ for a continuous beam:

$$[D_a] = \alpha \begin{pmatrix} 1/\tan(\theta) & 1/\sin(\theta) \\ 1/\sin(\theta) & 1/\sin(\theta) \end{pmatrix} \tag{3.3}$$

where $\alpha = EA\theta/L$, $\theta = L\sqrt{\rho(\omega^2 - 2i\gamma\omega)/E}$, γ is the damping constant, ω the angular frequency, L the length of the beam, A the cross section area of the beam, ρ the mass density of the beam.

The damping coefficient γ is described in detail in the next section.

The above matrices are the basic matrices for the axial vibration analysis of drill strings using the IDSM described in Chapter 2.

3.2.3. Damping mechanisms for axial motion

Damping is an essential parameter in determining the response and resonance amplitude. The main sources of damping of extensional waves are probably (Aarrestad et al 1986):

(a) Breathing effects of the pipe in the confined fluid;

(b) Viscous losses due to the interaction with the drilling fluid;

(c) Frictional forces due to wall contact;

(d) Bit/formation interaction;

(e) Losses in the suspension at the top of the drillstring;

(f) Dissipation in shock absorbers, if any.

The friction forces are usually non-linear. However, if the non-linear terms are small, it can then be modeled by an effective linear coefficient. In this chapter, we deal only with linear damping models.

There are two kinds of damping models: frequency-independent and frequency-dependent. The frequency-independent one was proposed by Dareing and Livesay (1968), Kreisle and Vance (1970).

The frequency-dependent model was proposed by Squire and Whitehouse (1979) based on the study of damping mechanisms of acoustic radiation and of viscous losses in the drilling fluid. According to their analysis the damping coefficient due to radiation is:

$$\gamma_r = \pi^2 v^2 r_0^2 \rho_f \omega k_\gamma \tag{3.4}$$

whereas the damping coefficient due to viscous losses is:

$$\gamma_v = \pi(r_i + r_0)\sqrt{2\omega\rho_f \eta} \tag{3.5}$$

where r_0 and r_i are the outer and inner radius (meters) of the drillstring, respectively. ρ_f is the density of mud (kg/m^3), η is the viscous coefficient of the mud, and v is the Poisson ratio of the drillstring. The coefficient k_γ takes a value between 0 and 3 (usually k_γ=2).

It is seen that both γ_r and γ_v are functions of frequency. The damping coefficient is then

$$\gamma = \gamma_r + \gamma_v \tag{3.6}$$

The numerical values given by equation (3.4) and (3.5) show that the viscous losses γ_v are negligible in comparison to the radiation damping γ_r.

The frequency-dependent damping model is believed to be more realistic than the frequency-independent one (Aarrestad et al, 1986).

3.2.4. Free axial vibrations

(1) Dynamic model

The free axial vibration analysis includes the calculation of eigenfrequencies and mode shapes. To this end, the drillstring shown in Fig.3.1 may be represented by an equivalent SDOF (single degree of freedom) model with bit axial displacement as the generalized coordinate for a given frequency using the IDSM described in Chapter 2. The following steps are used:

Step 1:

The drillstring consists of 9 elements, i.e. 7 beam elements, 1 lumped mass element and 1 lumped spring element with damping. Their corresponding frequency-dependent matrix (transfer matrix or dynamic stiffness matrix) are listed in section 3.2.2. The global transfer matrix is therefore obtained by:

$$[T_a^g] = [T_a^9][T_a^8].....[T_a^1] \tag{3.7}$$

Step 2:

The global dynamic stiffness matrix obtained without introducing any boundary conditions is derived by rearranging the global transfer matrix $[T_a^g]$ using equation (2.19). It is a 2×2 matrix. After introducing the boundary conditions at the top end, the restrained dynamic stiffness matrix reduces to a scalar for a given frequency. Hence, the dynamic equation of motion is:

$$F_a^b = d_a^g(\omega) X_a^b \tag{3.8}$$

where F_a^b and X_a^b represent respectively the axial force and the axial displacement response at the bit, $d_a^g(\omega)$ is the restrained dynamic stiffness matrix (a frequency-dependent scalar in this case). The superscript b refers to the bit and the subscript a denotes the axial vibration.

Based on the restrained dynamic stiffness matrix $d_a^g(\omega)$, the free vibration of drillstring can be analyzed.

(2) Natural-frequencies

Table 3.2 gives the first seven natural frequencies predicted by the IDSM model and by FEM model. In the FEM model, 40 elements (Samcef Software, beam element type 1) are used.

Table 3.2: Eigenfrequencies (Hz) predicted by IDSM and FEM

Mode	ω_1	ω_2	ω_3	ω_4	ω_5	ω_6	ω_7
IDSM	1.194	3.615	7.293	12.843	17.446	22.394	26.701
FEM	1.194	3.615	7.299	12.887	17.568	22.584	27.709

Fig.3.2 depicts the transfer function at the bit predicted by the IDSM model (equation (3.8)) with small damping. It is found that the axial eigenfrequencies are always within the operational band. When the axial excitation frequency, for example the three pattern excitation for tricone bit (will be described in next section), is equal to one of the eigenfrequencies, resonance will happen and hence large dynamic loads will be induced. This problem may be partly solved by placing a shock absorber above the bit. The effects of a shock absorber on the dynamics of the drillstring will be discussed in section 3.2.7.

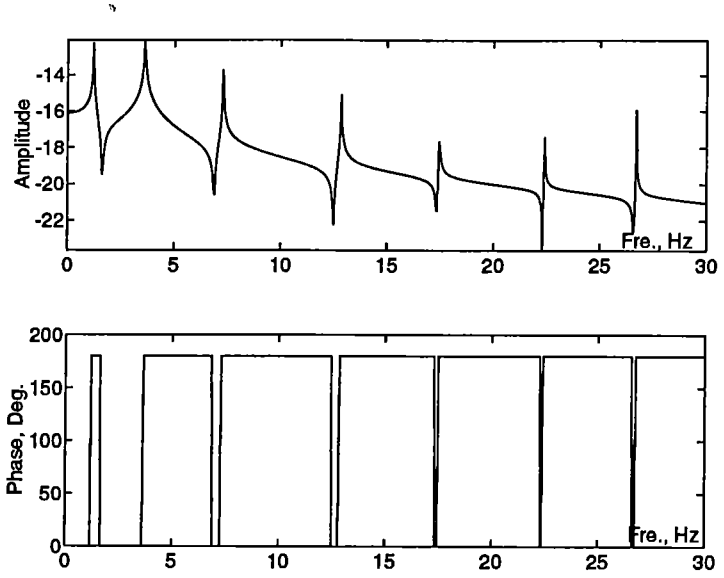

Fig.3.2: Transfer function predicted by the IDSM model

It should be noted that although the IDSM model uses only one dof, the eigenvalues predicted by the IDSM model are exact values. On the other hand, the FEM using 40 degrees of freedom gives only approximate results.

3.2.5. Forced axial vibrations

(1) Axial excitations

It is clear that the axial excitation source is the bit/formation interaction. It is therefore dependent on the bit type and the formation drilled. For tricone bits, for example, axial excitation is mainly produced by bottom hole surface unevenness, the so called three-lobe pattern (Besaisow and Payne, 1986, Dareing et al, 1983, Wolf et al, 1985 Aarestad et al, 1986). In other words, if the rotation speed is ω, then the excitation frequency is 3ω. Hence, for tricone bits, critical speeds are well within general operating range. If harder rocks are drilled by tricone bits, strong axial vibration may occur because of lower damping and rougher multi lobe pattern.

For the PDC bits, the excitation mechanisms are more complicated. The dynamic interaction between PDC cutters and formation may be one of the sources.

In addition, the variation of the weight on bit (WOB) and the fluctuation of the mud pressure (Dareing et al, 1983) may also be the excitation sources. In some cases the rock-bit teeth impacting and local formation singularities (Lutz et al, 1971) may induce small high frequency sollicitations.

Generally, from the above analysis it may be concluded that the actual excitation is a combination of non-random harmonic loads superimposed to random vibrations (Skaugen, 1987, Rixen, 1992a).

(2) Frequency domain response

It has been shown that the dynamic stresses caused by axial vibration are maximum on the bit (Dareing et al, 1983). Therefore, in this section the whole drillstring shown in Fig.3.1 may be modeled with one degree of freedom, i.e., with the bit axial displacement as the generalized coordinate. This is the case described in section 3.2.2..

Fig.3.3 shows the frequency responses with different damping levels. It is seen that the frequency dependent damping has a significant effect on the high frequency modes. It is because the damping constant calculated by equation (3.6) is almost a linear function of vibrating frequency. Another fact which can be observed from the figure is that the first two eigenmodes are difficult to be damped out. Note that the first two eigenfrequencies are usually in the range of operational speed of the drillstring. Therefore, the first two eigenmodes play an important role in the axial vibration control of the drillstring.

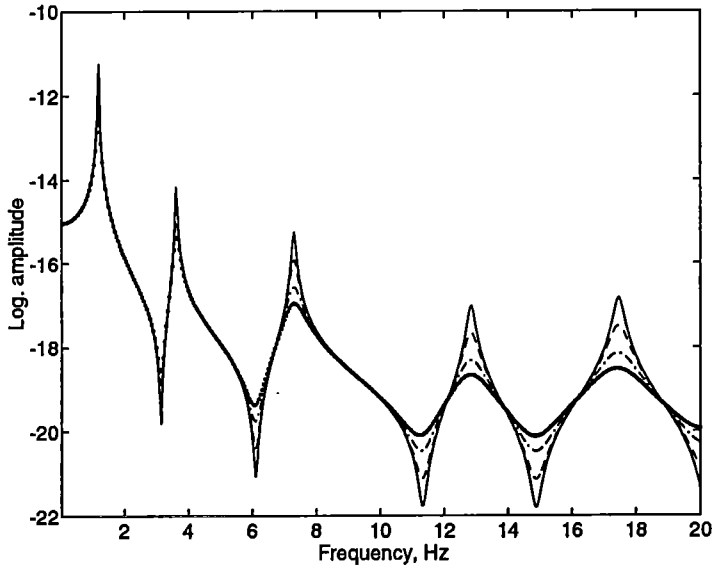

Fig.3.3 : Frequency responses with different damping
—: $k_\gamma = 0.5$; - -: $k_\gamma = 1.0$; -.-.: $k_\gamma = 2$; ....: $k_\gamma = 3$

(3) Time domain response

Fig.3.4 shows the down hole bit axial responses under sine and triangular excitations, respectively. For comparison, the responses obtained by the finite element model, i.e. Samcef software (Samtech, 1994) are also shown. In the IFFT, 4096 points and frequency step

$\Delta f = 0.05$ Hz are used. In this figure, both IDSM and FEM use frequency-independent damping ($\gamma = 100 Ns/m$) because in the FEM model it is difficult to deal with frequency-dependent damping. It is seen that the results obtained by the two methods agree very well. However, the CPU time needed by the present method is greatly reduced.

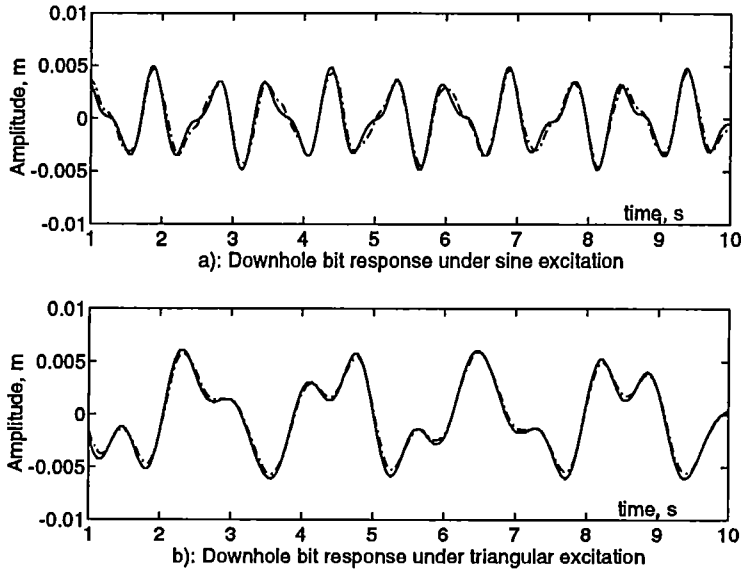

Fig.3.4: Down hole bit axial response under two different excitations
——: IDSM with IFFT; -.-.-.: HHT integration

3.2.6. Identification of dynamic bit axial force and motion

During the drilling, it is very difficult or expensive to measure directly the down hole bit forces and motions. In this section, we propose a method to identify the down hole bit axial and torsional forces and responses using the surface measurements based on the IDSM.

(1) Modeling procedure

Because the measurements are performed often at the surface, it is necessary to establish the model with the coordinates at the surface and at the bit as the generalized coordinates. To this end, following steps are used:

Step 1: The whole drillstring is divided into two substructures as shown in Fig.3.1b. Substructure 1 is further subdivided into four elements (1 spring-damper element, 1 lumped mass element and 2 beam elements). Substructure 2 is subdivided into five beam elements.

Step 2: The element dynamic stiffness matrices are transformed into element transfer matrices using equation (2.16). The global transfer matrices for each substructure, $[T_s^1]$ and $[T_s^2]$, are obtained by multiplying all the element transfer matrices.

For substructure 1: $[T_s^1] = [T_4][T_3][T_2][T_1]$

For substructure 2: $[T_s^2] = [T_9][T_8]...[T_5]$

The global dynamic stiffness matrices for each substructure, $[D_s^1]$ and $[D_s^2]$, are obtained by rearranging the matrices $[T_s^1]$ and $[T_s^2]$ using equation (2.15).

Step 3: The global dynamic stiffness matrix $[D_g]$ for the whole drillstring may be assembled from $[D_s^1]$ and $[D_s^2]$ by applying the standard assembly procedure of the finite element method. It is noted that the unrestrained global dynamic stiffness matrix has 3 x 3 dimension in this case. After introducing the boundary conditions at the topside, one finally obtains the dynamic equilibrium equation:

$$\begin{pmatrix} F_m \\ F_b \end{pmatrix} = [D_g^r(\omega)]_{2\times 2} \begin{pmatrix} X_m \\ X_b \end{pmatrix} \tag{3.9}$$

where subscript b and m represent respectively the bit and the measurement point, and $[D_g^r]$ is the restrained global dynamic stiffness matrix. It is of interest to point out that the force F_m and displacement X_m can be measured at the surface during drilling, therefore, the bit displacement X_b and bit force F_b can be predicted by equation (3.9).

(2) Identification principle

Equation (3.9) can be rewritten in the form

$$\begin{pmatrix} X_b(\omega) \\ F_b(\omega) \end{pmatrix} = \begin{pmatrix} A(\omega) & B(\omega) \\ C(\omega) & D(\omega) \end{pmatrix} \begin{pmatrix} X_m(\omega) \\ F_m(\omega) \end{pmatrix} \tag{3.10}$$

where $A(\omega), B(\omega), C(\omega), D(\omega)$ are scalar complex elements obtained by rearranging the matrix $[D_g^r]$.

Performing IFFT on equation (3.10) yields

$$x_b(t) = ifft[A(\omega)X_m(\omega) + B(\omega)F_m(\omega)] \tag{3.11a}$$

$$f_b(t) = ifft[C(\omega)X_m(\omega) + D(\omega)F_m(\omega)] \tag{3.11b}$$

where $x_b(t)$ and $f_b(t)$ are respectively the down hole bit axial displacement and force in the time domain. In equation (3.11), the functions $A(\omega)$, $B(\omega)$, $C(\omega)$ and $D(\omega)$ can be calculated and stored in advance because they depend only on the drillstring eigenproperties. The surface measurement force $f_m(t)$ and displacement $x_m(t)$ have to be transformed to the frequency domain by the FFT before using equation (3.11). The IFFT and FFT procedures are extremely fast, therefore the real time bit motion and force, $x_b(t)$ and $f_b(t)$, may be identified while drilling.

In order to compare the results obtained by the present method with those obtained by the finite element method (Samcef,1994), the frequency-independent damping is considered here. The damping force per unit length, γ, is taken as 100 Ns/m according to Aarrestad (1986). However, the damping mechanism in the drillstring is usually frequency-dependent. The

frequency-dependent damping can easily be taken into account in the analysis without any difficulty because both the dynamic stiffness matrix and the transfer matrix are frequency-dependent.

(3) Identification examples

Fig.3.5 and Fig.3.6 depict the predicted dynamic bit axial displacement and force using the IDSM-based method.

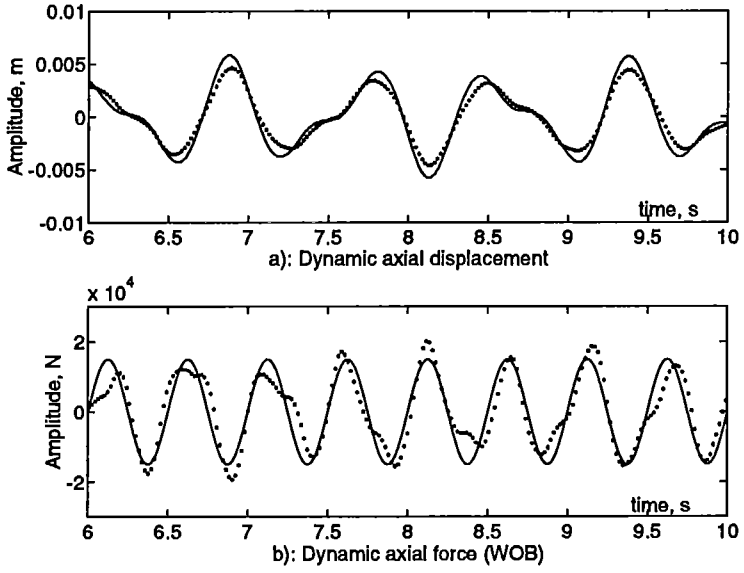

Fig.3.5: Identified dynamic down hole bit axial displacement and force
——: true value; .....: predicted

The assumed bit exciting forces (true values in the figures) are sine (Fig.3.5) and triangular (Fig.3.6) forces, respectively. They are also shown in the figure. The displacement and force at the surface measurement point are first calculated by the Mecano software using the HHT technique. From the figure, it is seen that both the bit displacement and bit force are predicted with satisfactory accuracy. The difference between the true and predicted values may be explained as follows. In the IDSM-based method, the input force and response at surface measurement are actually calculated by using Mecano software (Samtech, 1994). As will be pointed out in chapter 6, the beam element in Mecano is nonlinear. Therefore, nonlinear effects are taken into consideration in the responses and forces. When these values are used as the inputs of the IDSM-based linear model, the outputs must have errors. However, this will not influence the practical application of the method because in practice, the inputs of the IDSM-based linear model are measured directly during drilling.

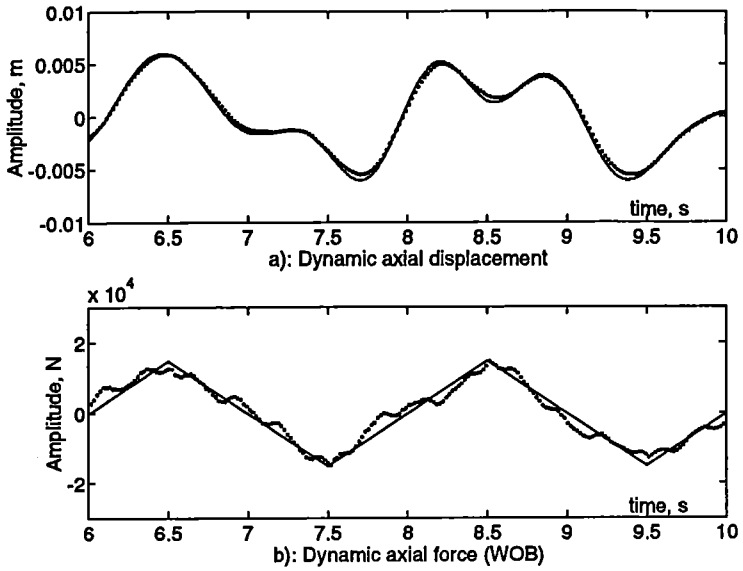

Fig.3.6: Identified dynamic down hole bit axial displacement and force
——: true value; .....: predicted

3.2.7. Shock absorber design and its effects on the axial dynamics

The purpose of the shock absorber is to reduce the dynamic loads on the drillstring, to enhance drillstring and bit life and to increase penetration rates by minimizing the shock and vibration experienced by the drillstring and the bit during drilling operations.

Like most of the dynamic absorbers, the shock absorber for drillstring is designed so that one of the natural frequencies (usually the first one) is detuned from a drill bit excitation frequency by choosing appropriately the stiffness constant. Therefore, there are two issues in the design of a shock absorber for drillstring. The first issue is the design of the stiffness and damping of the shock absorber. The second issue is the placement of the shock absorber in the drillstring. Usually, the shock absorber is placed near the bit as close as possible because the largest dynamic forces occur at the bit (Dareing, 1984, Vandiver et al, 1993).

The determination of the stiffness and the damping of a shock absorber is affected by many factors which include well depth, rock type, BHA design, bit type, RPM, WOB and so on. For example, softer springs are usually required with roller bits than with diamond or PDC bits due to the lower vibration frequencies and larger displacements with roller bits.

Although the use of shock absorber is common in practice, the design of the shock absorber and the implementation in the drillstring are often based mainly on the experience of the designer or on some simple models (for example, Kreisle and Vance, 1970). Only recently, Lee (1991) has investigated the design of a shock absorber based on the transfer matrix model.

In this section, the design of the shock absorber and its effect on the axial dynamics of the drillstring is studied based on the IDSM model. Because the largest dynamic force often occur at the bit, we are concerned with the effect of the absorber on the bit vibrations. Therefore, the entire drillstring is reduced exactly to a SDOF with the bit displacement as the generalized coordinate. The model procedure is exactly the same as described in section 3.2.4, except that the shock absorber is taken into account here. The consideration of the shock absorber does not increase the dimension of the global matrix. As shown in Fig.3.7, the shock absorber is directly placed above the bit.

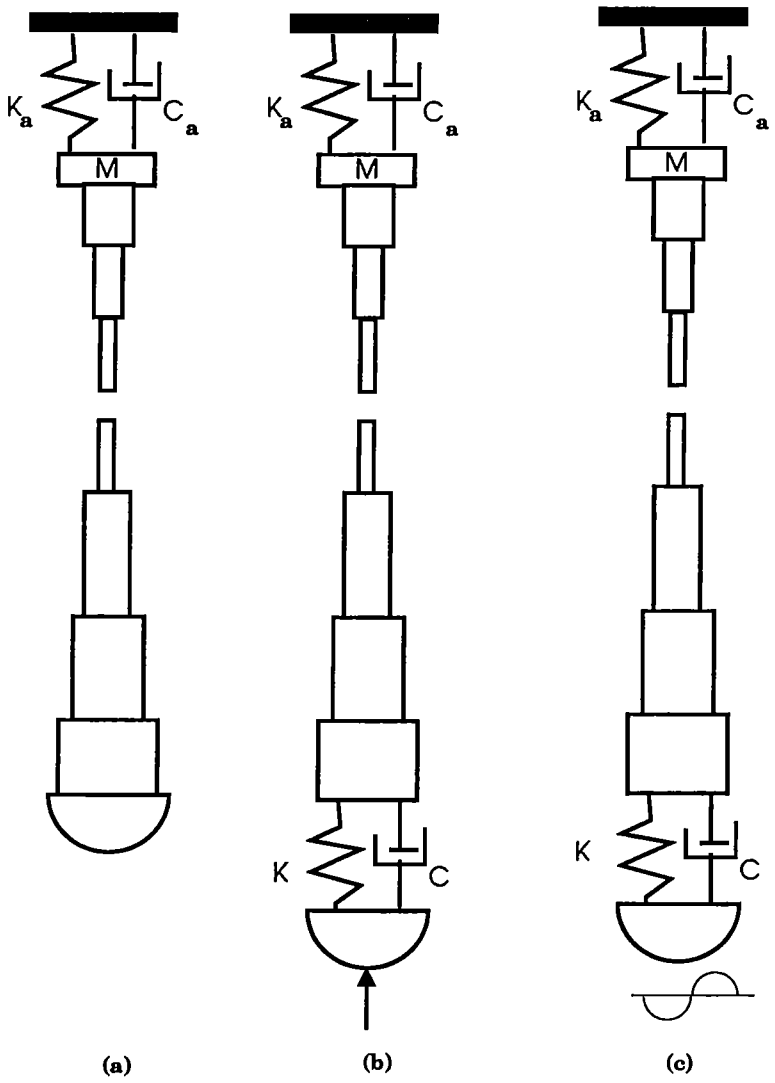

Fig.3.7: Drillstring with and without shock absorber
(a): Without absorber; (b): Constant bit force; (c): Constant bit displacement.

Two cases are analyzed. The first case studies the influence of the shock absorber on the bit amplitude. The second case considers the influence of the shock absorber on the bit dynamic force. Three types of shock absorbers are studied, their parameters are:

Sub No.1: $K_1 = 80000\ lb/inch$ and $C_1 = 800\ Ns/m$

Sub No.2: $K_2 = 50000\ lb/inch$ and $C_2 = 500\ Ns/m$

Sub No.3: $K_3 = 30000\ lb/inch$ and $C_3 = 300\ Ns/m$

Case 1: Influence on the bit displacement

In this case we are interested in the influence of the shock absorber on the bit axial displacement. Therefore, the transfer function with a constant force input at the bit is calculated based on the IDSM model. The predicted peaks represent the resonances of the BHA with a free boundary condition at the bit as shown in Fig.3.7b.

Fig.3.8 depicts the transfer functions under the condition of three types of shock absorber. From the figure, it is seen that (1) The first eigenmode dominates the response, any kind of shock absorber has almost no influence on the first mode. In other words, it is very difficult to detune the first eigenfrequency by a shock absorber. (2) At most of the frequencies, the amplitude is amplified when a shock absorber is used. In other words, the dynamic displacement at the bit is increased due to the shock absorber. The softer is the spring of the absorber, the larger is the amplification factor.

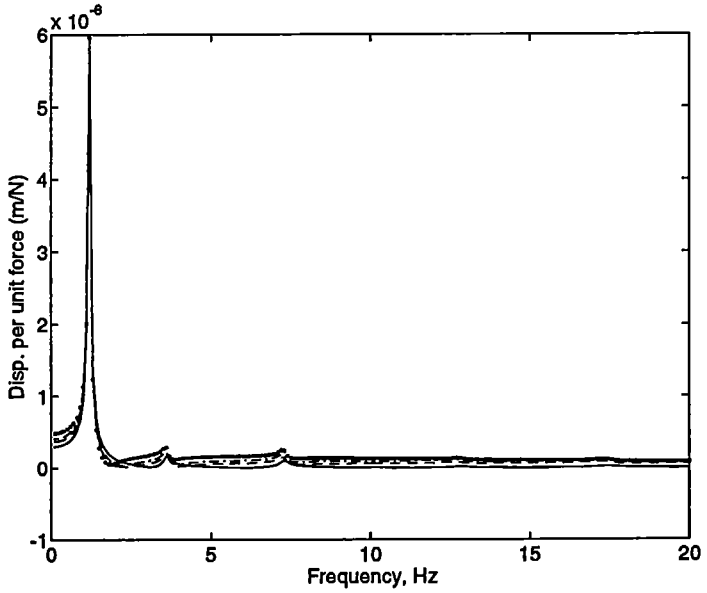

Fig.3.8: Influence of shock absorber on the frequency response at the bit
—: without sub; - -: sub type 1; -.-.: sub type 2; ....: sub type 3

Case 2: Influence on the bit dynamic force

In this case we are interested in the influence of the shock absorber on the bit dynamic force. To this end, we specify a constant displacement input at the bit and calculate the corresponding dynamic force amplitude at the bit.

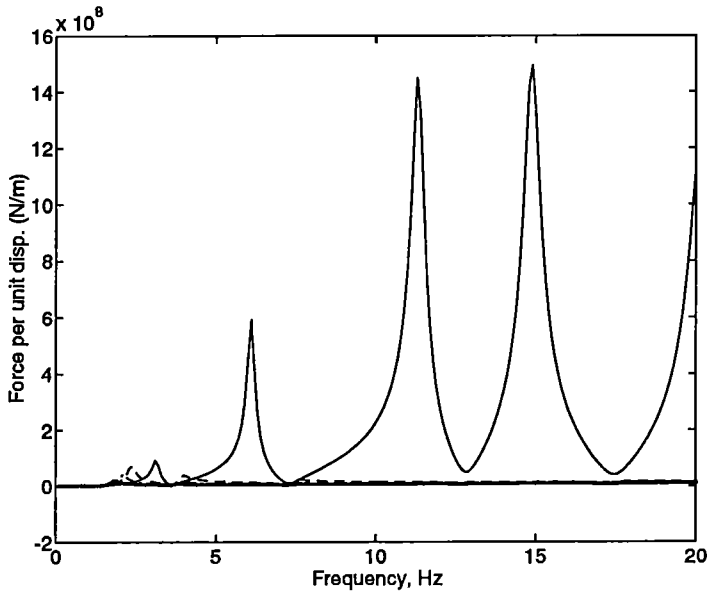

Fig.3.9: Influence of shock absorber on the dynamic force at the bit
—: without sub; - -: sub type 1; -.-.: sub type 2; ....: sub type 3

Shown in Fig.3.9 is the predicted dynamic force amplitudes when different shock absorbers are used. It is obviously seen that the dynamic force is reduced significantly by the shock absorber. The softer is the spring of the absorber, the larger is the reduced factor.

From the above analysis, it may be concluded that the shock absorber can reduce significantly the dynamic force on the bit. However, at the same time, the displacement of the bit is increased. Some of the previous work on shock absorbers, for example, Kreisle and Vance (1970) and Dareing (1984), concluded that a shock absorber reduces the dynamic bit force through detuning the natural frequency from excitation frequency. This conclusion was obtained on the basis of the simple model of the drillstring, usually only the BHA. However, from our full model, namely from bit to rig, one may conclude that it is very difficult to detune the natural frequencies of the drillstring. The shock absorber does reduce the bit dynamic force with the cost of increasing the bit displacement.

3.3 TORSIONAL VIBRATION ANALYSIS

Since the differential equation of motion for a basic element and the boundary conditions for the axial and torsional vibrations are similar, the theory described in section 3.2 may be directly expanded to torsional vibration analysis.

3.3.1. Mechanical model

The mechanical model of the drillstring for torsional vibration is exactly the same as shown in Fig.3.1a except that the equivalent lumped mass, spring and damping are replaced respectively by the equivalent polar mass moment, J_p, equivalent torsional spring constant K_t and damping constant C_t. These parameters are assumed to take the following values (Clayer, vandiver and Lee, 1990):

$$J_p=2000\ Kgm^2 \qquad K_t=400\ \text{Nm/rad} \qquad C_t=8000\ \text{Nm/s}$$

3.3.2. Basic frequency-dependent matrices

As in the case of axial vibration, there are also three kinds of basic elements in the torsional vibration of drillstring, namely the lumped torsional spring with damping, the lumped polar mass moment and the continuous beam element.

(1) Transfer matrix of a lumped torsional spring K_t with damping C_t

$$[T_t^{kc}] = \begin{pmatrix} 1 & 1/(K_t + i\omega C_t) \\ 0 & 1 \end{pmatrix} \tag{3.12}$$

where the subscripts t denotes the torsional vibration, $i = \sqrt{-1}$.

(2) Transfer matrix of a lumped polar mass moment J_p

$$[T_t^m] = \begin{pmatrix} 1 & 0 \\ -J_p\omega^2 & 1 \end{pmatrix} \tag{3.13}$$

(3) Torsional dynamic stiffness matrix for a beam

If we replace EA by GJ, E by G, respectively in equation (3.3), we obtain the torsional dynamic stiffness matrix for a beam element.

3.3.3. Free torsional vibration

(1) Dynamic model

For the free vibration analysis, the drillstring system can be reduced exactly to an equivalent single dof model with the bit angular displacement as the generalized coordinate. The modeling procedure for torsional vibration is exactly the same as in the case of axial vibration. One can also obtain the dynamic equilibrium equation in the form:

$$M_t^b = d_t^g(\omega)\theta_t^b \tag{3.14}$$

where M_t^b and θ_t^b represent the torque and the torsional displacement at the bit, $d_t^g(\omega)$ is restrained dynamic stiffness matrix. The superscript b refers to the bit and the subscript t denotes the torsional vibration.

Based on the restrained dynamic stiffness matrix $d_g^t(\omega)$, the free and forced vibrations of drillstring may be analyzed.

(2) Natural-frequencies

Table 3.3 gives the first eight undamped torsional natural frequencies predicted by the present model and by FE model. In the FE model, 40 elements (Samcef Software, beam element type 1) are used.

Table 3.3: Torsional eigenfrequencies (Hz) predicted by IDSM and FEM

Mode	ω_1	ω_2	ω_3	ω_4	ω_5	ω_6	ω_7
IDSM	0.0645	0.715	3.979	7.615	10.495	13.287	15.848
FEM	0.0645	0.734	4.097	7.863	10.859	13.775	16.555

Fig.3.10 depicts the transfer function at the bit predicted by the present model (equation 3.14).

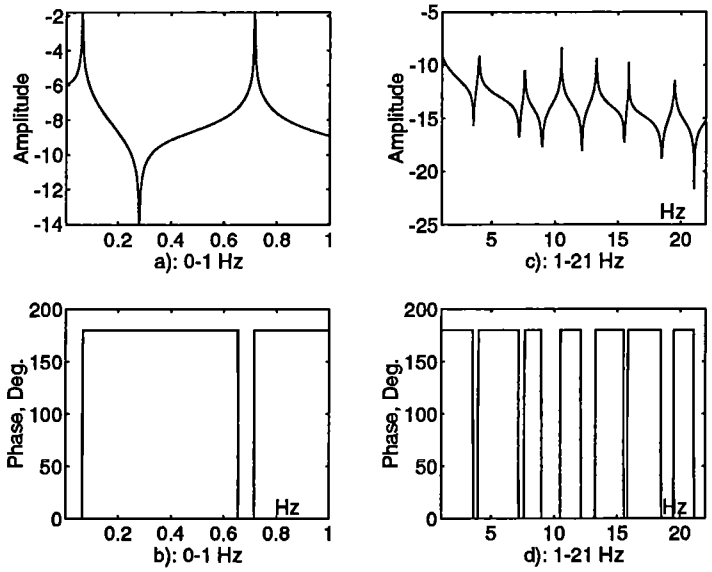

Fig.3.10: Transfer function predicted by the model

From Tab.3.3, it is seen that the torsional natural frequencies are much lower than the axial natural frequencies. It means that the torsional degree of freedom of a drillstring has a low associated stiffness and a relatively high inertia. It is found that frequency-dependent damping is small for low frequency, therefore, high torsional vibration amplitude may easily be achieved.

The forced responses, the estimations of down-hole bit torque and angular motion as well as the design of torsional shock absorber (if necessary) can also be investigated. The procedures developed for axial vibration can be followed for the parallel studies of torsional vibration.

3.4 CONCLUSIONS

As pointed out in the introduction of this chapter, the study of linear axial and torsional vibrations of drillstring is not a new subject. The analytical model and the model based on transfer matrix are often used. The analytical model can consider only simple cases such as uniform drillstring. Although the transfer matrix based model can give accurate solution for free vibration such as eigen-frequencies, mode shapes and harmonic response, the other model parameters such as modal mass, modal stiffness cannot be obtained. Another main disadvantage associated with the transfer matrix based model is that the explicit equations of motion of the original system are lost. This disadvantage makes the procedure of the estimation of down hole bit forces and motions using surface measurements very tedious because the global transfer matrix relates only the boundary ends of the original system.

In this chapter, the axial and torsional vibrations of the drillstring are studied by the IDSM developed in Chapter 2. It is demonstrated how the disadvantages of the traditional transfer matrix method are overcome by the IDSM.

Compared to the transfer matrix method and to the finite element method or the dynamic stiffness method, the IDSM has the following advantages for axial and torsional vibrations of drillstrings:

(1.) For free vibration, the whole drillstring can be exactly reduced to a single degree of freedom with the bit displacement (either axial or torsional) as the generalized coordinate. The reduced model can predict exactly the eigen-frequencies. The other modal parameters can be also calculated based on this model.

(2.) For estimation of down-hole bit forces and motions, the whole drillstring can be modeled with two degrees of freedom, one is the bit displacement and the other is the displacement of the surface measurement point. In other words, the forces and motions at the bit and at the surface measurement point are related explicitly.

(3.) The consideration of shock absorber changes neither the procedure of the analysis, nor does it change the dimension of the global matrix. This fact makes it possible to design the shock absorber based on the exact reduced model of drillstring. An important observation is made based on the exact model that it is difficult to detune the eigenfrequency (especially the first one) through the use of shock absorber for the drillstring. The shock absorber reduces the bit dynamic force with the cost of increasing the bit dynamic displacement.

CHAPTER 4

LINEAR LATERAL VIBRATION AND BUCKLING OF BHAS

4.1. INTRODUCTION

The lateral vibration of drillstring has become a project of investigation later than axial and torsional vibration because it does not appear uphole (Chin, 1988, Shyu, 1990). Lateral vibration can only be observed downhole because the travelling speed of lateral waves being low, it takes many wave lengths for the vibration to reach the top of the drillstring (Dareing, 1983, Wolf et al, 1985). The lateral motion is thus completely damped out by wall contact losses and by structural and fluid damping along the drillstring. However, downhole measurements have given clear evidence that severe lateral vibrations occur in the BHA (Deily and Dareing, 1968, Vandiver et al, 1988, Wolf et al, 1985).

For the lateral vibration analysis, the finite element method (FEM) seems to be the most powerful and versatile. However, as pointed out in chapter 2 and chapter 3, the FEM model requires usually a large number of degrees of freedom which limits its application to the oil-well fields.

In this chapter, the IDSM developed in chapter 2 is directly applied to the lateral vibration and buckling analysis of drillstring. Based on the consistent equations of motion of rotating Timoshenko shafts subject to axial loads (Choi, Pierre and Ulsoy, 1992) and following the similar procedure used by Lee et al (1991), an exact transfer matrix is developed which includes the effects of rotary inertia, gyroscopic, transverse shear and axial loads. The axial load may either be constant or distributed along the shaft. The transfer matrix for a curved beam is also derived. Using the IDSM, the BHA system can be modeled with arbitrary selected degrees of freedom. The free and forced vibrations for a typical BHA are studied in detail. The buckling loads for different BHA systems are calculated.

4.2. LINEAR LATERAL VIBRATION

4.2.1. Mechanical Model of BHA

The BHA (Bottom Hole Assembly) used for the drilling of oil and gas wells is often made up of different sizes of drill collars, stabilizers and down hole tools. It is usually subject to large axial compression force (or WOB). The main purpose of drill collars is to apply force to the drill bit for penetration. Compression developed within drill collars causes them to buckle inside the wellbore and this creates side loads on the bit. It is necessary to use stabilizers to control the direction of the borehole and to increase the buckling stability. Depending on the location of the stabilizers, BHAs can be categorized as building, holding and dropping assemblies (Dareing, 1988).

The building assemblies, as shown in Fig.4.1, are used to increase hole angle or to build angle. In this assembly the stabilizers are placed so that side forces on a drill bit push the

bit upward while the bit drills ahead. The selection of a given building assembly depends on the desired curvature to be drilled.

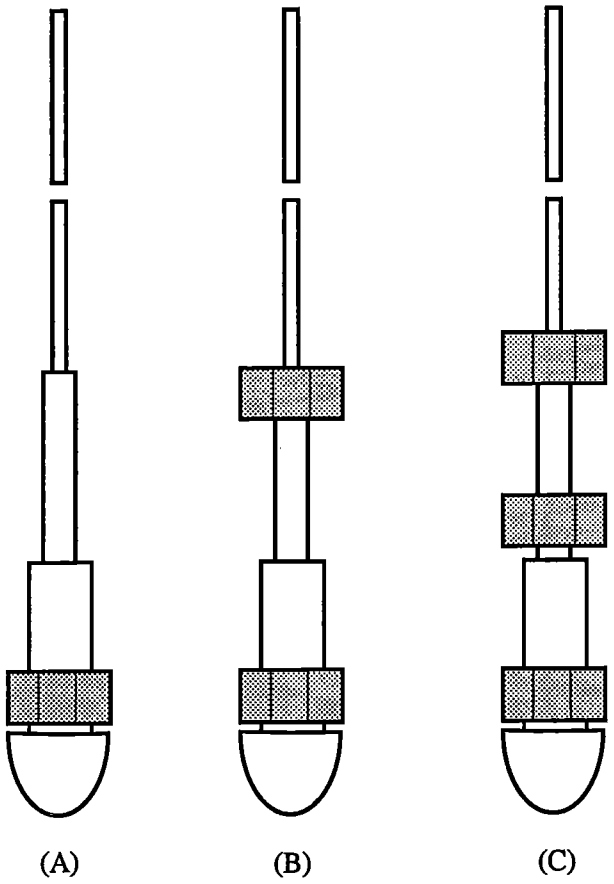

Fig.4.1: Building assemblies

The main purpose of holding assemblies is to drill straight sections of well. To this end, stabilizers are positioned within drill collars so that relatively small side forces are developed at the bit (Fig.4.2).

Unlike building and holding assemblies, dropping assemblies do not have near bit stabilizers as shown in Fig.4.3. The drill bit stands alone and is pushed downward by the weight of drill collars suspended between the bit and the first stabilizer. The dropping assembly is sometimes called pendulum assembly. This kind of assembly is used mostly for vertical wells.

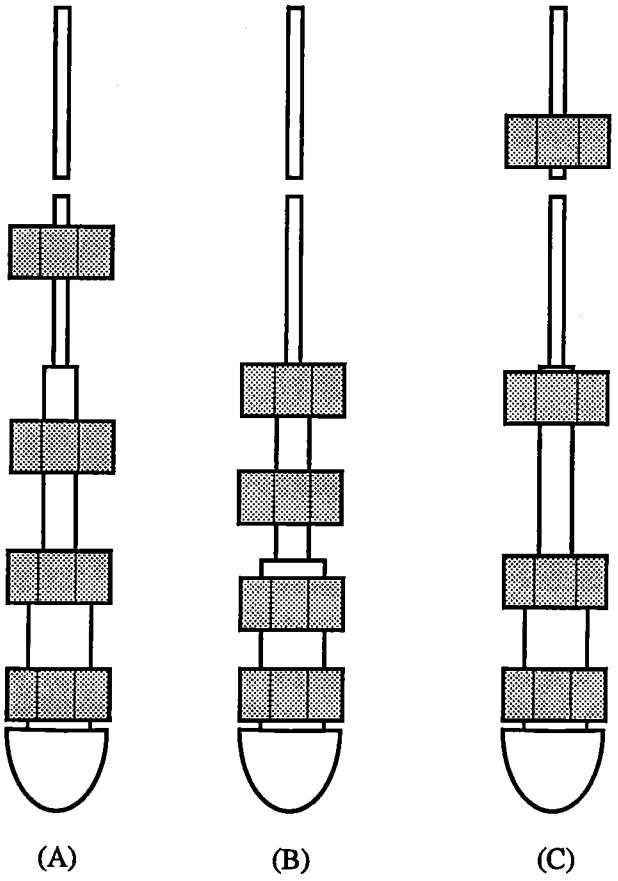

Fig.4.2: Holding assemblies

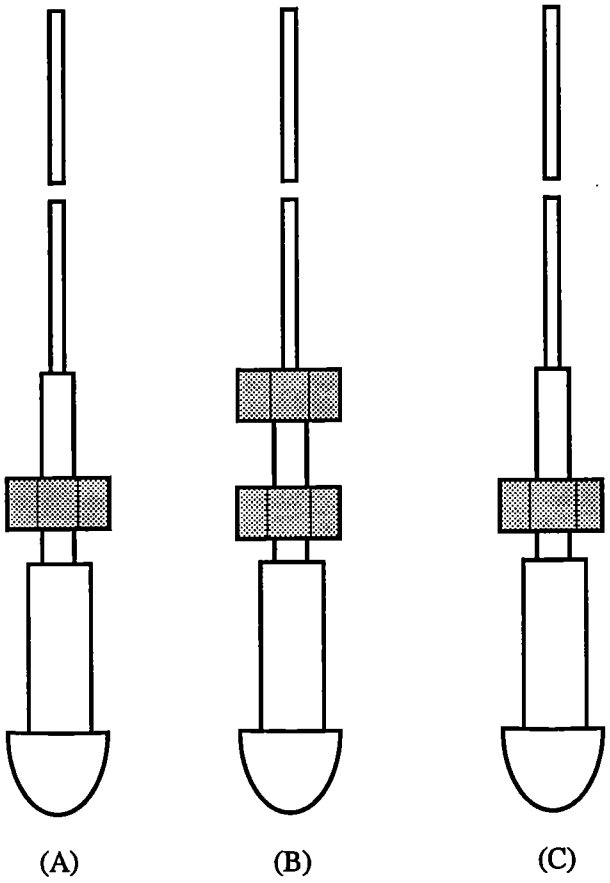

Fig.4.3: Dropping assemblies

The effects of the stabilizers on the directional drilling have been studied based on the static mechanics (Millheim, 1978a,b, 1979a,b,c,d). However, it is obvious that the placement of the stabilizers also affects the dynamic behaviors and buckling stability. These effects are studied in this chapter.

4.2.2. Exact Transfer Matrix of a Straight BHA Section

(1) Governing Equations

Let us first examine a uniform shaft subject to constant compression axial load as shown in Fig.4.4. For such a shaft, the consistent equations of motion have been derived recently using the finite strain beam theory by Choi, Pierre and Ulsoy (1992).

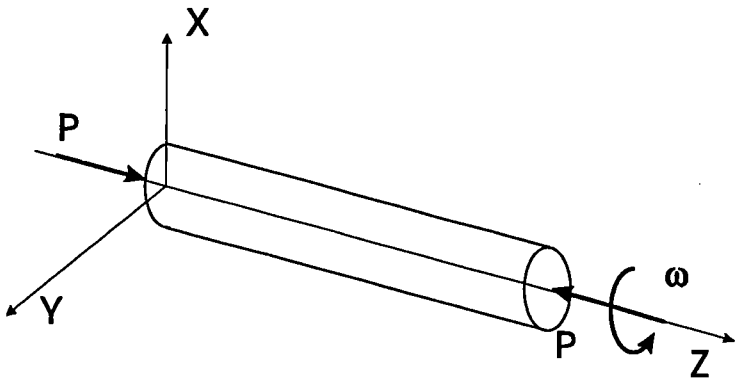

Fig. 4.4: Rotating Timoshenko shaft subject to axial load

In the XZ plane:

$$\frac{\partial^4 X}{\partial Z^4} - (\frac{\rho}{KG} + \frac{\rho}{E})\frac{\partial^4 X}{\partial Z^2 \partial t^2} + \frac{\rho^2}{KEG}\frac{\partial^4 X}{\partial t^4} + \frac{\rho A}{EI}\frac{\partial^2 X}{\partial t^2} - \frac{2\rho\omega}{E}(\frac{\partial^3 Y}{\partial Z^2 \partial t} - \frac{\rho}{KG}\frac{\partial^3 Y}{\partial t^3})$$
$$+\frac{P}{EI}(1 + \frac{P}{KAG})\frac{\partial^2 X}{\partial Z^2} + \frac{\rho P}{EIKG}\frac{\partial^2 X}{\partial t^2} - \frac{P^2}{E^2 AI}\frac{\partial^2 X}{\partial Z^2} + (-\frac{2P}{EA} - \frac{P^2}{EAKAG} + \frac{P^2}{(EA)^2})\frac{\rho A}{EI}\frac{\partial^2 X}{\partial t^2} = 0 \quad (4.1a)$$

In the YZ plane:

$$\frac{\partial^4 Y}{\partial Z^4} - (\frac{\rho}{KG} + \frac{\rho}{E})\frac{\partial^4 Y}{\partial Z^2 \partial t^2} + \frac{\rho^2}{KEG}\frac{\partial^4 Y}{\partial t^4} + \frac{\rho A}{EI}\frac{\partial^2 Y}{\partial t^2} + \frac{2\rho\omega}{E}(\frac{\partial^3 X}{\partial Z^2 \partial t} - \frac{\rho}{KG}\frac{\partial^3 X}{\partial t^3})$$
$$+\frac{P}{EI}(1 + \frac{P}{KAG})\frac{\partial^2 Y}{\partial Z^2} + \frac{\rho P}{EIKG}\frac{\partial^2 Y}{\partial t^2} - \frac{P^2}{E^2 AI}\frac{\partial^2 Y}{\partial Z^2} + (-\frac{2P}{EA} - \frac{P^2}{EAKAG} + \frac{P^2}{(EA)^2})\frac{\rho A}{EI}\frac{\partial^2 Y}{\partial t^2} = 0 \quad (4.1b)$$

with the following quantities: E is the Young's Modulus, G the shear modulus, K the shear factor, ρ the mass density, A the cross section area, ω the rotation speed of the drillstring and P the axial compression load.

It is noted that not only the gyroscopic moments but also the axial load terms are consistently captured in the above equations.

(2) Exact Transfer Matrix

The steady-state solutions of equation (4.1) may be represented in the form

$$\begin{aligned} X(Z,t) &= X_s(Z)\sin\Omega t \\ Y(Z,t) &= Y_c(Z)\cos\Omega t \end{aligned} \quad (4.2)$$

where the subscripts s and c stand for the sine and cosine components, respectively.

where Ω is the whirling angular frequency.

Substituting equations (4.2) into (4.1) would result in two homogeneous equations as follows:

In the XZ plane

$$\frac{d^4X_s}{dZ^4}+(\frac{\rho\Omega^2}{E}+\frac{\rho\Omega^2}{KG})\frac{d^2X_s}{dZ^2}+(\frac{\rho^2\Omega^4}{KGE}-\frac{\rho A\Omega^2}{EI})X_s+\frac{2\rho\omega\Omega}{E}\frac{d^2Y_c}{dZ^2}+\frac{2\rho^2\omega\Omega^3}{KGE}Y_c$$
$$+\frac{P}{EI}(1+\frac{P}{KAG})\frac{d^2X_s}{dZ^2}-\frac{\rho P\Omega^2}{EIKG}X_s-\frac{P^2}{E^2AI}\frac{d^2X_s}{dZ^2}-\frac{\rho A\Omega^2}{EI}(-\frac{2P}{EA}-\frac{P^2}{EAKAG}+\frac{P^2}{(EA)^2})X_s=0 \quad (4.3a)$$

In the YZ plane

$$\frac{d^4Y_c}{dZ^4}+(\frac{\rho\Omega^2}{E}+\frac{\rho\Omega^2}{KG})\frac{d^2Y_c}{dZ^2}+(\frac{\rho^2\Omega^4}{KGE}-\frac{\rho A\Omega^2}{EI})Y_c+\frac{2\rho\omega\Omega}{E}\frac{d^2X_s}{dZ^2}+\frac{2\rho^2\omega\Omega^3}{KGE}X_s$$
$$+\frac{P}{EI}(1+\frac{P}{KAG})\frac{d^2Y_c}{dZ^2}-\frac{\rho P\Omega^2}{EIKG}Y_c+\frac{P^2}{E^2AI}\frac{d^2Y_c}{dZ^2}-\frac{\rho A\Omega^2}{EI}(-\frac{2P}{EA}-\frac{P^2}{EAKAG}+\frac{P^2}{(EA)^2})Y_c=0 \quad (4.3b)$$

The solutions of equations (4.3) take the form

$$\begin{aligned} X_s &= U_s e^{\lambda Z} \\ Y_c &= V_c e^{\lambda Z} \end{aligned} \quad (4.4)$$

where U_s, V_c are arbitrary real constants and λ are the roots of the determinant equation

$$\begin{vmatrix} \lambda^4+f\lambda^2+g & h\lambda^2+k \\ h\lambda^2+k & \lambda^4+f\lambda^2+g \end{vmatrix}=0 \quad (4.5a)$$

with

$$f=\frac{\rho\Omega^2}{E}+\frac{\rho\Omega^2}{KG}+\frac{P}{EI}+\frac{P^2}{KAGEI}-\frac{P^2}{E^2AI}$$

$$g=\frac{\rho^2\Omega^4}{KGE}-\frac{\rho A\Omega^2}{EI}-\frac{\rho P\Omega^2}{EIKG}+\frac{\rho A}{EI}\frac{2P\Omega^2}{EA}+\frac{\rho P^2\Omega^2}{E^2IAKG}-\frac{P^2\rho\Omega^2}{E^3AI}$$

$$h=\frac{2\rho\omega\Omega}{E}, \quad k=\frac{2\rho^2\omega\Omega^3}{KGE}$$

Equation (4.5a) is equivalent to the following two equations:

$$\lambda^4-b_1\lambda^2+c_1=0 \quad (4.5b)$$

$$\lambda^4-b_2\lambda^2+c_2=0 \quad (4.5c)$$

where $b_1=h-f, \quad c_1=g-k, \quad b_2=-(f+h), \quad c_2=g+k.$

Let us consider first equation (4.5b). The following two cases are considered.

Case 1: $\sqrt{b_1^2 - 4c_1} > b_1$. This is true for $c_1 < 0$. Physically, this case would correspond to lower frequency vibrations. Numerical investigation has shown that this is the case for most drill strings. The solutions for λ are given by:

$$\lambda = \pm\lambda_1, \pm i\lambda_2$$

in which

$$\lambda_1 = \sqrt{\frac{b_1 + \sqrt{b_1^2 - 4c_1}}{2}}$$

$$\lambda_2 = \sqrt{\frac{-b_1 + \sqrt{b_1^2 - 4c_1}}{2}}$$

Case 2: $\sqrt{b_1^2 - 4c_1} < b_1$. This is true for $b_1 > 0$, and $c_1 > 0$. Physically, this case would correspond to higher frequency vibrations. The solutions of equation (5b) in this case are given by:

$$\lambda = \pm\lambda_1, \pm\lambda_2$$

in which

$$\lambda_1 = \sqrt{\frac{b_1 + \sqrt{b_1^2 - 4c_1}}{2}}$$

$$\lambda_2 = \sqrt{\frac{b_1 - \sqrt{b_1^2 - 4c_1}}{2}}$$

Numerical investigation has shown that this case may happen only at very high frequency. This is not the case of drillstring applications.

Equation (4.5c) can be similarly considered following the above discussions.

Combining the solutions of equations (4.5b) and (4.5c), the roots of the characteristic function of equation (4.5a) may take the form:

$$\lambda = \pm\lambda_a, \pm i\lambda_b, \pm\lambda_c, \pm i\lambda_d$$

for a constant value of ω (see also Lee, Kang, Liu, 1993, Zu and Han, 1992).

In the same way as the displacements, the slopes, moments and shear forces may be defined as follows:

$$\begin{aligned}
\alpha(Z,t) &= \alpha_s(Z)\sin\Omega t \\
\beta(Z,t) &= \beta_c(Z)\cos\Omega t \\
M_x(Z,t) &= M_{xs}(Z)\sin\Omega t \\
M_y(Z,t) &= M_{yc}(Z)\cos\Omega t \\
Q_x(Z,t) &= Q_{xs}(Z)\sin\Omega t \\
Q_y(Z,t) &= Q_{yc}(Z)\cos\Omega t
\end{aligned} \tag{4.6}$$

Let us define the state vector by:

$$S = [X_s, Y_c, \alpha_s, \beta_c, M_{xs}, M_{yc}, Q_{xs}, Q_{yc}]^t$$

The state vector on the right hand side of the shaft is related to the state vector on the left hand side by the following matrix equation:

$$S_i = [T]S_{i-1} \tag{4.7}$$

where $[T]$ is the transfer matrix of a shaft element with dimension 8×8 and

$$[T] = [A]^{-1}[N][A] \tag{4.8}$$

The matrices [A] and [N] are given in Appendix B.

4.2.3. Exact Transfer Matrix of a Curved BHA Section

In actual drilling, the curvature of the drillstring is very common due to the combined effects of gravity, axial force, eccentricity of the collars and the non homogeneity of the formation.

(1). Equations of Motion

Fig.4.5 shows a circularly in-plane curved shaft and coordinate system. A local coordinate system, XZ , is used. The axis Z is tangent to the curved axis of the shaft. The following assumptions are made: (1) The material is elastic and homogeneous; (2) The local cross-sectional dimensions are small compared to the local radius of curvature; (3) Every cross section is rigid in its own plane; (4) Transverse displacements in the cross section plane are much larger than the longitudinal displacement, the condition of inextensibility $\partial Z/\partial X + X/R = 0$ is therefore hold.

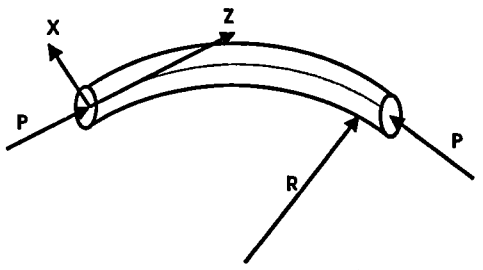

Fig.4.5: Curved beam subject to axial force

According to the Hamilton's principle, a set of governing differential equations of motion for the curved thin-walled beam without shear deformation has been developed by Yang and

Kuo (1986). Following the same procedure adopted by Yang and Kuo (1986) and Leung and Zhou (1993), neglecting the terms higher than the second order of smallness, and taking the shear deflection and rotary inertia into consideration, the equation of motion is finally obtained as follows:

$$\frac{\partial^4 X}{\partial Z^4} - (\frac{\rho}{KG} + \frac{\rho}{E})\frac{\partial^4 X}{\partial Z^2 \partial t^2} + \frac{\rho^2}{KEG}\frac{\partial^4 X}{\partial t^4} + (\frac{\rho A}{EI} - \frac{2\rho}{ER^2})\frac{\partial^2 X}{\partial t^2}$$

$$+\frac{P}{EI}(1 + \frac{P}{KAG})\frac{\partial^2 X}{\partial Z^2} + \frac{2}{R^2}\frac{\partial^2 X}{\partial Z^2} + (\frac{1}{R^4} + \frac{P}{EIR^2})X = 0 \tag{4.9}$$

In which

E—Young's Modulus; G—Shear Modulus; K—Shear factor; ρ—mass density; A—Cross section area; P—Axial compression load; R—Radius of the curvature.

It is noted that the effects of curvature, axial load, shear deflection and rotatory inertia are included in the above equation in an explicit manner.

It is seen that equation (4.9) is similar to equation (4.1). Therefore, using the same procedure described in the above section, the transfer matrix can also be derived. The obtained transfer matrix for the curved beam is given in Appendix C.

4.2.4. Transfer Matrices of Stabilizer and Bit

(1) Transfer matrix of stabilizer

The stabilizer may be modeled as a spring support as shown in Fig.4.6. The transfer matrix $[T_{st}]$ for such a support may be directly written as if the couple terms are not considered:

$$[T_{st}] = \begin{pmatrix} 1 & 0 & 0 & 0 & 0 & 0 & 0 \\ 0 & 1 & 0 & 0 & 0 & 0 & 0 \\ 0 & 0 & 1 & 0 & 0 & 0 & 0 \\ 0 & 0 & 0 & 1 & 0 & 0 & 0 \\ 0 & 0 & 0 & 0 & 1 & 0 & 0 \\ 0 & 0 & 0 & 0 & 0 & 1 & 0 \\ K_{xx} + i\Omega C_{xx} & 0 & 0 & 0 & 0 & 0 & 1 \\ 0 & K_{yy} + i\Omega C_{yy} & 0 & 0 & 0 & 0 & 0 \end{pmatrix} \tag{4.10}$$

where K_{xx}, K_{yy} are stiffnesses in X and Y directions, C_{xx} and C_{yy} are the damping constants, Ω is whirling frequency.

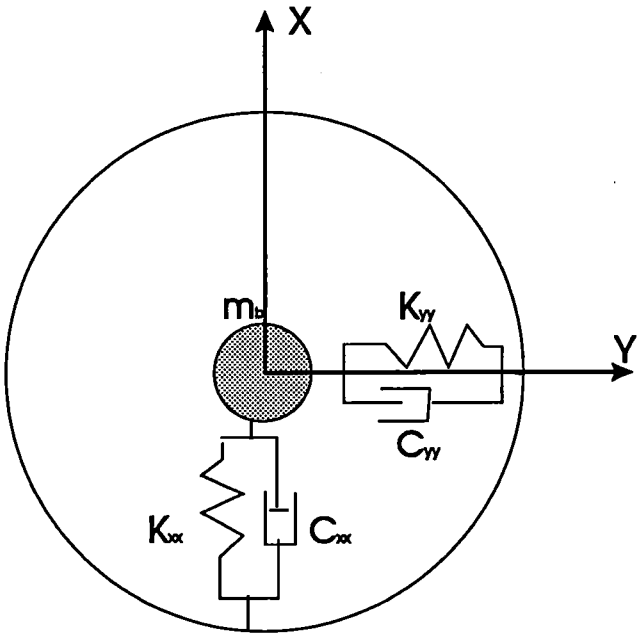

Fig.4.6: Model of a stabilizer

(2) Transfer matrix of bit

Compared to the flexibility of the BHA, the bit may be considered as a lumped mass. The transfer matrix $[T_b]$ is:

$$[T_b] = \begin{pmatrix} 1 & 0 & 0 & 0 & 0 & 0 & 0 & 0 \\ 0 & 1 & 0 & 0 & 0 & 0 & 0 & 0 \\ 0 & 0 & 1 & 0 & 0 & 0 & 0 & 0 \\ 0 & 0 & 0 & 1 & 0 & 0 & 0 & 0 \\ 0 & 0 & 0 & 0 & 1 & 0 & 0 & 0 \\ 0 & 0 & 0 & 0 & 0 & 1 & 0 & 0 \\ -M_b\Omega^2 & 0 & 0 & 0 & 0 & 0 & 1 & 0 \\ 0 & -M_b\Omega^2 & 0 & 0 & 0 & 0 & 0 & 1 \end{pmatrix} \tag{4.11}$$

where M_b is the lumped mass of the bit.

4.2.5. Mud-drillstring interaction

The drilling fluid confined between the drillstring and the hole-wall is submitted to a highly complicated motion. When lateral vibration occurs, the confined fluid is squeezed so that a complicated flow takes place and interacts with the structure (Rixen, 1992).

It is obvious that the mud-drillstring interaction is a very complicated phenomenon. However, under some conditions, the interaction effect may be represented by an added mass and a fluid damping coefficient (Chen, Wambsganss and Jendrzejczy, 1976, Allen, 1987, Jansen,

1990). According to Allen (1987), the effective density of the string is:

$$\rho_{eff} = \rho + \rho_{mud}\frac{(C_m A_o + A_i)}{(A_o - A_i)} \tag{4.12}$$

where ρ_{mud} is the mud density, C_m is the added mass coefficient (usually equal to 1), A_o and A_i are areas defined by the outer and inner diameters of the drillstring, respectively. It can be seen that the added mass increases when clearance decreases because the fluid is more squeezed. If the mud-drillstring interaction is taken into account, the mass density ρ in equation (4.1) should be replaced by the effective density ρ_{eff} given in equation (4.12). The added fluid damping is very complicated to estimate. It is usually taken as an equivalent damping value.

4.2.6. Modeling of boundary conditions

In lateral vibration analysis, the drill pipes above the BHA are usually not modeled. It is because the BHA dominates the lateral vibration (Shyu, 1989). In practice, there are three kinds of boundary conditions for the upper end of the BHA. The first one considers the contribution of the pipe above the BHA (Rixen, 1992a). This contribution is equivalent to lateral translation and bending springs (Fig.4.7a). However, the equivalent springs are difficult to determine. The second one is to fix the bending degrees of freedom and to release the lateral displacement (Fig.4.7b). The third one may be the simplest which fixes all the degrees of freedom at the upper end of the BHA (Fig.4.7c).

On the other hand, the boundary conditions at the bit may be modeled either as a spring (Fig.4.7d) or as free (Fig.4.7e). The spring model may not represent the reality if the bit is whirling and creates a over gauged hole. In this case, it might be more accurate to consider the bit as free (Rixen, 1992a).

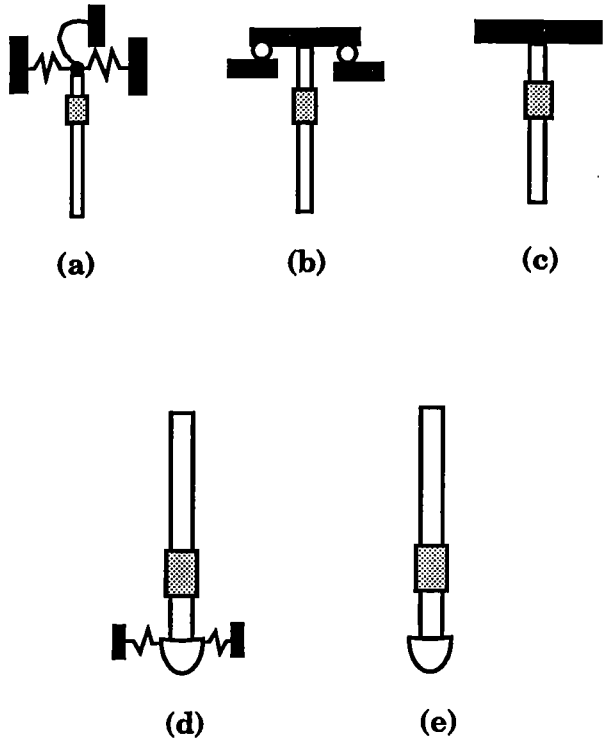

Fig.4.7: Upper and bottom boundary conditions of BHA

4.2.7. Free Lateral Vibration

(1) Dynamic model

Fig.4.8 shows a typical BHA system used for simulation. The geometry is listed in table 4.1.

Table 4.1: Geometry of the BHA of Fig. 4.8 (meters)

Section Nr.	**1**	**2**	**3**	**4**	**5**
Out Radius	0.085725	0.085725	0.085725	0.1016	0.1016
Inner Radius	0.071438	0.071438	0.071438	0.071438	0.071438
Length	3.81	19.812	10.67	10.67	6.238

The stiffness of the stabilizer is taken as $10^6 N/m$.

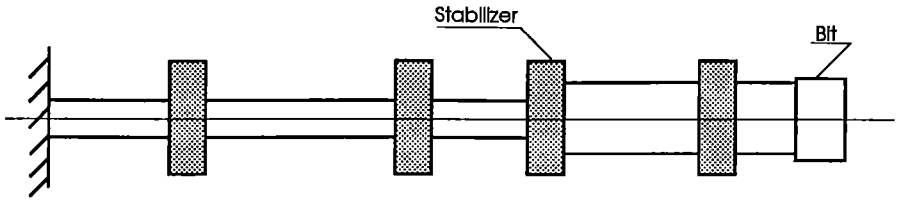

Fig.4.8: A typical BHA system

The upper end (left end in Fig.4.8) is modeled as a clamped end and the bit is assumed free. Because the lateral vibration can only be measured by the MWD system which is placed near the bit, in order to explain the measurement data, it is reasonable to model the BHA with the bit lateral displacements as the generalized coordinates. The following steps are needed according to the principle of the IDSM developed in Chapter 2:

Step 1: The whole BHA is divided into 10 elements (4 stabilizer, 5 shaft elements and 1 mass element) according to the discontinuities and the locations of the stabilizers. A uniform section can be taken as long as possible due to the exact element transfer matrix. Because the internal nodal coordinates are not needed, the BHA is treated as one substructure. The transfer matrix of this substructure is

$$[T_s] = [T_{10}][T_9].....[T_1] \tag{4.13}$$

where subscript s denotes substructure.

Step 2: The global dynamic stiffness matrix $[D_s]$ can be obtained from $[T_s]$ using equation (2.19). Note that the dimension of $[D_s]$ is 8×8 in this case. After introducing the boundary conditions at the left end, one finally obtains the dynamic equilibrium equation:

$$\begin{pmatrix} F_x^b \\ F_y^b \\ M_x^b \\ M_y^b \end{pmatrix} = [D_g(\omega, \Omega, P)]_{4\times4} \begin{pmatrix} X^b \\ Y^b \\ \theta_x^b \\ \theta_y^b \end{pmatrix} \tag{4.14}$$

where $[D_g(\omega, \Omega, P)]$ is the restrained global dynamic stiffness matrix which is a function of rotation speed ω, whirling speed Ω and axial force P, F_x^b, F_y^b, M_x^b and M_y^b are the forces and moments acting on the bit, X^b, Y^b, θ_x^b and θ_y^b are the corresponding displacements and rotation angle of the bit. The superscript b represents the bit, subscript x and y denote the directions in the coordinate system.

Step 3: The unwanted rotational degrees of freedom, θ_x^b, θ_y^b, may be eliminated by solving the linear set of equation (4.14) and setting their corresponding moments M_x^b, M_y^b to zero. Finally, we obtain:

$$\begin{pmatrix} F_x^b \\ F_y^b \end{pmatrix} = [D_2(\omega, \Omega, P)] \begin{pmatrix} X^b \\ Y^b \end{pmatrix} \tag{4.15}$$

It is important to note that the system shown in Fig.4.8 is exactly reduced to two degrees of freedom with displacements X^b and Y^b at the bit as generalized coordinates for a given

frequency and rotation speed. It is also noted that the reduced dynamic stiffness matrix $[D_2(\omega, \Omega, P)]$ of the system is both frequency and rotation speed dependent due to the gyroscopic effect. The frequency response function (FRF) matrix $[H(\omega, \Omega, P]) = [D_2(\omega, \Omega, P)]^{-1}$ determines completely the dynamic behavior of the system.

Step 4: The other frequency-dependent matrices such as mass matrix, gyroscopic matrix and stiffness matrix as well as the other modal parameters can be obtained from the dynamic stiffness matrix $[D_2]$ (see Chapter 2, 2.4.6).

(2) Eigen-frequency analysis

(a) Influence of rotation speed

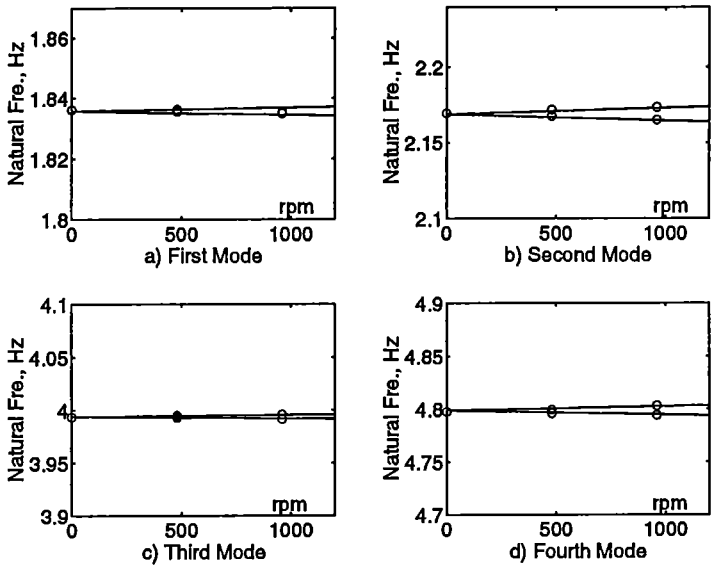

Fig.4.9: Natural frequencies versus rotating speed of the BHA
——: Present method; oooooo: FEM (Samcef)

Fig.4.9 depicts the first four natural frequencies predicted by the model versus the rotation speed. For comparison, the FEM results calculated by samcef software (Samtech, 1994) are also given. It is seen that (1) The results predicted by the model agree well with those predicted by the FEM model. (2) As long as the rotation speed Ω is small enough (usually 50-400 rpm in practice), the gyroscopic effects may be negligible. Under this condition, the rotating drillstring may be studied as a static beam.

(b) Influence of WOB

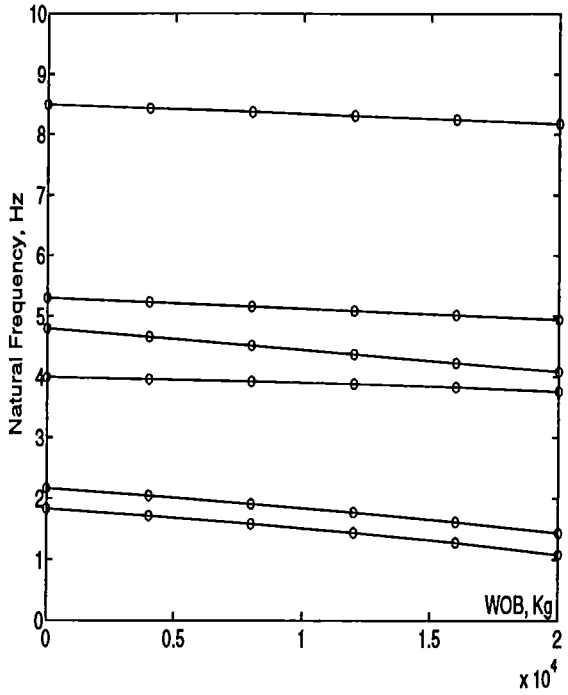

Fig.4.10: Natural frequencies versus WOB
——: Present method; oooooo: FEM (Samcef)

Fig.4.10 shows the influence of the WOB on the natural frequencies. With the increase of the WOB, the natural frequencies decrease. It is seen that the WOB decreases the first, second and third natural frequencies by about 41.7%, 35.6% and 8% respectively. Since the first three natural frequencies are usually within the range of rotation speed, the effects of WOB must be taken into account.

(c) Influence of curvature

The BHA used in the above analysis is used here. In order to describe the curvature explicitly, the degree of curvature of drillstring is described by a factor ξ which is defined as:

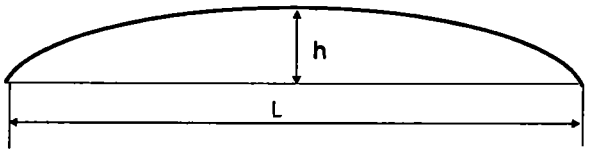

Fig.4.11: Definition of curvature

$$\xi = h/L \tag{4.17}$$

In Fig.4.11, L is the length of the BHA and the curvature takes circular form.

The transfer matrix for a curved beam subject to axial force has been derived above and is given in Appendix C. It is assumed that the stabilizer supports the BHA always in the radial direction (perpendicular to the local longitudinal axis of the curved drillstring).

Following the same procedure as described in the above section and neglecting the gyroscopic effects, the in-plane vibration of the curved BHA can be modeled by one degree of freedom system (for a given frequency) with the bit in-plane displacement X^b as the generalized coordinate.

Table 4.2: Influence of curvature on the natural frequencies (Hz)

ξ	ω_1	ω_2	ω_3	ω_4	ω_5	ω_6
0.0000	1.836	2.169	3.994	4.797	5.302	8.496
0.0437	1.835	2.169	3.993	4.796	5.302	8.494
0.0882	1.831	2.169	3.990	4.792	5.299	8.490
0.1340	1.825	2.168	3.985	4.785	5.296	8.484
0.1820	1.816	2.158	3.978	4.775	5.290	8.474
0.2332	1.805	2.147	3.970	4.762	5.284	8.462
0.2887	1.792	2.132	3.960	4.746	5.276	8.447
0.3501	1.776	2.120	3.948	4.728	5.266	8.429
0.4195	1.758	2.110	3.934	4.707	5.256	8.409
0.5000	1.739	2.100	3.920	4.683	5.245	8.386

Table 4.2 shows the influence of the curvature on the first six natural frequencies of the BHA. The natural frequencies decrease slightly with increasing curvature. Fig.4.12 depicts the influence of the WOB on the natural frequencies of curved drillstring. With the increase of the WOB, the natural frequencies decrease.

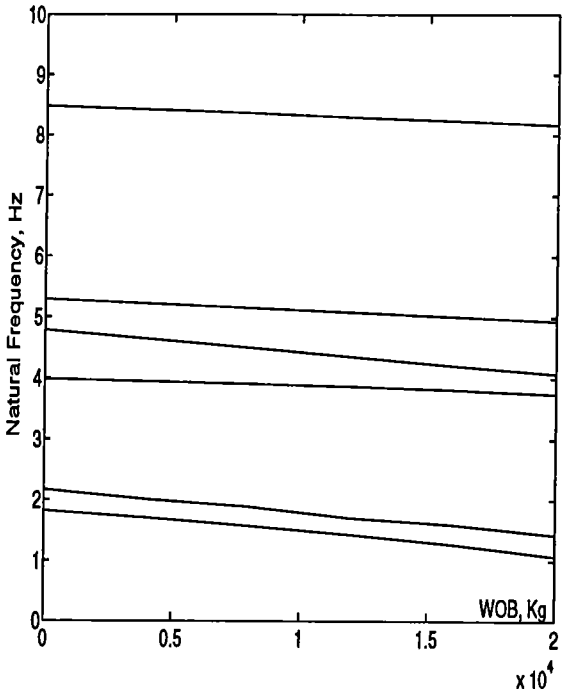

Fig.4.12: Natural frequencies of curved BHA versus WOB ($\xi = 0.4195$)

(d) Combined influence of curvature and WOB

From above results, it is seen that both the WOB and the curvature decrease the natural frequencies. Now we study the situation in which the curvature and the WOB are considered simultaneously.

Table 4.3: Combined effects of curvature and WOB on natural frequencies (Hz)

Conditions	ω_1	ω_2	ω_3	ω_4	ω_5	ω_6
WOB=0, ξ=0	1.836	2.169	3.993	4.797	5.302	8.496
WOB=0, ξ=0.4195	1.758	2.110	3.934	4.707	5.256	8.409
WOB=2E4 Kg, ξ=0	1.081	1.435	3.757	4.085	4.946	8.179
WOB=2E4 Kg, ξ=0.4195	1.051	1.415	3.689	4.023	4.928	8.102

Table 4.3 gives the natural frequencies in four different cases. If only the curvature ($\xi = 0.4195$) is considered, the first frequency is decreased by 4%. The WOB (20000 Kg) decreases the first natural frequency by 41 %. When the curvature ($\xi = 0.4195$) and WOB (20000 Kg) are taken into account simultaneously, the first natural frequency may

be decreased by 43%. Compared to the effect of WOB, the effect of the curvature may be negligible.

(e) Influence of surrounding mud

Table 4.4 gives a direct comparison in the cases of with and without the surrounding mud. The mud is taken as water. It is obviously seen that the surrounding mud decreases the eigenfrequencies, especially for the first one.

Table 4.4: Influence of surrounding mud on lateral eigenfrequencies (WOB=0)

Mode	ω_1	ω_2	ω_3	ω_4
Without mud	1.836	2.169	3.993	4.797
With mud	1.404	1.855	3.390	4.065

4.2.8. BHA Whirl Trajectory

(1) Exciting mechanism

Lateral vibration is mainly excited by centrifugal loads generated by unbalanced mass distribution around the rotation axis. The mass imbalance may be induced by axisymetry default, component misalignement, lateral deflection. Therefore, if the contact between drillstring and hole-wall is not considered, the lateral vibration initially results in synchronous forward whirling. The contact between drillstring and hole-wall will be considered in Chapter 5 and Chapter 6.

(2) Whirl trajectory

In order to study the bit whirl trajectory, an improved transfer matrix method (ITMM), instead of the IDSM, is used in this section. This is because the ITMM allows one to simulate the elliptical whirling orbit which may be more realistic than the circle orbit. The detailed description of the ITMM applied to bit whirl trajectory prediction has been given by Chen and Géradin (1993c).

In the ITMM the steady-state solution of equation (4.1) is assumed:

$$\begin{aligned} X(Z,t) &= X_c(Z)\cos\Omega t + X_s(Z)\sin\Omega t \\ Y(Z,t) &= Y_c(Z)\cos\Omega t + Y_s(Z)\sin\Omega t \end{aligned} \tag{4.17}$$

This solution form leads to an expanded transfer matrix with 16×16 in dimension.

The whirling motion of the bit is assumed to be known and is taken as an exciting source here in order to simulate the effects of the bit induced motion on the different points of the BHA.

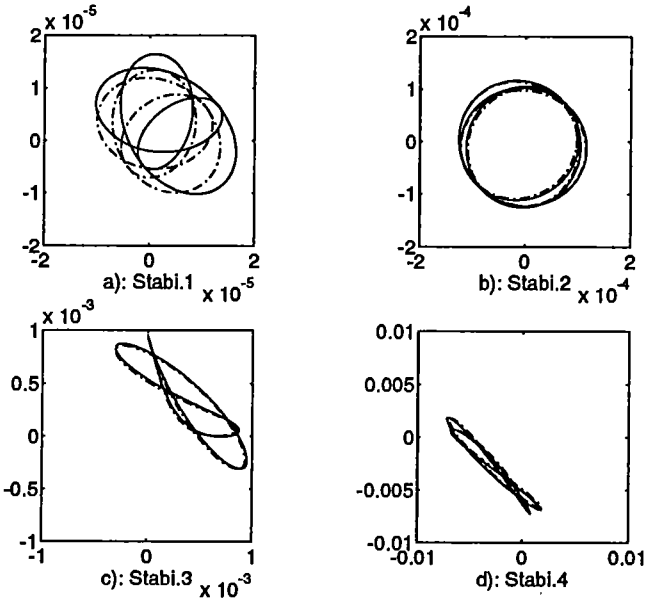

Fig.4.13: Nonsynchronous forward whirl orbits of the four stabilizers
——: WOB=0; -.-.-.: WOB=16000 Kg; $\omega = 2Hz, \Omega = 6Hz$

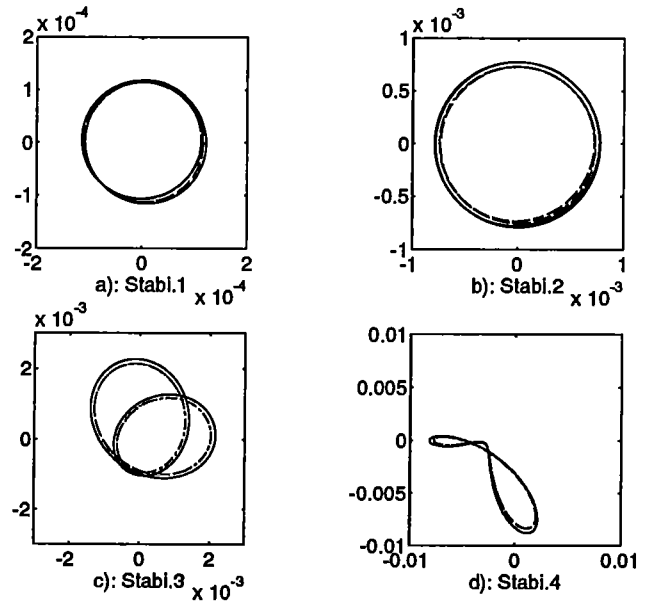

Fig.4.14: Backward whirl orbits of the four stabilizers
——: WOB=0; -.-.-.: WOB=16000 Kg; $\omega = 2Hz, \Omega = -8Hz$

It is assumed that the bit has an eccentricity with $M_b e_r = 0.1\ Kgm$ and the bit center has a known whirl orbit represented by $X_b = r\cos\Omega t$ and $Y_b = r\sin\Omega t$, where $r = 0.001m$.

From the superposition of the unbalance response and the bit whirl response, the multi-lobed whirling orbits for various bit whirling motions at the four stabilizers (Fig.4.8) are obtained by the transfer matrix method and shown in Fig.4.13 and Fig.4.14. In Fig.4.13, the rotation speed ω and the forward whirl speed Ω are taken respectively as 2 Hz and 6 Hz. In Fig.4.14, the rotation speed ω and the backward whirl speed Ω are taken respectively as 2 Hz and -8 Hz.

It is observed that under the same excitation, the whirl orbits of different points on the BHA are different. The trajectories may supply useful information for the stabilizer design.

4.3. BUCKLING ANALYSIS

The BHA is usually subject to large axial compression force or weight on bit (WOB). The magnitude of WOB has a significant influence on the rate of penetration (ROP) and on the drillstring failures. Therefore, it is very important to estimate the critical loads before the planning of drilling and during drilling.

The buckling analysis of drillstring was first recommended by Lubinski (1950) for vertical wells. Two kinds of buckling, i.e., sinusoidal and helical bucklings were analyzed since 1950 by different authors (Dawson and Paslay, 1984, Mitchell, 1986, Chen and Lin, 1990, Wu and Juvkam-Wold, 1993, 1994a,b). In these works the drillstring was treated as a constant cross-section shaft and the influence of the stabilizers on the critical load was usually ignored. Recently, Heisig (1993) studied the drillsting buckling using the finite element method (FEM) for vertical and horizontal wells. Although the FE model may include many factors such as stabilizers, contact between drillpipe and hole wall, the application of the method to drilling fields is limited due to its high computation cost.

In this section, the buckling of the drill strings is studied by the IDSM with emphasis on the influence of the locations of the stabilizers.

4.3.1. Special Problems

Three special problems associated with drill strings are considered:

(1) The drillstring may be divided into two parts. The upper part (drill pipe) is subject to extensional load and the lower part or BHA is subject to compression load;

(2) The compression load is generated by the weight of the lower part. Therefore, the compression force is linearly distributed along the BHA;

(3) The length of the compression part increases with the weight on bit. This makes the buckling analysis difficult if standard FEM software is used because the geometry of the system is a function of the buckling load.

4.3.2. Analysis Procedure

There are two ways to calculate the buckling loads of the drillstring. The first way is to observe the disappearance of the natural frequencies for a given load. For example, if the first eigenfrequency disappears for a given load P_1, then P_1 is the first critical load. If the load is continuously increased, one may find the second and higher critical loads. Obviously, the procedure of this method is exactly the same as the case of free lateral vibration analysis, but the effects of rotation speed can be disregarded. This method may be tedious if the calculated critical mode number is high.

The second way is to calculate directly the critical load and is described as follows. The stiffness matrix $[K^e]$ of a Timoshenko beam subject to axial load has been developed by Howson (1983) and is given in Appendix D. According to the principle of the IDSM, the BHA can always be reduced to an equivalent low order system. Let $[K(P)]$ be the global stiffness matrix (usually 2×2 in dimension), the critical load may directly be obtained by solving the following equation:

$$det[K(P)] = 0 \tag{4.18}$$

The buckling modes may be obtained as below:

(1.) The displacement vectors at both ends are calculated by solving the following linear equation for a given critical load P:

$$[K(P)]X = 0 \tag{4.19}$$

(2.) The displacements at a given internal node are then calculated by the transfer relation between the end node and the internal node

$$S_i = [T_i]S_0 \tag{4.20}$$

where S_i is the state vector of the internal node i and S_0 is the state vector of the end node.

(3.) The mode shape within an element (or between two nodes) can be recovered by the shape function given in Chapter 2.

Usually the knowledge of the mode shapes for drillstring is not as important as the knowledge of the buckling loads. The IDSM for buckling analysis of beam structures has been validated by Chen and Géradin (1994g).

4.3.3. Critical Loads for BHA

For sake of simplicity, the following assumptions have been made:

(1.) The influence of the rotation speed of the drillstring is neglected because the rotation speed is usually low (60-400 rpm).

(2.) The plane in which the buckling occurs is the plane of smallest flexural rigidity. This simplifies the 3D problem to a 2D problem.

(3.) The buckling mode is not constrained by the hole radius drilled. In other words, the contact between the drillstring and the hole wall is not considered. In practice, if such contact occurs due to the buckling, the drillstring operates in postbuckling mode and hence is theoretically unstable.

(4.) The influence of the hydrostatic pressure is neglected.

(5.) Only the compression part (BHA) is analyzed.

As outlined above, the compression load of the BHA is generated by its weight. This fact leads to the whole length of the BHA being the function of the WOB. For sake of simplicity, the geometries of the lower two drill collars are fixed (parameters in Table 4.5) and only the length of the third part (L_3 in Fig.4.15) is a function of WOB. This function may be determined by:

$$M_1 + M_2 + M_3 = WOB \tag{4.21}$$

where $M_i = \pi L_i \rho (R_i - r_i)$, i=1,2,3, with R_i, r_i and L_i being the outer radius, inner radius and the length of the corresponding section (Fig.4.15) and ρ the mass density.

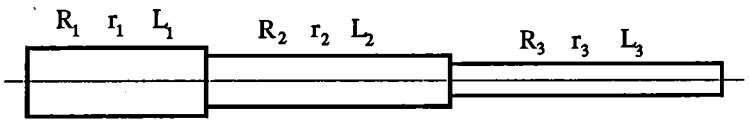

Fig.4.15: Geometry of the BHA

Table 4.5: Geometry of the BHA of figure 4.15 (meters)

R_1	r_1	L_1	R_2	L_2	R_3	L_3
0.1397	0.07143	10	0.1143	20	0.1016	Eq.(4.21)

$r_3 = r_2 = r_1$

Table 4.6: Buckling loads (Newton) of building assembly (Fig.4.1)

Type	P_1	P_2	P_3	P_4
A	86592	136178	152650	193850
B	97477	152150	192350	218950
C	173400	206450	239950	268750

The stabilizers are modeled as elastic supports with stiffness $k = 10^6$ N/m. The upper node is supposed to be clamped. Three kinds of bottom hole assemblies, namely building assembly (Fig.4.1), holding assembly (Fig.4.2) and dropping assembly (Fig.4.3) are studied here. Tables 4.6, 4.7, 4.8 list respectively the first four buckling loads of the different types of assemblies.

Table 4.7: Buckling loads (Newton) of holding assembly (Fig.4.2)

Type	P_1	P_2	P_3	P_4
A	173050	212050	238750	273250
B	161950	191750	231350	258750
C	155950	167750	187580	206950

Table 4.8: Buckling loads (Newton) of dropping assembly (Fig.4.3)

Type	P_1	P_2	P_3	P_4
A	142250	175550	213750	240650
B	173650	206650	240450	269050
C	140250	174850	212650	239750

The main roles of the building assemblies are to increase the hole angle or to build the angle. From table 4.5, it is seen that the buckling capacity of the building assembly increases with the number of the stabilizers. Type A in Fig.4.1 is the weakest.

Holding assemblies are used to drill a straight hole. Table 4.6 shows that the type A in Fig.4.2 has the strongest buckling capacity.

The buckling capacity of the dropping assemblies is almost of the same level as the holding assemblies but with fewer stabilizers. In the drilling practice, a general rule for the determination of the number of stabilizers is "the fewer the better" (Dareing, 1988). Therefore, dropping assemblies should be recommended in vertical wells.

4.3.4. Discussions about the buckling loads

The boundary conditions at upper and bottom ends of the BHA have a very big influence on the vibration behavior (Clayer, Vandiver, Lee, 1990). There is no doubt that the buckling loads depend strongly on the boundary conditions. In the above analysis the upper end is supposed to be fixed. Introducing other boundary conditions at both upper and bottom ends will not change the analysis procedures.

The hydrostatic and buoyancy forces are neglected in the analysis. However, they can easily be taken into account in the program without any difficulty.

Most of the recent work on drillstring buckling analysis were based on the assumption that the hole wall confines the buckling development. Therefore, the sinusoidal buckling and helical buckling will occur successively if the load is large enough. In this case, the contact between drill pipe and hole wall is, of course, very important. The FEM analysis may be the only way to obtain accurate buckling loads if contacts are taken into account.

4.4. CONCLUSIONS

The lateral vibration of the drillstring and buckling of the BHA are modeled exactly using the IDSM developed in Chapter 2 which leads to more accurate determination of modal parameters and buckling loads than those available from the FE approach. For lateral vibration, the drillstring is modeled as an equivalent two degrees of freedom system for a given frequency and rotation speed. The axial force (WOB) has a significant influence on the lateral vibration. Both the WOB and curvature decrease the lateral natural frequencies of the drillstring. The influence of the rotation speed may be neglected.

An outstanding advantage of the method for buckling analysis is that the size of the global stiffness matrix is the same as the size of the element stiffness matrix, irrespective of the number of elements. This fact makes it possible to calculate the buckling loads and modes during drilling.

Three types of BHA are studied. The results show that the locations of the stabilizers have a significant influence on the buckling loads, especially on the first one.

The simplicity of the method makes it possible to analyse the vibration and buckling of the drillstring during drilling.

CHAPTER 5:

BIT WHIRL KINEMATICS AND BACKWARD WHIRL DUE TO BIT-HOLEWALL CONTACT BY LUMPED MODEL

5.1. INTRODUCTION

In chapter 4, the linear lateral vibration including the free and forced vibrations are analyzed. Due to the nature of linear vibration, the bit- holewall contact, the stabilizer-holewall contact, as well as the drillcollar-holewall contact were not considered.

Actually, because the drillstring is designed to rotate from 60 $\sim$ 400 *rpm* for conventional tricone and PDC bit drilling, the lateral vibration, strictly speaking, should include both bending and whirling vibration.

It is well known that the bending vibration is mainly excited by unbalanced mass distribution of the bit and the drillstring. Therefore, bending vibration initially results in synchronous forward whirl, i.e., the string rotates as a whole around the well axis in the same direction and with the same speed as it rotates around its proper axis [Rixen, 1992]. However, as the vibration amplitude increases, not only the bit, but also the stabilizers and even the drillcollar will be in contact with the holewall (Fig.5.1).

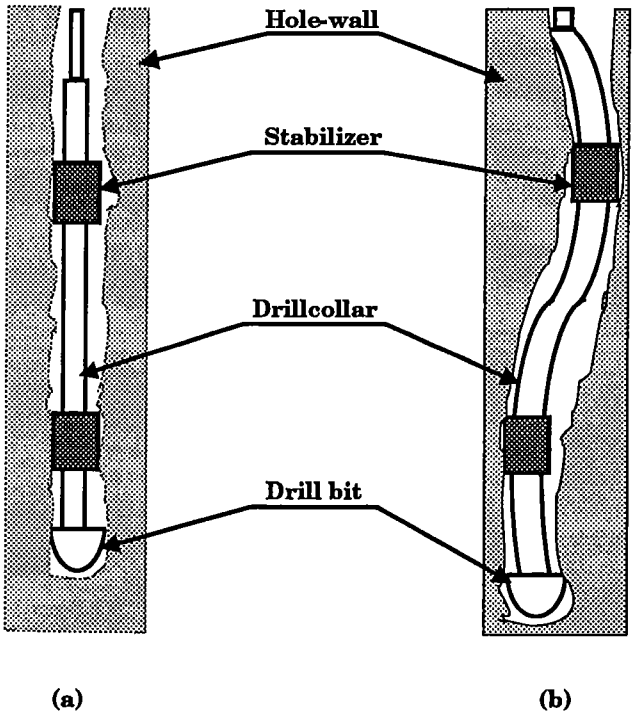

Fig.5.1: Drillstring in bore-hole. (a) Straight; (b) Curved.

In this case, the wall friction force may be able to change the forward whirl motion to backward whirl motion (Jansen, 1992).

There is an enormous established literature on the subject of whirling vibration of rotor systems. For example, among others, Crandall (1987) has shown that the continuous contact between rotor and stator can involve forward or backward whirling. The analytical and experimental investigations of the backward whirl due to rotor-stator contact (Lingener, 1990, Crandall, 1990, Crandall et al, 1993) have lead to the conclusion that stable backward whirl may occur under some conditions. Jansen (1991, 1992, 1993) studied the whirling and chaotic motion of drillstring using the rotor dynamic theory and found that the stabilizer-holewall contact, drillcollar-holewall contact as well as the bit-holewall contact can induce backward whirl.

Based on the observation at the drilling fields, Brett et al (1989) found that the backward whirl motion is an important source of PDC bit premature damage, because backward whirl can generate high impact loading on PDC cutters. The downhole measurements have also given clear evidence of bit whirl motion during drilling (Vandiver et al, 1988, Shyu, 1989).

However, because of its complexity, the bit whirl phenomenon is not completely clear. In this chapter, the PDC bit whirl kinematics is described first. The relationship between the cutter path, the bottomhole shape and whirl speed are obtained. The bit whirl kinematics is not only useful for PDC bit designer but also is the basis of bit whirl identification by experiments (discussed in chapter 7).

The dry friction induced steady-state backward whirl motion is studied both analytically and numerically based on a simple model. The formula to calculate the whirl speed and the whirl radius have been derived in a closed form. It is shown that once backward whirl is initiated, the whirl frequency is not only dependent on the rotation speed, but also on the eigenfrequency of the system. The maximum backward whirl frequency is limited by the eigenfrequency of the joint drillstring-formation system. The analytical results are compared with the experimental work performed by Lingener (1990) and Crandall (1990) for a flexible rotor.

The work presented in this chapter is based on Chen, Rixen and Géradin (1992, 1994) and Chen, Golinval and Géradin (1994a, 1994b).

5.2. BIT WHIRL KINEMATICS

5.2.1. Definition of bit whirl

The bit whirl motion is such that the center of the bit rotates about the hole center at a speed Ω. This whirl speed Ω may be different from bit rotation speed ω both in magnitude and in direction. They may have the following relationships:

$\Omega = \omega$ —— synchronous forward whirl;

$\Omega = m\omega, \quad m > 0, \quad m \neq 1$ —— nonsynchronous forward whirl;

$\Omega = -\omega$ —— synchronous backward whirl;

$\Omega = -m\omega, \quad m > 0, \quad m \neq 1$ ——nonsynchronous backward whirl;

5.2.2. Cutter trajectory during bit whirling

In order to describe the cutter trajectory during bit whirling, two coordinate systems are used (Fig.5.2). The first coordinate $X_hY_hZ_h$ is the inertial frame, fixed in the formation. The second coordinate $X_bY_bZ_b$ rotates with the drill bit at a constant speed ω. The subscripts h and b represent the hole and the bit respectively.

Fig.5.2 shows the parameters of whirl motion, in which

O_h is the geometrical hole center;

O_b is the geometrical center of the bit body;

R_h is the hole radius;

R_b is the bit radius;

ω is the rotation speed of the bit around O_b;

Ω is the bit whirl speed around O_h;

r_c, θ_c are the polar coordinates of any point in the reference system $X_bO_bY_b$;

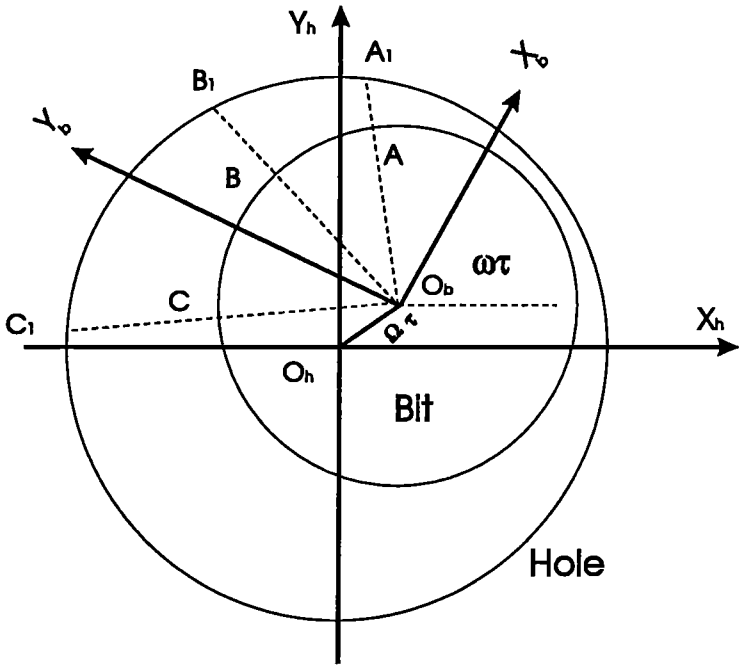

Fig.5.2: Bit whirl motion

Let us assume that the O_hX_h and O_bX_b axes coincide at $t = 0$. At any time t, the coordinate of any point in the absolute frame $X_hO_hY_h$ is:

$$\begin{aligned} X_h &= \Delta R\cos(\Omega t) + r_c\cos(\theta_c + \omega t) \\ Y_h &= \Delta R\sin(\Omega t) + r_c\sin(\theta_c + \omega t) \end{aligned} \tag{5.1}$$

where ΔR is called whirl radius and in the case of bit-holewall contact $\Delta R = R_h - R_b$. The first part of equation (5.1) is the bit center trajectory which is a circle with ΔR as its radius and Ω as its angular frequency.

Equation (5.1) is the general equation of any cutter path. After the bit and hole radii have been determined, the path of any cutter is dependent only on the whirl speed Ω and bit rotation speed ω.

Fig.5.3 and Fig.5.4 depict respectively the cutter trajectories during bit forward whirl motion and backward whirl motion.

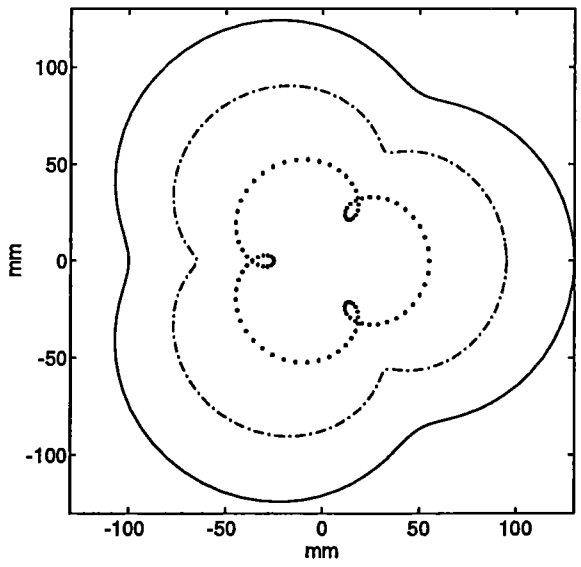

Fig.5.3: Forward whirl path of cutters, $\omega = 1Hz$, $\Omega = 4Hz$, $\Delta R = 5mm$
——: $r_c = 115\ mm$; -.-.-.: $r_c = 80\ mm$; .....: $r_c = 40\ mm$

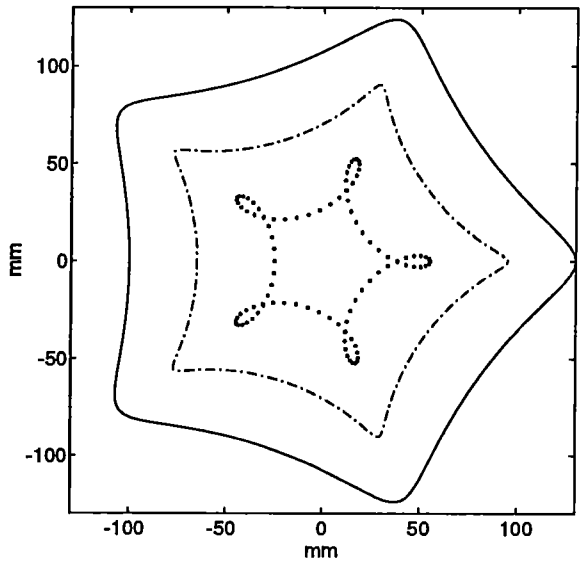

Fig.5.4: Backward whirl path of cutters, $\omega = 1Hz$, $\Omega = -4Hz$, $\Delta R = 5mm$
——: $r_c = 115\ mm$; -.-.-.: $r_c = 80\ mm$; .....: $r_c = 40\ mm$

5.2.3. Overlap condition of cutter path

Let A and B be any two cutters on the bit body. They are located on the same circle r_1 but cutter B has a phase lag, α, relative to cutter A. Hence for cutter A, according to equation (5.1) we have

$$\begin{aligned} X_h^a &= \Delta R\cos(\Omega t) + r_a\cos(\theta_a + \omega t) \\ Y_h^a &= \Delta R\sin(\Omega t) + r_a\sin(\theta_a + \omega t) \end{aligned} \tag{5.2}$$

Similarly, for cutter B we have:

$$\begin{aligned} X_h^b &= \Delta R\cos(\Omega t) + r_b\cos(\theta_b + \omega t) \\ Y_h^b &= \Delta R\sin(\Omega t) + r_b\sin(\theta_b + \omega t) \end{aligned} \tag{5.3}$$

where θ_b and θ_a , r_a and r_b are related by:

$$\begin{aligned} \theta_b &= \theta_a - \alpha \\ r_a &= r_b = r_1 \end{aligned} \tag{5.4}$$

where α is taken positive.

The so called overlap condition is such that during bit whirling, cutter A and cutter B have the same path, i.e., cutter B moves always following the path of cutter A in the absolute coordinate system $X_hY_hZ_h$.

Let t_1 be the relative time for cutter B to move to the position of cutter A in consideration of whirling and rotation of the bit. Then at any time t_0 one must have following relationship for overlap condition:

$$\begin{aligned} X_h^b(t = t_0 + t_1) &= X_h^a(t = t_0) \\ Y_h^b(t = t_0 + t_1) &= Y_h^a(t = t_0) \end{aligned} \tag{5.5}$$

Inserting equations (5.2), (5.3), (5.4) into equation (5.5), we have:

$$\begin{aligned} \omega t_1 &= \alpha \\ \Omega t_1 &= 2\pi n \end{aligned} \tag{5.6a}$$

It leads to the following overlap condition:

$$\alpha = 2\pi n \frac{\omega}{\Omega}, \quad n = \pm 1, 2, 3..... \tag{5.6b}$$

where n is a positive integer for forward whirl, and a negative integer for backward whirl.

The physical interpretation of condition (5.6b) is fairly obvious: indeed, the only way for point B to reach the same position as point A while the bit is whirling is that the bit has whirled an integer number of rounds while B has undergone an angle displacement α relative to the bit, hence $n/\Omega = \alpha/2\pi\omega$, yielding equation (5.6b).

When the bit has Z cutter edges (usually Z=3,4,5...), then α is equal to $2\pi/Z$ for conventional bit. In this case, the overlap condition is:

$$\frac{\Omega}{\omega} = nZ \tag{5.7}$$

Equation (5.7) means that when the bit center rotates about the hole center at a speed equal to nZ times the bit rotation speed itself, the cutters having the same radius move along the same path and overlap thus each other.

To verify the overlap condition, Fig.5.5 and Fig 5.6 shows the cutter path under the condition of $\Omega/\omega = -4 = -1 * 4$ and $\Omega/\omega = 4 = 1 * 4$, respectively. It is proved that the cutters having the same radius have the same path even during the bit whirling.

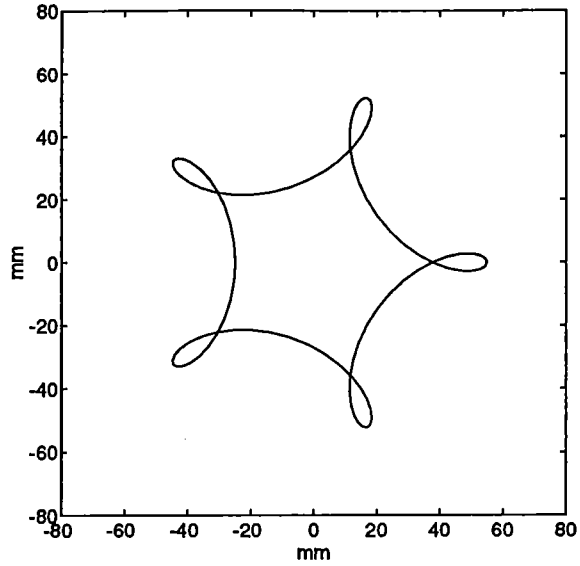

Fig.5.5: Backward whirl path of cutters, $\omega = 1Hz$, $\Omega = -4Hz$, $\Delta R = 5mm$
All the cutters have the same radius positions but with different angle θ_c

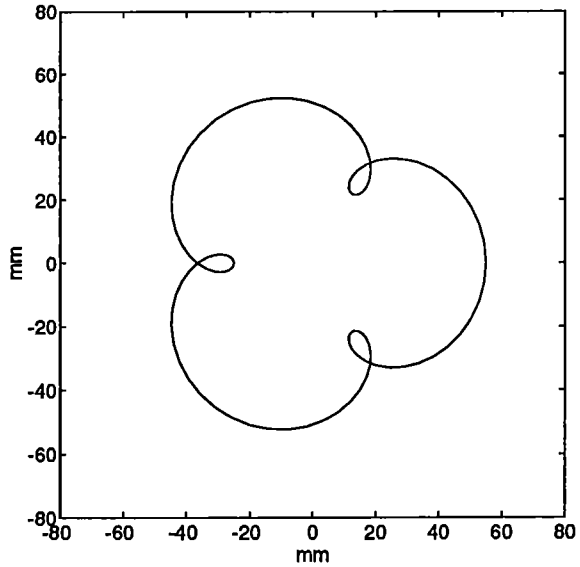

Fig.5.6: Forward whirl path of cutters, $\omega = 1Hz$, $\Omega = -4Hz$, $\Delta R = 5mm$
All the cutters have the same radius positions but with different angle θ_c

5.2.4. Number of hole lobes

According to equation (5.1), the path of any cutter can be rewritten in the polar coordinate system:

$$R = \sqrt{(x^2 + y^2)} = \sqrt{\Delta R^2 + r_c^2 + 2\Delta R r_c \cos[(\Omega/\omega - 1)\omega t - \theta_c]} \tag{5.8}$$

Equation (5.8) shows that the number of hole lobes N is:

$$N = abs(\frac{\Omega}{\omega} - 1) \tag{5.9}$$

For the bit having Z edges, we have:

$$N = abs(nZ - 1) \tag{5.10}$$

where n is an integer, $n = \pm 1, 2, 3.....$

This conclusion can be tested from Fig.5.3 and Fig.5.4.

The number of hole lobes may be used as an information to identify the whirling speed of the bit. From equation (5.9), the whirling frequency Ω can be obtained when rotation speed of the bit and number of hole lobes are known.

5.2.5. Rolling factor k

(1) Rolling factor k for backward whirl

If there is no slip between the bit gauge and the wall, then the instantaneous center of rotation will be the contact point at that time during backward whirling. In this case, we have:

$$(R_h - R_b)\Omega + R_b\omega = 0 \tag{5.11}$$

So:

$$\frac{\Omega}{\omega} = -\frac{R_b}{(R_h - R_b)} \tag{5.12}$$

Note that equation (5.11) and equation (5.12) are based on the assumption that the wall is rigid, i.e., no deformation during whirling. If wall deformation is considered, $R_h - R_b$ should be replaced by whirl radius ΔR. Section 5.3 gives a detailed description of this case.

Generally there is some slip between the bit and the wall, and the instantaneous center is no longer the contact point. In this case, let r_w be the distance between the bit center and the instantaneous center, then $r_w \leq R_b$. It has the following meaning: the instantaneous center of rotation of the bit is on the circle of radius r_w. In the case of backward whirl the instantaneous center C must be outside the distance of O_hO_b, Fig.5.7a. We have:

$$\frac{\Omega}{\omega} = -\frac{r_w}{(R_h - R_b)} \tag{5.13}$$

Let $k = r_w/R_b$, then we have

$$\frac{\Omega}{\omega} = -\frac{k}{R_h/R_b - 1} \tag{5.14}$$

If $k = 1$, there is no slip between bit and wall (pure roll). If $k = 0$, there is no whirling motion of the bit. Usually, $0 \leq k \leq 1$. We call k rolling factor.

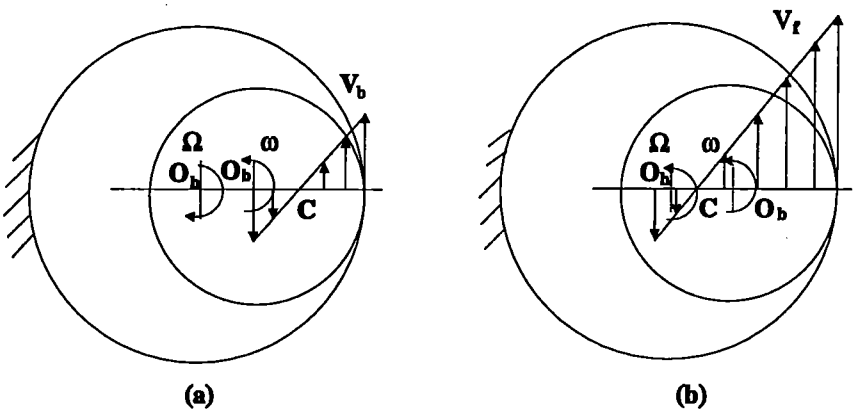

Fig.5.7: Distribution of sliding velocity. (a) Backward whirl; (b) Forward whirl

The sliding velocity between bit gauge and wall is defined by

$$V_b = \omega(R_b - r_w) = \omega R_b(1 - k) \tag{5.15}$$

The sliding velocity V_b is a linear function of k. The larger the V_b is, or the larger the factor k is, the larger is the bit wear.

From equation (5.14) it is seen that backward whirl speed Ω is dependent on bit rotation speed, the radius of bit and hole, and the rolling factor k.

(2) Rolling factor k for forward whirl

In the case of forward whirl the instantaneous center of rotation of the bit must be inside the distance of O_hO_b (Fig.5.7b). Similarly we have:

$$\frac{\Omega}{\omega} = -\frac{k}{R_h/R_b - 1} \tag{5.16}$$

where $k = -r_w/R_b$, usually, $-1 \leq k \leq 0$.

The sliding velocity between bit gauge and wall is defined by:

$$V_f = \omega(R_b - r_w) = \omega R_b(1 - k) \tag{5.17}$$

If $k = 0$, V_f reaches its minimum value

$$V_{fmin} = \omega R_b \tag{5.18}$$

If $k = -1$, V_f reaches its maximum

$$V_{fmax} = 2\omega R_b \tag{5.19}$$

In practice, synchronous forward whirl usually occurs. In this case the sliding velocity is:

$$V_f = \omega R \tag{5.20}$$

It is noted that the sliding velocity V_f for forward whirl is always larger than V_b for backward whirl.

Now let us consider two cases, i.e., synchronous forward whirl and backward whirl with no slip. In the first case, the bending stress frequency $(\Omega - \omega)$ is equal to zero and the sliding velocity V_f is equal to ΩR_h. In the second case, the bending stress frequency is $|\Omega| + |\omega|$ and the sliding velocity is equal to zero. It means that synchronous forward whirl generates large wear but no bending fatigue, while backward whirl with no slip implies no wall contact wear but high dynamic bending fatigue (Shyu, 1989, Rixen, 1992a).

Generally, forward whirl generates larger wear but smaller bending fatigue than backward whirl.

5.2.6. Velocity and acceleration of the cutters

From equation (5.1), it is easy to obtain the velocity of the cutter:

$$\begin{aligned} \dot{X} &= -\Delta R\Omega \sin \Omega t - r_c\omega \sin(\theta_c + \omega t) \\ \dot{Y} &= \Delta R\Omega \cos \Omega t + r_c\omega \cos(\theta_c + \omega t) \\ v &= \sqrt{(\dot{X}^2 + \dot{Y}^2)} \end{aligned} \tag{5.21}$$

and the acceleration:

$$\begin{aligned} \ddot{X} &= -\Delta R\Omega^2 \cos \Omega t - r_c\omega^2 \cos(\theta_c + \omega t) \\ \ddot{Y} &= -\Delta R\Omega^2 \sin \Omega t - r_c\omega^2 \sin(\theta_c + \omega t) \\ a &= \sqrt{\ddot{X}^2 + \ddot{Y}^2)} \end{aligned} \tag{5.22}$$

Equation (5.22) will be used in chapter 7 to identify the whirl parameters by using accelerometers.

5.3. BACKWARD WHIRL INDUCED BY BIT-HOLEWALL CONTACT

5.3.1. Equation of motion

For sake of simplicity and without missing the major characteristics, the following assumptions are made for the analysis of the whirling vibration of a drillstring:

(1) The drillstring is rotating at a constant rate ω.

(2) The bit can deflect only in the plane perpendicular to the drillstring axis.

(3) The borehole has a perfect circular cross-section.

(4) The contact between bit and borehole obeys the Coulomb friction law.

(5) Only the contact between bit gauge and borehole is considered.

(6) The rock or formation removal process is not considered.

Two coordinate frames are used (Fig.5.8). The first frame XYZ is the inertial frame, fixed in the formation whose Z axis is the longitudinal axis of the hole. The second frame, xyz, rotates with the drill bit at a constant rotation speed ω and its z axis is the longitudinal axis of the bit.

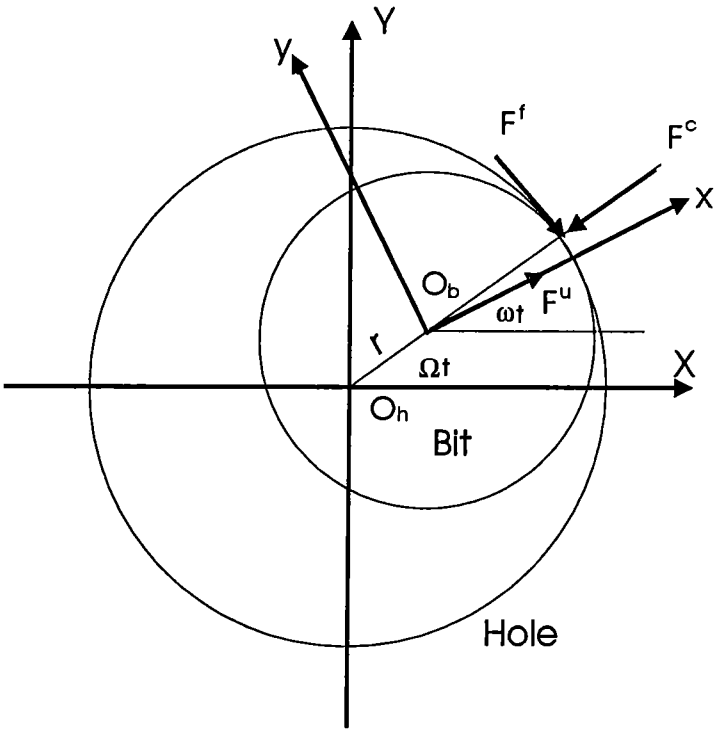

Fig.5.8: Coordinate systems and forces

In Fig. 5.8, with X and Y defined as the horizontal displacements of the bit, and with M, K, C defined as the equivalent mass, the equivalent bending rigidity of the drillstring, and the equivalent damping coefficient, the equations of motion of transverse drillstring vibration are expressed as:

$$[M]\ddot{U} + [C]\dot{U} + [K]U = F^c + F^f + F^u \tag{5.23}$$

where $U = [X, Y]^T$.

It is noted that the gyroscopic effect of the rotating drillstring is neglected in the equation due to the low rotation speed ($60 \sim 400$ rpm). In the above equation, F^c, F^f , and F^u represent the contact restoring forces, friction forces, and unbalance forces, respectively. They are described as follows.

(a) Contact Forces

The contact forces are due to the clearance between the bit gauge and the hole wall. A typical model for the contact forces is shown in Fig.5.9(a). The contact force acts as a linear spring with a deadband threshold region. For displacement below the deadband threshold, the contact force is zero. Mathematically, the contact force can be described as:

$$F^c = K_c\gamma(1 - \frac{\Delta r}{r})r \tag{5.24}$$

where $\gamma = 1$ if $r > \Delta r$, otherwise, $\gamma = 0$; r is the instantaneous whirling radius.

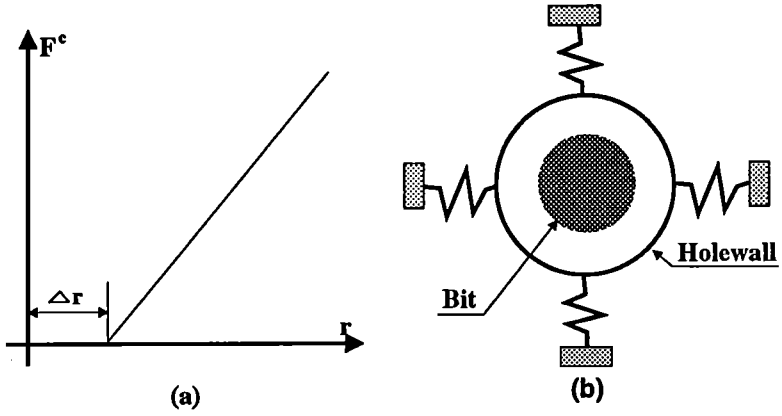

Fig.5.9: Contact model with deadband nonlinearity

Let

$$K_e = K_c\gamma(1 - \frac{\Delta r}{r}) \tag{5.25}$$

then the contact forces in the X and Y directions are:

$$\begin{aligned} F_X^c &= -K_e X \\ F_Y^c &= -K_e Y \end{aligned} \tag{5.26}$$

(b) Friction Forces

Since the bit is rotating relatively to the hole wall, a friction force is induced:

$$F^f = S\mu_c F^c \tag{5.27}$$

where μ_c is the coefficient of friction. S is the sign function defined by:

$$S = sign(r\Omega + R_b\omega) \tag{5.28}$$

where r is the whirling amplitude, R_b the bit radius, Ω the whirl speed and ω the rotation speed.

The need to introduce the sign function is obvious. Due to the whirling motion of the bit, the direction of the slip velocity of the bit gauge changes with time. The introduction of the sign function makes the direction of the friction force be always opposite to the direction of the slip velocity of the bit gauge at the point of contact with the borehole wall.

The friction forces in the X and Y directions are:

$$\begin{aligned} F_X^f &= S\mu_c K_e Y \\ F_Y^f &= -S\mu_c K_e X \end{aligned} \tag{5.29}$$

(c) Unbalance Force

The unbalance force is produced by the eccentricity of the bit. Its amplitude is given by:

$$F^u = m_b e\omega^2 \tag{5.30}$$

where m_b is the mass of the bit and e the eccentricity.

In this study the direction of F^u is assumed to coincide with the bit local axis x for the sake of simplicity.

Based on the above discussion, the equations of motion of transverse drillstring vibration are expressed as follows:

$$\begin{aligned} M\ddot{X} + C\dot{X} + KX &= -K_e X + S\mu_c K_e Y + m_b e\omega^2 \cos\omega t \\ M\ddot{Y} + C\dot{Y} + KY &= -K_e Y - S\mu_c K_e X + m_b e\omega^2 \sin\omega t \end{aligned} \tag{5.31}$$

It is noted that in the above equation, K_e is function of X and Y (equation (5.25)). Hence, equation (5.31) is a nonlinear equation.

5.3.2. Analytical Solutions For Steady-state Backward Whirl Motion

There are two forms of solutions of equation (5.31): forward whirl motion and backward whirl motion. We look only for the backward whirl motion in this section.

To this end, a complex variable is introduced:

$$R = X + iY = re^{i\theta} \tag{5.32}$$

In addition, two assumptions are made:

(i) The bit is always in contact with the hole wall, and therefore $\gamma \equiv 1$. This assumption is necessary for existence of backward whirl motion. Indeed if no contact exists with holewall, the dry-friction induced backward whirl vibration will be never happen.

(ii) The bit unbalance force $F^u = m_b e\omega^2$ may be negligible compared to the whirling unbalance force $F^\Omega = Mr\Omega^2$, in which r is the whirl radius and Ω is the whirl angular

speed. This is true in practice because the bit unbalance mass and eccentricity are usually small.

Substituting equation (5.32) into equation (5.31), we obtain the equations of motion in polar complex form as follows:

$$M(\ddot{r} - r\dot{\theta}^2) + C\dot{r} + Kr + K_c(r - \Delta r) = 0 \tag{5.33a}$$

$$M(r\ddot{\theta} + 2\dot{r}\dot{\theta}) + Cr\dot{\theta} + S\mu_c K_c(r - \Delta r) = 0 \tag{5.33b}$$

Under the condition of steady-state backward whirl, we have:

$$\dot{\theta} = \Omega, \quad \ddot{r} = 0, \quad \dot{r} = 0 \tag{5.34}$$

Inserting equation (5.34) into equation (5.33a), we get the whirl radius:

$$r = \frac{K_c \Delta r}{(K + K_c) - M\Omega^2} \tag{5.35}$$

In the case of backward whirl without slip, the whirl kinematics gives:

$$\Omega = -\frac{R_b}{r}\omega \tag{5.36}$$

Inserting equation (5.35) into equation (5.36), we get the whirl angular speed:

$$\Omega = \frac{R_b\omega(K + K_c - M\Omega^2)}{K_c \Delta r} \tag{5.37a}$$

Or in another form:

$$M\Omega^2 - \frac{K_c \Delta r}{R_b \omega}\Omega - (K + K_c) = 0 \tag{5.37b}$$

Solving equation (5.37b) and taking only the negative solution of Ω (backward whirl), we have:

$$\Omega(\omega) = -\sqrt{\omega_2^2 + (\omega_2^2 - \omega_1^2)^2(\frac{\Delta r}{2R_b\omega})^2} + (\omega_2^2 - \omega_1^2)\frac{\Delta r}{2R_b\omega} \tag{5.38}$$

where $\omega_2^2 = \frac{K+K_c}{M}$, and $\omega_1^2 = \frac{K}{M}$.

Substituting equation (5.38) into equation (5.35), we have:

$$r(\omega) = \frac{K_c \Delta r}{(K + K_c) - M\Omega(\omega)^2} \tag{5.39}$$

Equations (5.38) and (5.39) give the closed form solution for steady-state backward whirling motion. It is seen that both the whirl speed Ω and radius r are functions of the rotation speed ω, the geometry of the drillstring (equivalent stiffness K, bit radius R_b) and the hole conditions (hole clearance Δr and equivalent formation stiffness K_c).

If $\omega \rightarrow \infty$, from equation (5.38), we get the possible maximum backward whirl speed:

$$|\Omega|_{max} = \omega_2 = \sqrt{\frac{K + K_c}{M}} \tag{5.40}$$

In other words, there is an upper limit frequency for backward whirl. This upper limit frequency is equal to the eigenfrequency of the joint drillstring-formation system.

5.3.3. Numerical simulation conditions

Shown in Fig.5.10 is a commonly used BHA in the field. The modal parameters of the first mode are obtained using the finite element method (Samtech, 1994) as follows:

Eigenfrequency ω_1=2.22 Hz;

Modal mass $M = 1095.0Kg$;

Modal stiffness $K = 213124.5N/m$

Modal damping ratio is assumed to be 0.05

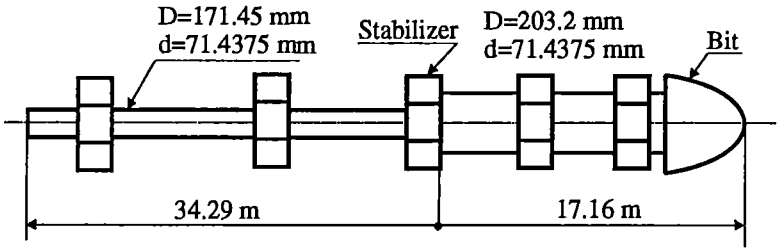

Fig.5.10: Drillstring used in the simulation

The hole wall is supposed to be isotropic around the bit and the contact stiffness K_c is taken equal to 10^7 N/m. The mass participation of the hole wall is not considered. If the bit or drillstring remains in close contact with the hole wall, the eigenfrequency of the joined system should become

$$\omega_2 = \sqrt{\frac{K + K_c}{M}} \tag{5.41}$$

The bit radius (R_b) is taken to be 100 mm and the deadband (dr) in Fig.5.9 is 5 mm. The friction coefficient between bit and hole wall, μ_c, and mass eccentricity, e, are varied so that the backward whirl can be initiated.

An automatic step size Runge-Kutta-Fehlberg algorithm with a pair of 4th and 5th order formulas was used in order to solve the differential equation (5.31) numerically. In the analysis, the initial conditions are equal to zero, i.e., the bit center coincides with the hole center at $t = 0$.

5.3.4. Numerical results

As stated before, we are not concerned with the initiation mechanism of backward whirl. What we are interested in is the possibility of steady state backward whirl. Therefore, in the numerical simulation the unbalance force is assumed to be large enough (about 1000 N) so that the bit can always be in contact with the hole-wall ($r \geq \Delta R$). Such a high mass unbalance force may be unpractical for the drillstring because the rotation speed is low. However, the side unbalance force generated by the bit/formation interaction during drilling may be as high as 5000 N depending on the bit type and the operating conditions (Chen and Géradin, 1993a).

(1) Influence of friction coefficient

Fig.5.11 and Fig.5.12 show respectively the influence of friction coefficient on the backward whirl frequency and amplitude. The whirl speed is obtained from the numerical integration results as follows:

$$\Omega = \frac{d}{dt}(atan(\frac{Y}{X})) = \frac{X\dot{Y} - Y\dot{X}}{X^2 + Y^2} \tag{5.42}$$

If Ω is positive, forward whirl occurs. Otherwise, backward whirl occurs.

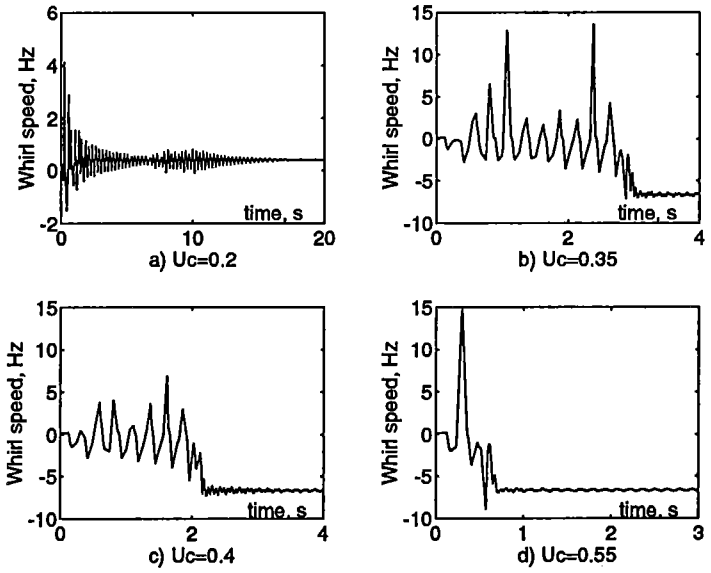

Fig. 5.11: Influence of friction coefficient on the backward whirl frequency ($\omega = 0.4$ Hz)

There is a critical friction coefficient below which synchronous forward whirl occurs (Fig.5.11a) and above which backward whirl occurs (Fig.5.11b,c,d). In Fig.5.11b,c,d, all the backward whirl frequencies converge to about 6.63 Hz. On the other hand, after backward whirl is initiated, its amplitude converges to about 6 mm (Fig.5.12b,c,d). It means that once initi-

ated, the backward whirl frequency and amplitude do not depend on the value of the friction coefficient.

This observation coincides with the analytical solutions given by equation (5.38) and (5.39). The backward whirl speed Ω given by equation (5.38) and radius r given by equation (5.39) do not depend on the friction coefficient. If the above parameters are input to equation (5.38) and equation (5.39), the obtained backward whirl speed and radius are exactly the same as those obtained by numerical simulation.

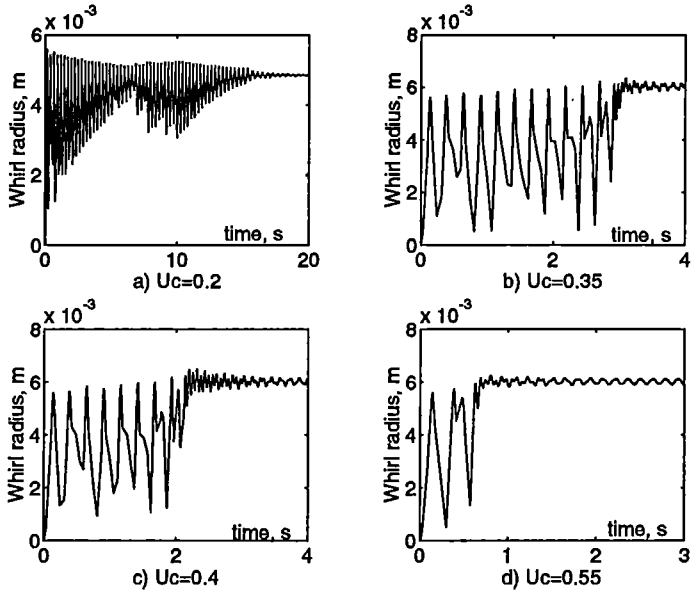

Fig. 5.12: Influence of friction coefficient on the backward whirl amplitude (ω = 0.4 Hz)

Fig.5.13 depicts the steady state backward whirl motion with constant amplitude and constant frequency after it is initiated. The amplitude is always larger than the clearance Δr. It means that during backward whirl, the bit is always in contact with the hole wall.

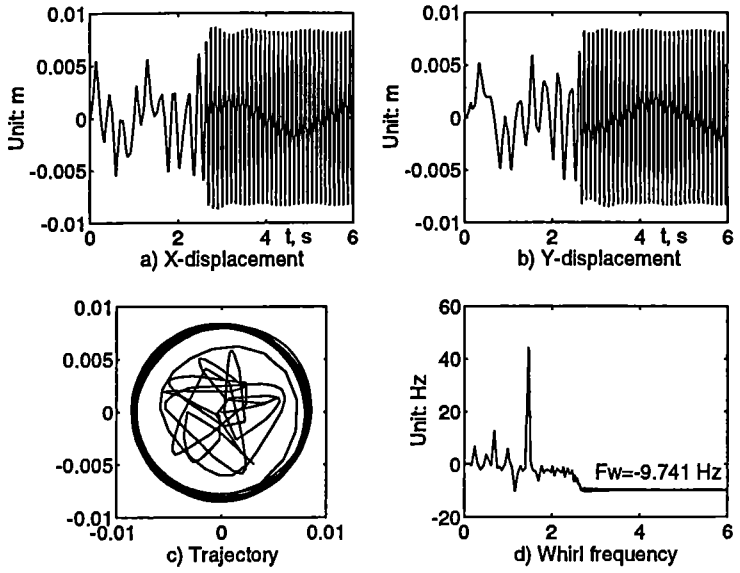

Fig.5.13: Steady-state backward whirl motion ($\omega = 0.8$ Hz, $\mu_c = 0.3$)

(2) Influence of rotation speed

Fig. 5.14 shows the influence of rotation speed of the drillstring on the backward whirl frequency (Fig.5.14a) and on the whirl radius (Fig.5.14b).

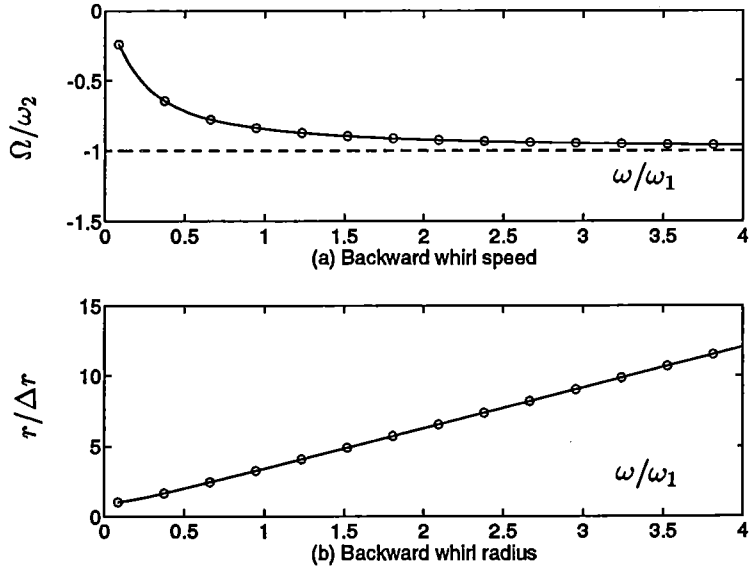

Fig.5.14: Influence of rotation speed on backward whirl motion
—: Analytical solutions; ooo: Numerical simulation.

It is observed that:

(1) The backward whirl frequency increases nonlinearly with the rotation speed;

(2) There is an upper limit frequency for backward whirl. This conclusion agrees well with the analytical prediction and also with the experimental results given by Lingener (1990) and Crandall (1990);

(3) The whirl amplitude is increased almost proportionally with the rotation speed.

(4) The backward whirl frequency is related to the rotation speed and to the whirl amplitude by the following relation:

$$\Omega = -\frac{R_b}{r(\omega)}\omega \tag{5.43}$$

In oil well drilling, it was usually accepted that the backward whirl frequency without slip can be given by:

$$\Omega = -\frac{R_b}{\Delta r}\omega \tag{5.44}$$

It means that the backward whirl frequency increases proportionally with the rotation speed and may be very high if Δr is very small. Unfortunately it is unlikely to observe such high backward whirl frequency in practice. Hence, the use of equation (5.44) may be questionable.

The differences between equation (5.44) and equation (5.43) are obvious. In equation (5.44), Δr is constant and the predicted backward whirl speed increases proportionally with the rotation speed. In equation (5.43), on the other hand, the predicted backward whirl speed is nonlinearly related to the rotation speed because the whirl amplitude r is a function of rotation speed ω.

5.4. CONCLUSIONS

In this chapter, the PDC bit whirl kinematics and the backward whirl vibration due to bit-holewall contact are studied both analytically and numerically. The bit whirl kinematics is not only useful for PDC bit designers but also the basis of whirl parameters identification by downhole measurements.

From the bit whirl dynamics, it is seen that

(1) Dry friction can induce steady-state backward whirl with frequency $\Omega = -R_b\omega/r(\omega)$ and with a very large amplitude $r(\omega)$.

(2) The maximum possible backward whirl frequency is the eigenfrequency of joint drillstring-formation system.

(3) The friction is responsible for the initiation of backward whirl. However, once initiated, the backward whirl frequency and amplitude do not depend on the friction coefficient.

(4) The differences between equation (5.44) and equation (5.43) are obvious. In equation (5.44), Δr is constant and the predicted backward whirl speed increases proportionally with

the rotation speed. In equation (5.43), on the other hand, the predicted backward whirl speed is nonlinearly related to the rotation speed because the whirl amplitude r is a function of rotation speed ω.

(5) The single mass-spring model used in this study may be too simple to be able to explain completely the backward whirling motion because a realistic assembly will exhibit several resonance frequencies in the range of rotation speed. This is a subject that will be studied in chapter 6 using finite element method.

CHAPTER 6

A FURTHER STUDY OF BACKWARD WHIRL DUE TO BIT-HOLEWALL CONTACT BY FEM

6.1 INTRODUCTION

6.1.1 Outline of the problem

In Chapter 2 to 4, the drillstring system is considered as a linear rotor-bearing system. The linear model is helpful to understand and to explain some important dynamic behaviors. Because of its simplicity, the linear model is also helpful to design the BHA system such as the placements of the stabilizers, the design of shock absorber and so on.

However, the drillstring is confined in a hole being drilled. During drilling, the drillstring may be curved due to the combined effects of gravity, WOB, TOB, the bit unbalanced side force and the non-homogeneity of the formation. In addition, some of the point along the drillstring may be in contact with the holewall. Therefore, strictly speaking, the drillstring is a nonlinear system. Following nonlinear phenomena are important:

(1) The nonlinearities induced by bit-holewall contact, stabilizer-holewall contact, BHA-holewall contact. These contacts introduce friction forces and a nonlinear restoring force (nonlinear stiffness). The friction coefficient is a dominant factor in this case. These contacts may be the main sources of bit backward whirl motion and stick-slip motion.

(2) The nonlinearties induced by bit-formation interaction. This is different from the contact induced nonlinearity. The bit-formation interaction may generate a very complicated force function which depends on, for example, the type of the formation and the bit, the cutter wear conditions and the operational parameters. The drilling forces are usually nonlinear functions of bit displacements and/or velocities. In addition, the bit-formation interaction is one of the coupling mechanisms because of interdependence of the drilling forces on the bit.

(3) The geometrically nonlinear behavior of the drillstring (Rixen, 1992). The drillstring structure is peculiar in the sense that its diameter to length ratio is very small so that it may be submitted to very large static deflections caused by axial compressive loading and by contact forces. Therefore, the drillstring can not be considered as straight and planar. The geometric non-linearities will appear in the sense that axial displacement will also involve bending and torsion along the drillstring. For the same reason, torsion generates bending and axial movements, and bending induces axial and torsional displacements. It can be thus seen that large displacement in drillstrings is the origin of geometric nonlinearities. The geometrically nonlinear behavior is also the source of the linear and parametric coupling (Rixen 1992, Shyu, 1989).

Modeling of the bit-formation interaction was initiated in 1987 in an effort to investigate the wear condition of PDC cutters (Glowka, 1987). Warren and Sinor (1989a,b) developed a similar 2D PDC bit model based on actual bit measurements. In a 2D model, it is assumed that the area of cut for any cutter on the bit is constant for a full revolution of the bit.

Hence, the bottom hole geometry is adequately described with just two dimensions. The constant area of cut assumption allows the force calculations for each cutter to be made only as it passes a fixed radial rock plane, thus the force on any cutter is also constant for a full rotation of the bit. This assumption is only valid for steady-state bit performance in homogeneous rock.

To be able to take the complex motions of the bit such as bit whirling motion into account, Behr and Warren (1991) developed a 3D PDC bit model which has the capability to evaluate cutter loading under the condition of nonhomogeneous rock and bit whirl. For the purpose of PDC bit dynamic analysis, Langeveld (1991) has developed a 3D bit/formation model which can calculate the instantaneous bit drilling force. A fully 3D model for PDC bit has been also developed by Chen and Géradin (1993a). This model has been successfully applied to bit force calculation, stability analysis of anti-whirl PDC bit (Chen and Géradin, 1993b), random bit force analysis (Chen and Géradin, 1992b) and PDC bit optimal design (Chen, Lamine et al 1993). However, the 3D bit-formation model has not been successfully combined with the drillstring dynamic model at this stage. Difficulties exist in updating the bottomhole condition and in the convergence of time integration. This remains a future research subject.

The linear and parametric couplings due to geometrically nonlinearities of the drillstrng have been studied by Shuy (1989).

It is shown in Chapter 5 that the bit-holewall contact may induce steady-state backward whirling. However, the single-mass-spring model may be unable to explain the complex whirling vibration. In order to better understand the nonlinear dynamics, especially the contact induced vibration, Hersig (1993) and Jansen (1993) have respectively established a FEM model for the drillstring. The contact between the drillstring and the holewall is modeled by a penalty function. Axial friction force is neglected in their model. Because the explicit time integration algorithm is used in Jansen's thesis, numerical instabilities may exist when strong nonlinearities occur (Jansen, 1993, pp177).

Simulation of the contact between drillstring and holewall at LTAS of University of Liège has been initiated in 1987 by Raeymakers and Géradin (1988) and later by Parisis and Géradin (1990). The work, namely the BHA project, consists of modifying the Mecano module of the Samcef software to adapt this module to the study of the behavior of the BHA. The initial goal of the project was the prediction of drilling direction. The contact element acts like an infinitely rigid disk which runs against an elastic cylindrical wall. During the contact the transverse and axial friction forces are taken into account. Although many modifications have been made during the second phase of the BHA project (Parisis and Géradin 1990), numerical difficulties still exist. In addition, the developed contact element is for static and quasi-static analysis and not for dynamic analysis.

6.1.2 The work of this chapter

The main purpose of this chapter is to develop a contact element for the simulation of drillstring holewall contact and to implement this element to the general multi-body dynamic analysis software, namely, Mecano module of Samcef (Samtech, 1994). The contact element

is located at some selected node along the drillstring. If the contact at one node occurs, the contact element at this node is introduced. In this way, all the contact points along the drillstring can be determined.

This chapter describes first the computational aspects behind the Mecano software. Secondly, the development of a contact element for dynamic analysis is described in detail. This contact element is based on the one developed by Parisis and Géradin (1990). Finally, the applications of the contact element to the drillstring are performed. Several numerical examples are given.

6.2 COMPUTATIONAL ASPECTS OF THE MECANO PROGRAM

Mecano is a software commercialized by Samtech, based on the research work carried out at LTAS (Aerospace Laboratory, University of Liège, Belgium). Although, it is tailored for multi-body systems, Mecano is suitable for dealing with static and dynamic, linear and nonlinear beam structures because it is based on the finite rotation concept and contains a nonlinear beam element. It is not the aim of this chapter to give a detailed description of the Mecano software (see Cardona and Géradin, 1987). However, it is necessary to understand the basic principle used in the software.

6.2.1. The Nonlinear Beam Element

The beam element developed in Mecano is geometrically exact, large displacement/small strain finite element which takes the shear effects into account. The element can undergo large rigid body displacements and rotations. Because the element is derived in 3 dimensional space, the axial, lateral and torsional couplings of the drillstring may be analyzed.

6.2.2. Hilber-Hughes-Taylor (HHT) α-Method

The general equations for a linear or a nonlinear system take the form:

$$\mathbf{M}\ddot{\mathbf{q}} + \mathbf{g}^{\mathbf{int}} = \mathbf{g}^{\mathbf{ext}} \tag{6.1}$$

For linear systems,

$$\mathbf{g}^{\mathbf{int}}(\mathbf{q}, \dot{\mathbf{q}}) = \mathbf{K}\mathbf{q} + \mathbf{C}\dot{\mathbf{q}} \tag{6.2}$$

For nonlinear systems,

$$\mathbf{K} = \frac{\partial \mathbf{g}^{\mathbf{int}}}{\partial \mathbf{q}} \tag{6.3a}$$

$$\mathbf{C} = \frac{\partial \mathbf{g}^{\mathbf{int}}}{\partial \dot{\mathbf{q}}} \tag{6.3b}$$

where $\mathbf{M}, \mathbf{K}, \mathbf{C}$ are the mass matrix, stiffness matrix and damping matrix, respectively, $\mathbf{g}^{\mathbf{int}}$ and $\mathbf{g}^{\mathbf{ext}}$ are the internal and external force vectors, respectively. $\mathbf{q}$ is displacement vector.

The one step Newmark integration scheme is implicit on accelerations and interpolates displacements and velocities between time steps n and $n+1$ according to coefficients β and γ and time step length h:

$$\dot{\mathbf{q}}_{n+1} = \dot{\mathbf{q}}_n + (1-\gamma)h\ddot{\mathbf{q}}_n + \gamma h\ddot{\mathbf{q}}_{n+1} \tag{6.4a}$$

$$\mathbf{q}_{n+1} = \mathbf{q}_n + h\dot{\mathbf{q}}_n + (\frac{1}{2} - \beta)h^2\ddot{\mathbf{q}}_n + \beta h^2\ddot{\mathbf{q}}_{n+1} \tag{6.4b}$$

where h is the time increment, β and γ are two free parameters of the method.

Instead of directly substituting the above scheme (6.4) into equation (6.1), Hilber, Hughes and Taylor have proposed an elegant way to introduce numerical damping without degrading the order of accuracy. In the HHT method, the time-discrete equations are modified by averaging elastic, inertia and external forces between both time instants. Therefore, if we know the displacements, velocities and acceleration at time t_n, the displacements and velocities at time t_{n+1} are given by equation (6.4). The acceleration at t_{n+1} is obtained by solving the following equation:

$$M\ddot{\mathbf{q}}_{n+1} + (1-\alpha)\mathbf{g}^{int}_{n+1} + \alpha\mathbf{g}^{int}_{n} = (1-\alpha)\mathbf{g}^{ext}_{n+1} + \alpha\mathbf{g}^{ext}_{n} \tag{6.5}$$

where α is the numerical damping coefficient. If the parameters are chosen so that $\alpha = 0 \sim 1/3$, $\gamma = 0.5 + \alpha$ and $\beta = 0.25(1+\alpha)^2$, the result is an unconditionally stable second order schema (Géradin and Rixen, 1994).

Because the presence of the internal forces term $\mathbf{g}^{int}$, the implicit equation (6.5) is usually nonlinear in $\mathbf{q}_{n+1}$. We have thus to solve it by using an iterative method such the Newton-Raphon method (Cardona and Géradin, 1987). The iteration matrix of the Newton-Raphson process is:

$$\mathbf{S} = \frac{1}{\beta h^2}\mathbf{M} + \frac{\gamma}{\beta h}\mathbf{C} + (1-\alpha)\mathbf{K} \tag{6.6}$$

An automatic control of time step size has also been introduced in version 5.0 of Mecano (Samtech, 1994). The time step control algorithm is based on the comparison of the HHT interpolation scheme and the Taylor development to the third order. This scheme saves much computational time because it takes larger time steps where the solution is more slowly changing.

6.2.3. The User Element

The user element in Mecano allows to introduce an element with variable number of nodes and a behavior law programmed by the user himself to meet his specific needs and applications. This behavior law may be function of time and depends on nodal displacements, velocities and accelerations of the element.

This very general approach guarantees a good opening of the package. In practice, the element is written in a Fortran subroutine, the programming of which is made easily by resorting to the library of general subroutines available in the software. This element has been used to simulate the 2 dimensional bit/formation contact problems (Chen, Rixen and Géradin, 1994).

6.3 A CONTACT ELEMENT FOR BHA DYNAMIC ANALYSIS

6.3.1 Problem Description and Assumptions

In order to simulate the contact between drillstring and holewall, two essential issues are important. The first issue is how to determine the contact point along the drillstring at a given time. The second issue is how to introduce the contact law after the contact occurs, such as friction force evaluation, contact stiffness.

Consider Fig.6.1. There are two coordinate systems. The global coordinate system, xyz, is fixed in the space.

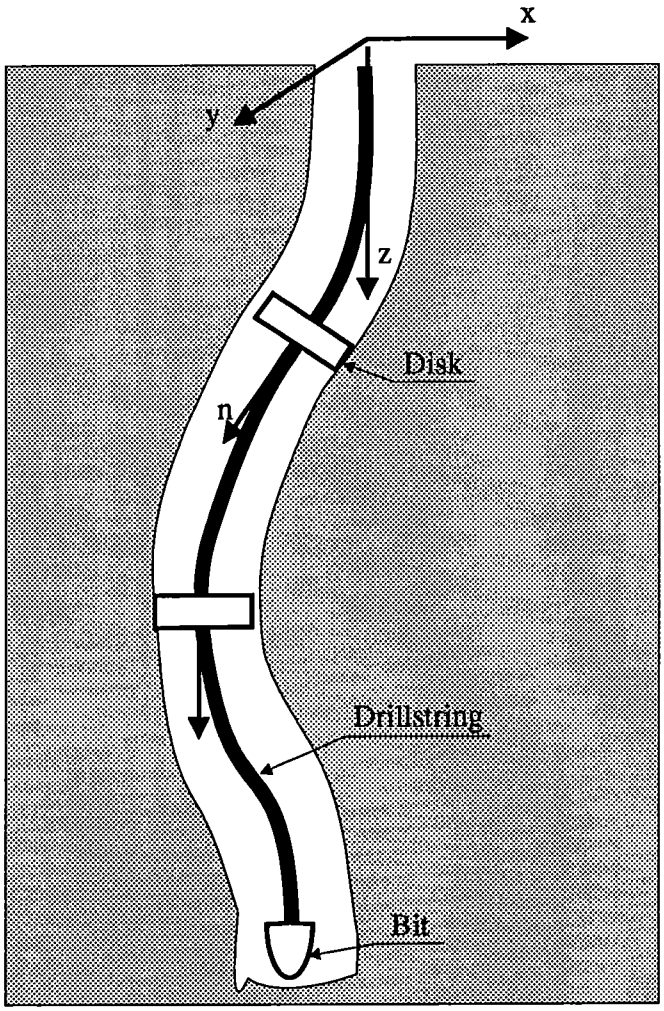

Fig.6.1: Drillstring and the hole drilled

The movement of the drillstring is expressed in terms of this cartesian coordinate. The hole geometry may be determined according to the initial position of the drillstring. In other words, the tangent of the initial curvature of the drillstring is a good representation of the

hole curve itself. This assumption is reasonable because the hole is drilled by the movement of the drillstring.

The second coordinate system is a local coordinate frame which is represented by the disk normal direction **n** at the disk center. The initial coordinate of the disk center, x_0, y_0, z_0, is the reference point of this contact element. It is assumed that the normal disk vector **n** has the same direction as the tangent direction of the reference point and does not change during the vibration simulation. It is also assumed that the contact occurs only in the disk plane (reference plane).

In summary, the following assumptions are made for the sake of simplicity without loss of the main characteristics:

(1) The disk is infinitely rigid without mass.

(2) The cross section of the hole in the disk plane is circular.

(3) The vibration of the disk is small so that its normal vector **n** may be considered to be constant during the simulation. Therefore, the disk normal direction may be determined by the reference point.

(4) The disk is rotating around its normal vector **n** with a constant speed ω. Thus the rotating vector is $\omega = \omega \mathbf{n}$.

(5) The Coulomb friction law is applied at the contact point.

6.3.2 Contact Condition

Let us consider the local coordinate at the contact point (Fig.6.2).

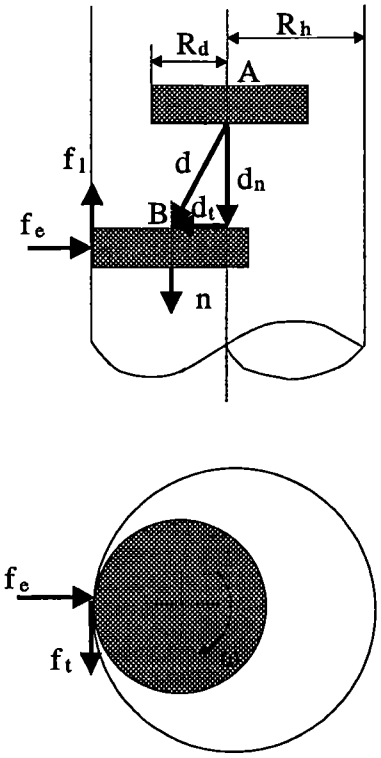

Fig.6.2: Model of disk-holewall contact

At time t, the reference point moves from $A(x_0, y_0, z_0)$ to $B(x, y, z)$. Therefore, the element displacement is

$$\mathbf{d} = (x - x_0 \quad y - y_0 \quad z - z_0)^T \tag{6.7}$$

The projection of the displacement vector $\mathbf{d}$ on the vector $\mathbf{n}$ is given by

$$\mathbf{d_n} = (\mathbf{d} \bullet \mathbf{n})\mathbf{n} = \begin{pmatrix} (x-x_0)n_1^2 + (y-y_0)n_1n_2 + (z-z_0)n_1n_3 \\ (x-x_0)n_1n_2 + (y-y_0)n_2^2 + (z-z_0)n_2n_3 \\ (x-x_0)n_1n_3 + (y-y_0)n_2n_3 + (z-z_0)n_3^2 \end{pmatrix} \tag{6.8}$$

where $\mathbf{n} = (n_1 \quad n_2 \quad n_3)^T$.

The transversal displacement $\mathbf{d_t}$ is then:

$$\mathbf{d_t} = \mathbf{d} - \mathbf{d_n} = \begin{pmatrix} (x-x_0)(1-n_1^2) - (y-y_0)n_1n_2 - (z-z_0)n_1n_3 \\ -(x-x_0)n_1n_2 + (y-y_0)(1-n_2^2) - (z-z_0)n_2n_3 \\ -(x-x_0)n_1n_3 - (y-y_0)n_2n_3 + (z-z_0)(1-n_3^2) \end{pmatrix} \tag{6.9}$$

If the module $|\mathbf{d_t}|$ is greater than the clearance $\Delta R = R_h - R_d$, i.e., if

$$|\mathbf{d_t}| - \Delta R > 0 \tag{6.10}$$

then there is a contact between the disk and the holewall.

The unit vector of $\mathbf{d}_t$ may be determined by:

$$\mathbf{u} = \frac{\mathbf{d}_t}{|\mathbf{d}_t|} = \begin{pmatrix} u_1 \\ u_2 \\ u_3 \end{pmatrix} \tag{6.11}$$

The unit vector $\mathbf{u}$ represents the contact direction. In the following sections, it will be shown that the unit vectors $\mathbf{u}$ and $\mathbf{n}$ are the two basic vectors for determination of the contact forces.

6.3.3 Forces Induced by Contact

As shown in Fig.6.2, the contact between the massless disk and the holewall will generate four forces, i.e., elastic force, damping force, transversal friction force and longitudinal friction force. They are expressed below.

(a) Elastic force

The elastic forces or the restoring forces induced by the contact between the disk and the holewall are due to the elasticity of the holewall. Shown in Fig.6.3 are three kinds of models for the elastic forces, i.e., the linear spring model, the hard spring model and the soft spring model.

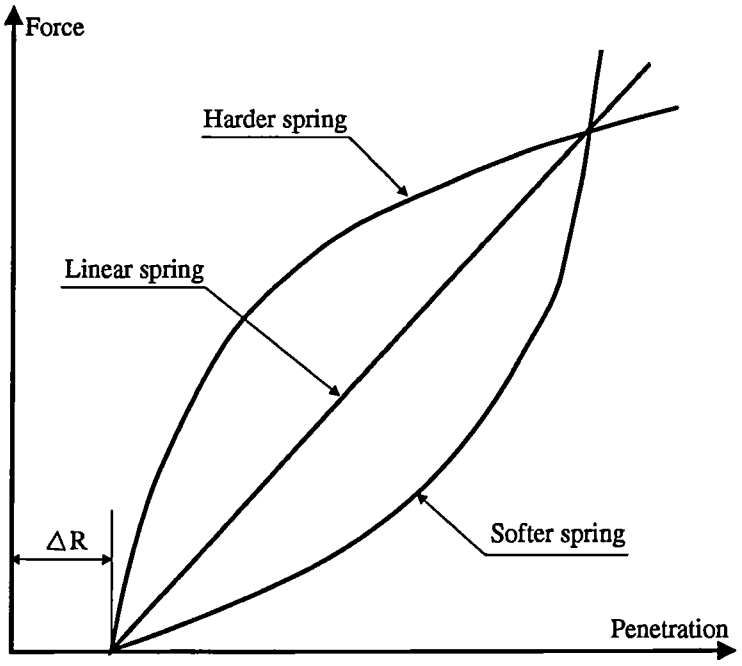

Fig.6.3: Elastic force models

For displacement below the deadband threshold, the elastic force is zero. Mathematically, the modulus of the elastic force can be described by

$$f_e = \begin{cases} k_e(|\mathbf{d}_t| - \Delta R)^m, & \text{if contact occurs;} \\ 0, & \text{otherwise.} \end{cases} \tag{6.12}$$

where k_e is the stiffness of the holewall at contact point and ΔR is the clearance between the disk and the holewall. The value of m is:

$$m = \begin{cases} 1, & \text{linear spring model;} \\ > 1, & \text{hard spring model (usually m=3/2);} \\ < 1, & \text{soft spring model (usually m=2/3);} \end{cases} \tag{6.13}$$

The direction of $\mathbf{f_e}$ is shown in Fig.6.2. Therefore, the elastic force vector is:

$$\mathbf{f_e} = f_e\mathbf{u} = \begin{pmatrix} f_e u_1 \\ f_e u_2 \\ f_e u_3 \end{pmatrix} \tag{6.14}$$

(b) Damping force

The damping force modulus is:

$$f_d = Cv_t \tag{6.15}$$

where v_t is the modulus of the disk velocity in the contact direction. If $\mathbf{v}$ is the velocity vector of the disk center, v_t can be written:

$$v_t = \mathbf{v} \bullet \mathbf{u} = v_1u_1 + v_2u_2 + v_3u_3 \tag{6.16}$$

where $\mathbf{v} = (v_1 \quad v_2 \quad v_3)^T$.

The damping force vector is then:

$$\mathbf{f_d} = f_d\mathbf{u} = \begin{pmatrix} f_d u_1 \\ f_d u_2 \\ f_d u_3 \end{pmatrix} \tag{6.17}$$

(c) Transverse friction force and moment

The modulus of the transverse friction force is:

$$f_t = \mu_t(f_e + f_d) \tag{6.18}$$

This force lies in the disk plane. In order to define its direction, however, two cases have to be considered:

Case 1: Static analysis

In this case, the direction of the transverse friction force can be determined by the disk rotation:

$$\mathbf{f_t} = f_t(\mathbf{u} \times \mathbf{n}). \tag{6.19}$$

It is noted that the disk rotating vector ω coincides with the vector $\mathbf{n}$.

Case 2: Dynamic analysis

In the case of dynamic analysis, the disk rotates around its center, meanwhile, the disk center vibrates. It means that the contact velocity at the contact point includes two terms: (1) the term $\mathbf{v}^{t\omega}$ induced by disk rotation ω and (2) the term $\mathbf{v}^{tt}$ induced by the vibration of the disk center. These two terms can be evaluated respectively as follows:

$$\mathbf{v}^{t\omega} = R_d(\mathbf{u} \times \omega) \tag{6.20a}$$

$$\mathbf{v}^{tt} = \mathbf{v} - (\mathbf{v} \bullet \mathbf{u})\mathbf{u} \tag{6.20b}$$

Therefore, the contact velocity is:

$$\mathbf{v}^{t} = \mathbf{v}^{t\omega} + \mathbf{v}^{tt} \tag{6.21}$$

Finally, the transversal friction force vector in the dynamic case is:

$$\mathbf{f}_t = -f_t \frac{\mathbf{v}^t}{|\mathbf{v}^t|} \tag{6.22}$$

In order to avoid the singularities in the computation, equation (6.22) is modified by

$$\mathbf{f}_t = \begin{cases} -f_t \frac{\mathbf{v}^t}{|\mathbf{v}^t|}, & \text{if } |\mathbf{v}^t| \geq \epsilon; \\ -f_t(2 - \frac{|\mathbf{v}^t|}{\epsilon})\frac{\mathbf{v}^t}{\epsilon}, & \text{otherwise.} \end{cases} \tag{6.23}$$

where ϵ is a small value, usually equal to 10^{-3}.

Because the friction force acts at the surface of the disk, it generates an additional friction moment. For both static and dynamic analysis, this additional friction moment is obtained by

$$\mathbf{m}_t = R_d(\mathbf{u} \times \mathbf{f}_t) \tag{6.24}$$

(d) Longitudinal friction force and moment

The force modulus is:

$$f_l = \mu_l(f_e + f_d) \tag{6.25}$$

The longitudinal velocity at the contact point is:

$$v_l = \mathbf{v} \bullet \mathbf{n} = v_1 n_1 + v_2 n_2 + v_3 n_3 \tag{6.26}$$

Therefore, the longitudinal friction force vector is

$$\mathbf{f}_l = S_l f_l \mathbf{n} \tag{6.27}$$

where

$$S_l = sign(v_l) = \begin{cases} 1, & \text{if } v_l < 0; \\ 0, & \text{if } v_l = 0; \\ -1, & \text{if } v_l > 0; \end{cases} \tag{6.28}$$

In order to avoid the singularity of the derivative at $v_l = 0$, equation (6.28) is modified by

$$S_l = \begin{cases} \frac{v_l}{|v_l|}, & \text{if } |v_l| \geq \epsilon; \\ (2 - \frac{v_l}{\epsilon})\frac{v_l}{\epsilon}, & \text{if } |v_l| < \epsilon \end{cases} \tag{6.29}$$

Like as the transversal friction force, the longitudinal force generates also an additional moment which can be given by

$$\mathbf{m}_l = f_l S_l R_d(\mathbf{n} \times \mathbf{u}) = \begin{pmatrix} f_l S_l R_d(n_2 u_3 - n_3 u_2) \\ f_l S_l R_d(n_3 u_1 - n_1 u_3) \\ f_l S_l R_d(n_1 u_2 - n_2 u_1) \end{pmatrix} \tag{6.30}$$

6.3.4 Element Matrices

Because the disk is massless, only stiffness and damping matrices are needed for the contact element. The stiffness and the damping matrices are the sum of four terms, respectively:

$$\mathbf{K} = \mathbf{K_e} + \mathbf{K_d} + \mathbf{K_f^t} + \mathbf{K_f^l} \tag{6.31}$$

$$\mathbf{C} = \mathbf{C_e} + \mathbf{C_d} + \mathbf{C_f^t} + \mathbf{C_f^l} \tag{6.32}$$

where $\mathbf{K_e}, \mathbf{K_d}, \mathbf{K_f^t}, \mathbf{K_f^l}$ are stiffness matrices corresponding to the elastic force, damping force, transverse friction force and longitudinal friction force, respectively. $\mathbf{C_e}, \mathbf{C_d}, \mathbf{C_f^t}, \mathbf{C_f^l}$ are damping matrices associated with these forces. These matrices are derived below.

(a) $\mathbf{K_e}$ and $\mathbf{C_e}$

According to equations (6.3) and (6.14), we have the stiffness matrix $\mathbf{K_e}$:

$$K_e(i,j) = \frac{\partial(f_e u_i)}{\partial q_j} = \frac{\partial f_e}{\partial q_j} u_i + f_e \frac{\partial u_i}{\partial q_j}, \quad i,j = 1,2,3. \tag{6.33}$$

where

$$\frac{\partial f_e}{\partial q_j} = k_e \frac{\partial |d_t|}{\partial q_j} \tag{6.34}$$

with

$$\frac{\partial |d_t|}{\partial q_j} = u_j - \sum_{k=1}^{3} u_k n_k n_j \tag{6.35}$$

and

$$\frac{\partial u_i}{\partial q_j} = \frac{\delta_{ij} - n_i n_j - u_i \frac{\partial |d_t|}{\partial q_j}}{|d_t|} \tag{6.36}$$

with δ_{ij} is the Kroneker's symbol and $\mathbf{q} = (x \quad y \quad z)$.

The damping matrix $\mathbf{C_e}$ is obviously a zero matrix:

$$C_e(i,j) = \frac{\partial(f_e u_i)}{\partial \dot{q}_j} = 0, \quad i,j = 1,23. \tag{6.37}$$

(b) $\mathbf{K_d}$ and $\mathbf{C_d}$

Based on equation (6.17), the stiffness matrix $\mathbf{K_d}$ is:

$$K_d(i,j) = \frac{\partial(f_d u_i)}{\partial q_j} = \frac{\partial f_d}{\partial q_j} u_i + f_d \frac{\partial u_i}{\partial q_j}, \quad i,j = 1,2,3. \tag{6.38}$$

with

$$\frac{\partial f_d}{\partial q_j} = c(v_1 \frac{\partial u_1}{\partial q_j} + v_2 \frac{\partial u_2}{\partial q_j} + v_3 \frac{\partial u_3}{\partial q_j}) \tag{6.39}$$

and $\frac{\partial u_i}{\partial q_j}$ is given by equation (6.36).

The associated damping matrix $\mathbf{C_d}$ is

$$C_d(i,j) = \frac{\partial(f_d u_i)}{\partial \dot{q}_j} = c u_i u_j \tag{6.40}$$

(c) $\mathbf{K_f^t}$ and $\mathbf{C_f^t}$

It is seen that the transverse friction induces a nodal friction force and an additional moment. Therefore, the associated internal force vector has 6 components. Two cases are considered.

Case 1: Static analysis

In the static analysis, the internal force vector is:

$$\mathbf{g}_t^{int} = \begin{pmatrix} \mathbf{f}_t \\ \mathbf{m}_t \end{pmatrix} = \begin{pmatrix} f_t(n_3 u_2 - n_2 u_3) \\ f_t(n_1 u_3 - n_3 u_1) \\ f_t(n_2 u_1 - n_1 u_2) \\ f_t R_d n_1 \\ f_t R_d n_2 \\ f_t R_d n_3 \end{pmatrix} \tag{6.41}$$

If we note that:

$$\frac{\partial f_t}{\partial q_j} = \mu_t(\frac{\partial f_e}{\partial q_j} + \frac{\partial f_d}{\partial q_j}), \quad j = 1,2,3. \tag{6.42}$$

and

$$\frac{\partial f_t}{\partial \dot{q}_j} = \frac{\partial f_d}{\partial \dot{q}_j} = \mu_t c u_j, \quad j = 1,2,3. \tag{6.43}$$

the matrix $\mathbf{K_f^t}$ and $\mathbf{C_f^t}$ are obtained from:

$$K_f^t(1,j) = \frac{\partial f_t}{\partial q_j}(n_3 u_2 - n_2 u_3) + f_t(n_3 \frac{\partial u_2}{\partial q_j} - n_2 \frac{\partial u_3}{\partial q_j})$$

$$K_f^t(2,j) = \frac{\partial f_t}{\partial q_j}(n_1 u_3 - n_3 u_1) + f_t(n_1 \frac{\partial u_3}{\partial q_j} - n_3 \frac{\partial u_1}{\partial q_j})$$

$$K_f^t(3,j) = \frac{\partial f_t}{\partial q_j}(n_2u_1 - n_1u_2) + f_t(n_2\frac{\partial u_1}{\partial q_j} - n_1\frac{\partial u_2}{\partial q_j})$$

$$K_f^t(i,j) = R_d\frac{\partial f_t}{\partial q_j}n_i, \quad i = 4 \sim 6, \tag{6.44}$$

$$C_f^t(1,j) = \mu_t c u_j(n_3u_2 - n_2u_3)$$

$$C_f^t(2,j) = \mu_t c u_j(n_1u_3 - n_3u_1)$$

$$C_f^t(3,j) = \mu_t c u_j(n_2u_1 - n_1u_2)$$

$$C_f^t(i,j) = c\mu_t R_d u_j n_i, \quad i = 4,5,6.j = 1,2,3. \tag{6.45}$$

Case 2: Dynamic analysis

In the case of dynamic analysis, the expression of the transversal friction force, equation (6.23), is more complicated than that of the static case. The internal force vector is:

$$\mathbf{g}_t^{int} = \begin{pmatrix} \mathbf{f}_t \\ \mathbf{m}_t \end{pmatrix} \tag{6.46}$$

where $\mathbf{f_t}$ and $\mathbf{m_t}$ are given by equations (6.23) and (6.24).

The stiffness matrix is:

$$K_f^t(i,j) = \frac{\partial \mathbf{g}_t^{int}}{\partial q_j} \tag{6.47}$$

where $i = 1 \sim 6, \quad j = 1 \sim 3.$

And the damping matrix is:

$$C_f^t(i,j) = \frac{\partial \mathbf{g}_t^{int}}{\partial \dot{q}_j} \tag{6.48}$$

where $i = 1 \sim 6, \quad j = 1 \sim 3.$

The explicit expression of the above stiffness and damping matrices have been derived by using the symbolic computation software Maple V (Maple V, 1993).

(d) $\mathbf{K_f^l}$ and $\mathbf{C_f^l}$

The internal force vector associated with the longitudinal friction force is obtained by combining the nodal force and moment:

$$\mathbf{g}_l = \begin{pmatrix} \mathbf{f}_l \\ \mathbf{m}_l \end{pmatrix} = \begin{pmatrix} S_l f_l n_1 \\ S_l f_l n_2 \\ S_l f_l n_3 \\ f_l S_l R_d(n_2u_3 - n_3u_2) \\ f_l S_l R_d(n_3u_1 - n_1u_3) \\ f_l S_l R_d(n_1u_2 - n_2u_1) \end{pmatrix} \tag{6.49}$$

The stiffness matrix is explicitly given by:

$$K_f^l(i,j) = \frac{\partial f_l}{\partial q_j} n_i S_l, \quad i,j = 1,2,3.$$

$$K_f^l(4,j) = \frac{\partial f_l}{\partial q_j} R_d S_l (n_2 u_3 - n_3 u_2) + f_l R_d S_l (n_2 \frac{\partial u_3}{\partial q_j} - n_3 \frac{\partial u_2}{\partial q_j})$$

$$K_f^l(5,j) = \frac{\partial f_l}{\partial q_j} R_d S_l (n_3 u_1 - n_1 u_3) + f_l R_d S_l (n_2 \frac{\partial u_1}{\partial q_j} - n_3 \frac{\partial u_3}{\partial q_j})$$

$$K_f^l(6,j) = \frac{\partial f_l}{\partial q_j} R_d S_l (n_1 u_2 - n_2 u_1) + f_l R_d S_l (n_2 \frac{\partial u_2}{\partial q_j} - n_3 \frac{\partial u_1}{\partial q_j}) \tag{6.50}$$

where

$$\frac{\partial f_l}{\partial q_j} = \mu_l (\frac{\partial f_e}{\partial q_j} + \frac{\partial f_d}{\partial q_j}) \tag{6.51}$$

The damping matrix is:

$$C_f^l(i,j) = \mu_l c S_l u_j n_i, \quad i,j = 1,3;$$

$$C_f^l(4,j) = \mu_l c S_l u_j R_d (n_2 u_3 - n_3 u_2)$$

$$C_f^l(5,j) = \mu_l c S_l u_j R_d (n_3 u_1 - n_1 u_3)$$

$$C_f^l(6,j) = \mu_l c S_l u_j R_d (n_1 u_2 - n_2 u_1) \tag{6.52}$$

6.4 BACKWARD WHIRL DUE TO BIT-HOLEWALL CONTACT

6.4.1 Assumptions and Simulation Conditions

The purpose of this section is to study the possibility of steady-state backward whirl due to bit holewall contact. To this end, following assumptions are made:

(1.) Only bit-holewall contact is taken into account. The other possible contacts between drill collar and holewall, stabilizer and holewall are all disregarded. These contacts will be studied in a forthcoming report.

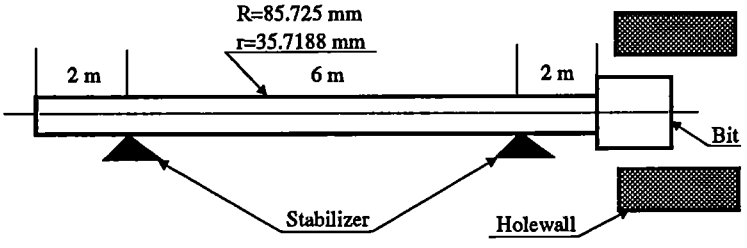

Fig.6.4: A BHA system

(2.) The stabilizer is assumed as a rigid supporter for simplicity. Its stiffness can be taken into account without any difficulty.

(3.) The axial vibration is not considered.

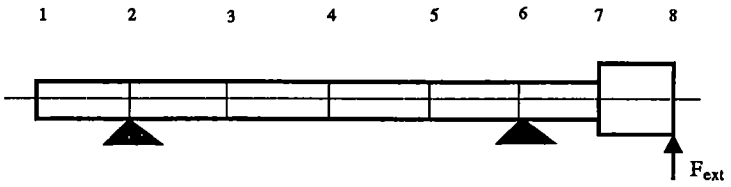

Fig.6.5: FE model for the BHA system

Fig.6.4 shows a BHA structure used for simulation. The geometry is also given in the figure. Fig.6.5 depicts the FEM model of the BHA system. The clearance is taken as 1 mm and the stiffness of the holewall is 5×10^7 N/m. The friction coefficient μ_t is taken as a variable parameter whose special value will be given in the corresponding figures.

Table 6.1: Eigenfrequencies (Hz) of the BHA system

Mode	ω_1	ω_2	ω_3	ω_4
Without contact	14.97	24.12	33.72	86.99
With contact	24.12	33.72	86.99	326.18

The modal properties of the BHA system are calculated by the module DYNAM of the Samcef software (Samtech, 1994). Table 6.1 lists the first 4 eigenvalues in the cases of with and without contact, respectively.

6.4.2 Steady-state Backward Whirl

The bit-holewall contact leads usually to synchronous whirl of the BHA. However, under certain conditions, such contact can lead to backward whirl, i.e., a rolling of the BHA along the inner surface of the holewall in the opposite direction of the BHA rotation. Fig.6.6 depicts an example of steady-state backward whirl due to bit-holewall contact. In the figure, the rotation speed $\omega = 3\ Hz$, the friction coefficient $\mu_t = 0.5$. The bit keeps always in contact with the inner surface of the holewall by applying an external force $F_{ext} = F_0 exp(i\omega_{ext})$.

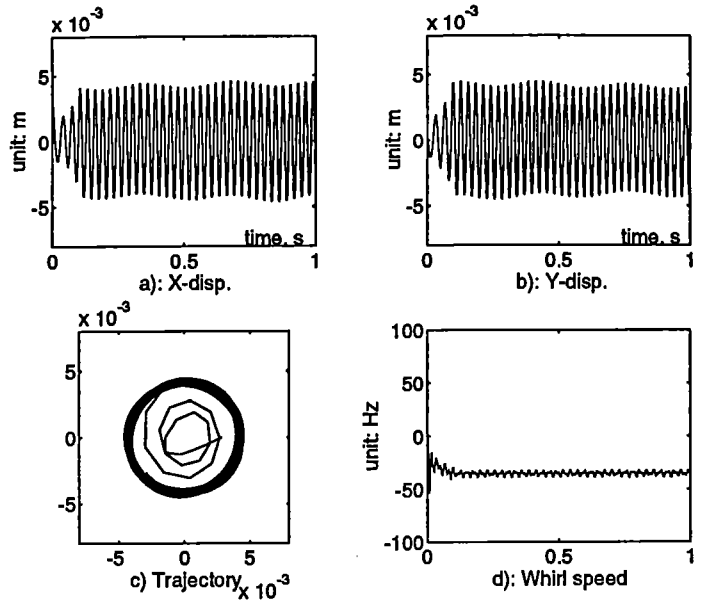

Fig.6.6: Steady-state backward whirl motion
$\mu_t = 0.5, \omega = 3Hz$

The influences of friction coefficient, the external exciting force, the contact damping, the elastic stiffness as well as the rotation speed of the BHA on the backward whirl motion are discussed below.

(a) Friction coefficient μ_t

The effects of friction coefficient μ_t on the backward whirl motion are shown in Fig.6.7 and Fig.6.8 in which the rotation speed $\omega = 3\ Hz$ and the clearance is $\Delta R = 1\ mm$. When $\mu_t = 0.3$, the motion is synchronous forward whirl (Fig.6.7a) with radius $r = 1.1\ mm$ (Fig.6.8a). Note that the whirl radius r is greater than the clearance ΔR. In other words, the bit is in contact with the holewall, but no backward whirl occurs.

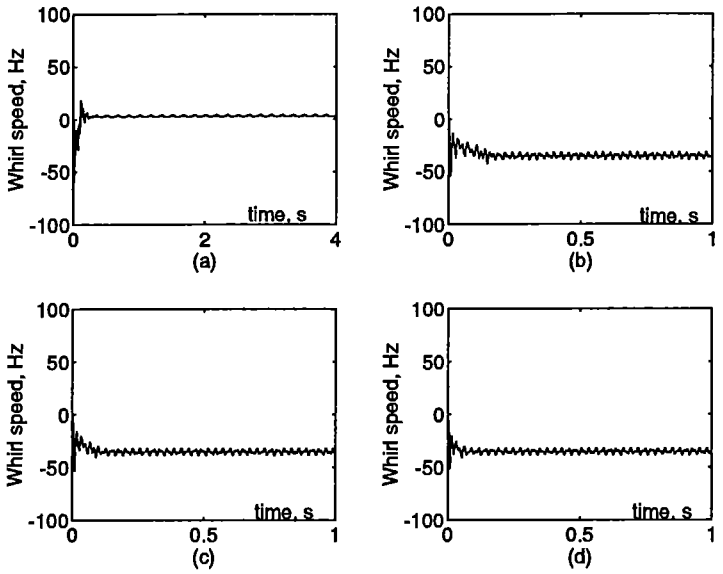

Fig.6.7: Influence of friction coefficient on the backward whirl frequency ($\omega = 3Hz$)
(a): $\mu_t = 0.3$, (b): $\mu_t = 0.45$. (c): $\mu_t = 0.5$. (d): $\mu_t = 0.6$.

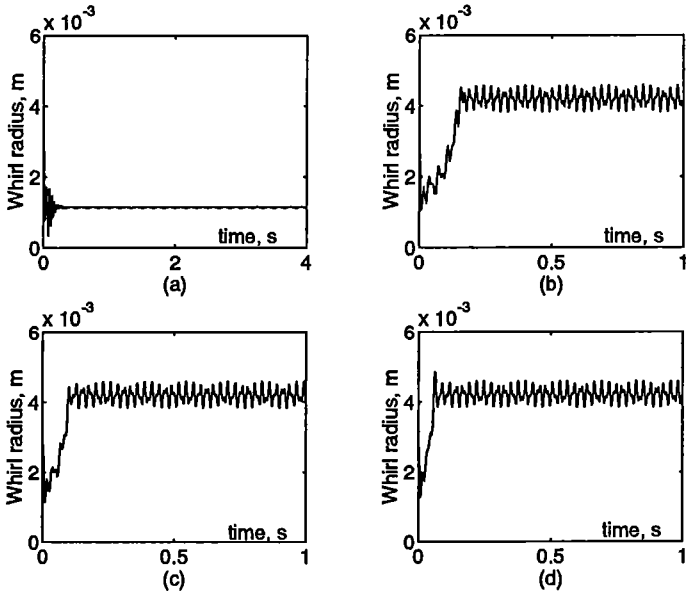

Fig.6.8: Influence of friction coefficient on the backward whirl radius ($\omega = 3Hz$)
(a): $\mu_t = 0.3$, (b): $\mu_t = 0.45$. (c): $\mu_t = 0.5$. (d): $\mu_t = 0.6$.

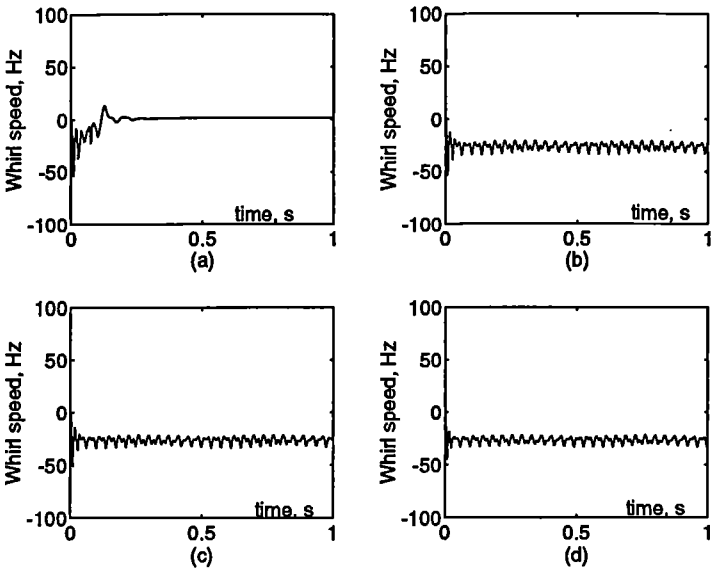

Fig.6.9: Influence of friction coefficient on the backward whirl frequency ($\omega = 1Hz$)
(a): $\mu_t = 0.3$, (b): $\mu_t = 0.45$. (c): $\mu_t = 0.5$. (d): $\mu_t = 0.6$.

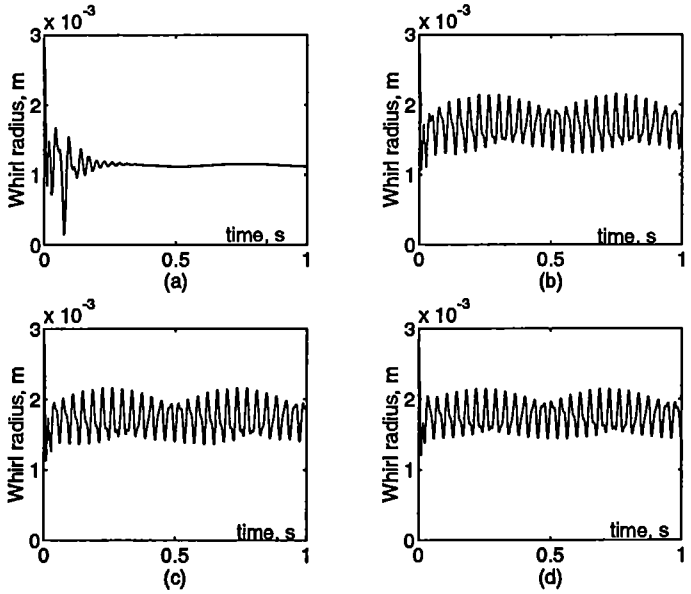

Fig.6.10: Influence of friction coefficient on the backward whirl radius ($\omega = 1Hz$)
(a): $\mu_t = 0.3$, (b): $\mu_t = 0.45$. (c): $\mu_t = 0.5$. (d): $\mu_t = 0.6$.

If the friction coefficient is increased to $\mu_t = 0.45$, the backward whirl motion with a constant speed (Fig.6.7b) and a constant radius (Fig.6.8b) occurs. The radius in backward whirl (4.2

mm) is much larger than that in forward whirl (1.1 mm). For further increase of the friction coefficient to $\mu_t = 0.5$ and $\mu_t = 0.6$, the radius and speed of the backward whirl motion do not change. Similar observations can also be made when we change the rotation speed to $\omega = 1\ Hz$ (Fig.6.9 and 6.10).

These observations depict that (1) There is a critical friction coefficient below which synchronous forward whirl occurs and above which backward whirl occurs. (2) Once initiated, the backward whirl speed and radius do not depend on the value of the friction coefficient. These two facts coincide with the conclusions made in chapter 5 where a lumped model is used. The first fact may explain why the bit with low friction pad does not move backwards in most cases.

(b) External force

In order to ensure that the bit is always in contact with the holewall, it is necessary to apply an external force on the bit in the simulation. In practice, this force may be generated by bit/formation interaction. In fact, the side force generated by bit/formation interaction during drilling may be as high as 5000 $Newton$ depending on the bit type and the operating conditions (Chen and Géradin, 1993a). For the sake of simplicity and in order to simulate the bit side force, the assumed external force is taken the form

$$F_{ext} = F_0 exp(i\omega_{ext} t) \tag{6.53}$$

where F_0 is amplitude and ω_{ext} is angular frequency.

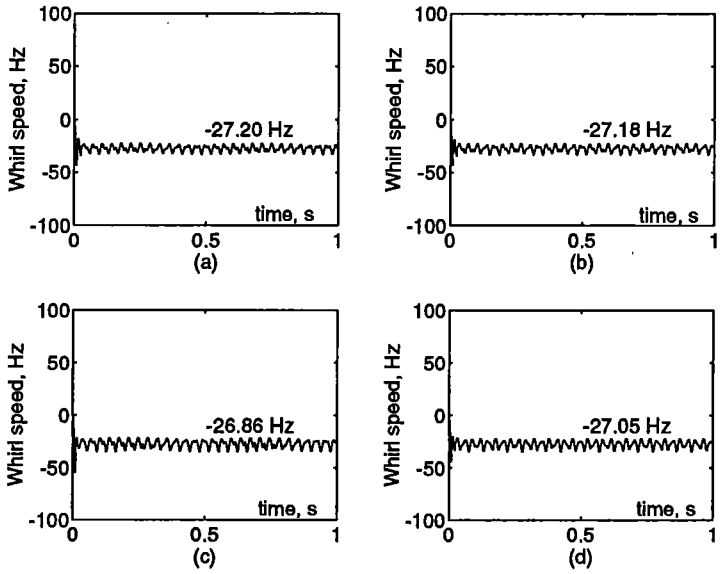

Fig.6.11: Influence of external force type on the backward whirl frequency ($\omega = 1Hz$)
(a): $F_0 = 3000N$, $\omega_{ext} = 1Hz$. (b): $F_0 = 3000N$, $\omega_{ext} = 3Hz$.
(c): $F_0 = 4000N$, $\omega_{ext} = 1Hz$. (d): $F_0 = 3000N$, $\omega_{ext} = 7Hz$.

The angular frequency ω_{ext} is usually not the same as the rotation speed of the bit except the case of bit unbalance force.

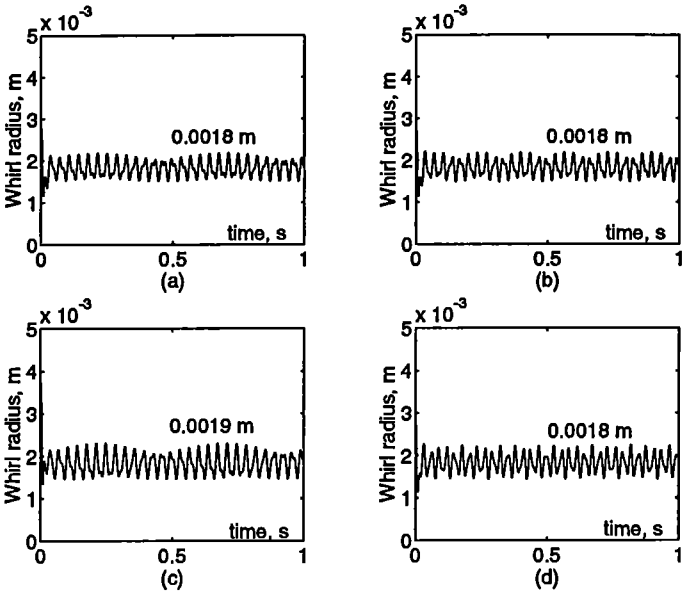

Fig.6.12: Influence of external force type on the backward whirl radius ($\omega = 1Hz$)
(a): $F_0 = 3000N$, $\omega_{ext} = 1Hz$. (b): $F_0 = 3000N$, $\omega_{ext} = 3Hz$.
(c): $F_0 = 4000N$, $\omega_{ext} = 1Hz$. (d): $F_0 = 3000N$, $\omega_{ext} = 7Hz$.

Fig.6.11 and 6.12 show the influence of the external forces on the backward whirl motion. Four different types of external force types are considered with different amplitudes and frequencies. It is seen that in spite of the external force type, the backward whirl motion has almost the same speed and the same radius. The small difference may be due to the numerical accuracy. Therefore, the external force has no influence on the backward whirl motion. The only requirement on the external force is that its amplitude must be large enough in order to put the bit in contact with the holewall.

(c) Contact damping

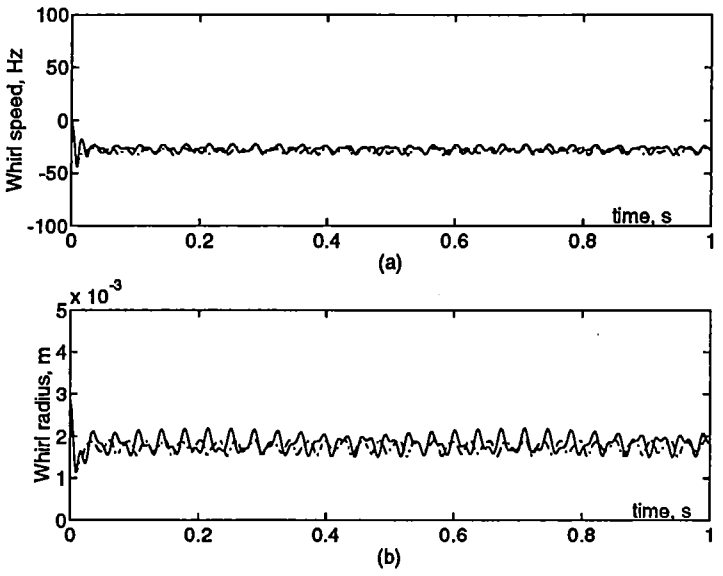

Fig.6.13: Influence of contact damping on backward whirl motion
$\omega = 1Hz$, $\mu_t = 0.6$, —: c=0; -.-.: $c = 1.5 \times 10^5 sN/m$

Fig.6.13 shows the influence of the contact damping on the backward whirl speed and radius. In the figure, the contact damping is assumed to be 1.5×10^5 sN/m and the stiffness is 1.5×10^7 N/m. The contact damping has almost no influence on the whirl speed (Fig.6.13a) but reduces a slightly the whirl radius.

(d) Contact stiffness

The value of the contact stiffness k_e is dependent mainly on the kind of formation being drilled. k_e is lower for soft formation and higher for hard formation.

In the drilling practice, the bit may have opportunities to meet many kinds of formation. To simulate this situation, simulations have been performed for the contact stiffness $k_e = 10^4$, 10^6, 10^7, $10^8 N/m$, respectively. In all these cases, the friction coefficient μ_t is taken as 0.5. The shaft is rotating at speed $\omega = 1$ Hz and the clearance is 1 mm.

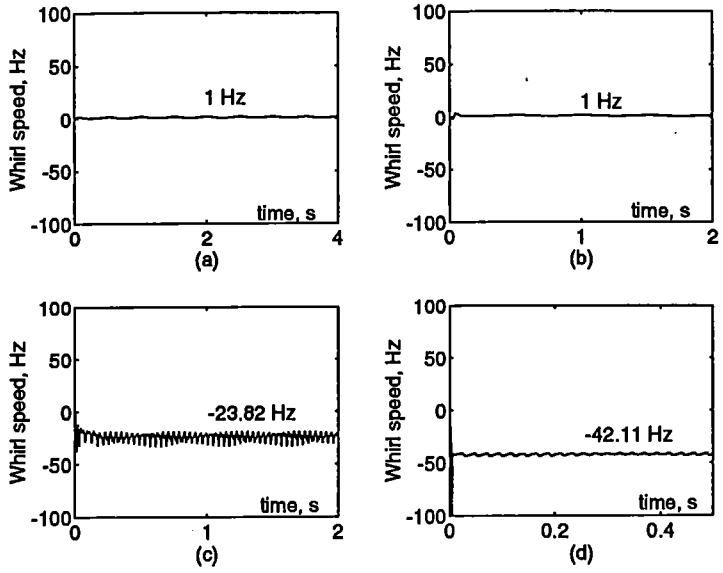

Fig.6.14: Influence of contact stiffness on whirl speed
(a): $k_e = 10^4 N/m$; (b): $k_e = 10^6 N/m$; (c): $k_e = 10^7 N/m$; (d): $k_e = 10^8 N/m$;

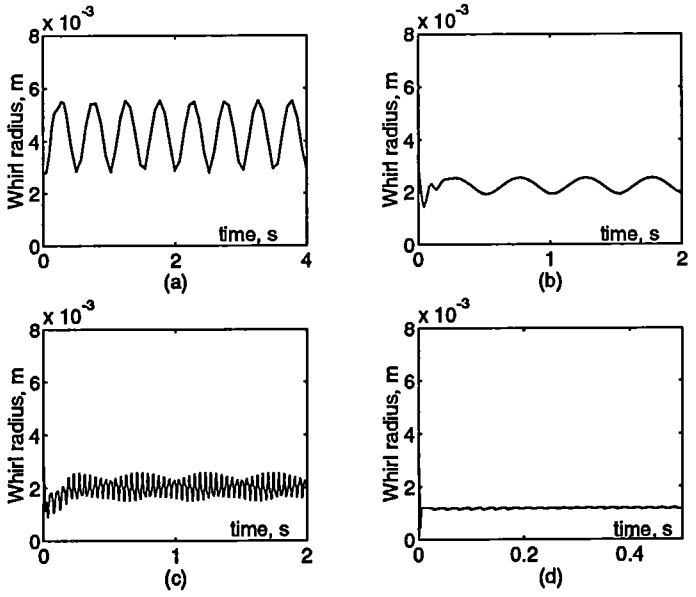

Fig.6.15: Influence of contact stiffness on whirl radius
(a): $k_e = 10^4 N/m$; (b): $k_e = 10^6 N/m$; (c): $k_e = 10^7 N/m$; (d): $k_e = 10^8 N/m$;

Fig.6.14 and 6.15 show respectively the whirl speed and radius under the condition of different contact stiffnesses. For the stiffness $k_e = 10^4 N/m$ and $k_e = 10^6 N/m$ (Fig.6.14 a,b), the whirl is forward ($\Omega > 0$). This is due to the fact that the friction force induced by the contact is not enough to move the shaft backwards when k_e is low. For the stiffness

$k_e = 10^7 N/m$ and $k_e = 10^8 N/m$ (Fig.6.14 c,d), the whirl is backward ($\Omega < 0$). It means that there is a critical stiffness (for a given friction coefficient μ_t) below which forward whirl occurs and above which backward whirl occurs. This fact may explain why backward whirl occurs often in the cases of hard formations. Another observation is that with the increase of the stiffness, the backward whirl speed increases. This is because the eigenfrequencies of the BHA system under contact have been changed. This means also that the backward whirl speed induced by the contact is dependent on the eigen-properties of the BHA system.

(e) Rotation speed

Rotation speed ω of the BHA is one of the two most important control parameters in the drilling field (the other is WOB). Fig.6.16 depicts the influence of the rotation speed of the BHA on the backward whirl speed and radius, respectively. In the figure, $k_e = 1.5 \times 10^7$, $\mu_t = 0.5$, $\Delta R = 1mm$. During the simulation, we find that it is very difficult to generate backward whirl motion if the rotation speed is lower than 1 Hz. Once initiated, the speed of the backward whirl is greater than the lowest bending eigenfrequency of the BHA system. More clearly, there is a minimum backward whirl speed which is near to but greater than the lowest bending eigenfrequency of the BHA system. This fact is not predicted by the single mass model given in Chapter 5. However, the fact agrees with the experimental observations made by Lingerner (1990) and Crandall (1990) for backward whirl due to rotor-stator contact.

With the increase of the rotation speed, the backward whirl radius $r(\omega)$ increases proportionally. A least square fitting has been made for the relationship between the rotation speed and the whirl radius. The function obtained is:

$$r(\omega) = 1.2338\omega + 0.4908, \quad mm \tag{6.54}$$

Once the backward whirl is initiated, its speed always follows the following relation:

$$\Omega(\omega) = \frac{-R_d\omega}{r(\omega)} \tag{6.55}$$

where R_d is the disk radius. In the practice, a very large penetration into the formation for the bit is very difficult. After the penetration is large enough, slide must occur at the contact point. Therefore, the whirl speed will be smaller than the value predicted by equation (6.55). In this sense, the backward whirl speed is also limited for the continuous model. However, which parameters determine the maximum backward whirl speed is not clear so far.

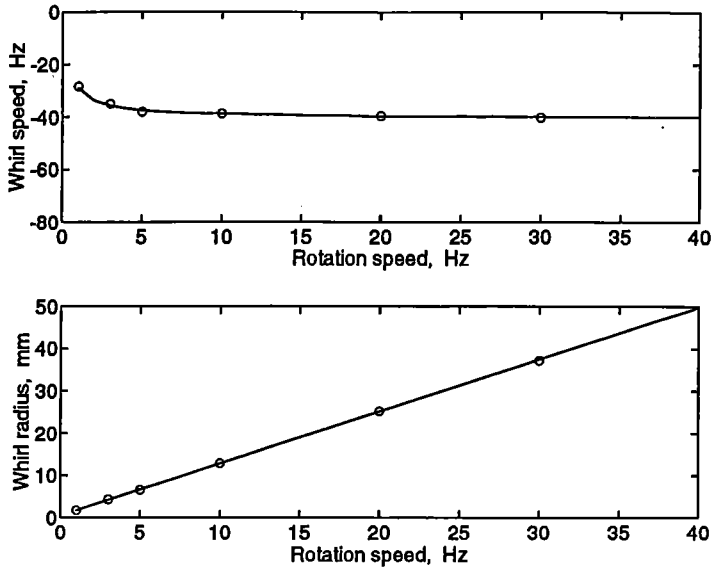

Fig.6.16: Influence of rotation speed on the backward whirl motion
—: FEM results; ooo: fitting results; $k_e = 1.5 \times 10^7$, $\mu_t = 0.5$, $\Delta R = 1mm$

6.5. CONCLUSIONS

In this chapter the backward whirl due to bit-holewall contact is investigated by finite element model. The bit-holewall contact is modeled by a special contact element which can be used not only for static but also for dynamic analysis. The following conclusions may be made:

(1) The bit-holewall contact can lead to steady-state backward whirl under certain conditions. These conditions include a large bit side force and friction coefficient. However, once initiated, the backward whirl motion does not depend on the values of side force amplitude and friction coefficient.

(2) There is a critical friction force below which forward whirl occurs and above which backward whirl occurs. In other words, there is a critical friction coefficient (for a given formation stiffness) or a critical formation stiffness (for a given friction coefficient). This fact may explain why a PDC bit with low friction pad can resist backward whirl and why backward whirl occurs often in the hard formations.

The above conclusions agree with the conclusions made in chapter 5.

(3) Once initiated, the backward whirl frequency is greater than the lowest bending eigenfrequency of the BHA system in the case of contact. In other words, there is a lowest backward whirl speed which is near to but greater than the first bending eigenfrequency of the system. This fact is not predicted by the single mass model given in chapter 5.

(4) The backward whirl radius is almost proportional to the rotation speed. However the backward whirl speed seems to be limited by a maximal value (Fig.6.16). After the whirl radius is large enough, slide at the contact point must occur. It is because a very large penetration into the formation for the bit is difficult in practice.

The contact element developed in this chapter may also be used for analysis of rotor-bearing systems such as the whirling motion due to rotor-stator contact.

CHAPTER 7:

EXPERIMENTAL IDENTIFICATION OF DOWNHOLE BIT WHIRL DURING DRILLING

7.1. INTRODUCTION

As discussed in chapter 5, bit whirl and particularly bit backward whirl, has an adverse effect on the rate of penetration (ROP) and causes heavy dynamic loading of the cutters in general and of the gauge cutters in particular. This heavy dynamic loading of the cutters reduces the overall bit life, especially in harder formations.

Recently, there has been much interest in the elimination of the bit backward whirl during drilling. One way is to use anti-whirl PDC bit (Brett et al, 1989, Sinor, 1990, 1992, Clegg, 1992). However, both laboratory and field tests have shown that the anti-whirl PDC bit may still whirl under certain conditions depending on the weight on bit (WOB) applied, the bit rotation speed (RPM) and the actual hole size drilled (Langeveld, 1991, Shyu, 1989).

Another more popular way to eliminate the backward whirl is to change the WOB and/or the RPM when whirl is initiated. Hence, the identification of bit whirl during drilling becomes a critical issue.

There are three main difficulties in the identification of bit whirl during drilling. The first one is that the bit whirl can not be detected directly at the surface as mentioned in chapter 4. The second one is that the sensors must be mounted on the rotating drillstring or on the bit body. This makes it complicated to obtain directly the bit center trajectory which is very useful in the identification of bit whirl. The third one is that there are many excitation sources acting on the drillstring and on the bit due to the dynamic interaction of the bit/formation.

Some noticeable work has been done in the bit whirl identification using measured bending moment and acceleration (Vandiver et al, 1988, Shyu, 1989) or using the hole pattern drilled (Brett et al, 1989). However, these attempts were focused only on the bit whirl frequency identification. In fact, not only the whirl frequency but also the whirl radius (or hole radius), the bit center trajectory and the instantaneous bit rotation speed are important in order to eliminate the whirl motion during drilling.

In this chapter several methods have been developed to identify bit whirl motion (including whirl frequency, whirl radius, bit rotation speed, bit center trajectory) using accelerometers and contact sensors. The contact sensors are used here to measure the distance between the bit gauge and the hole-wall. Two identification examples are given using laboratory experimental data. The analysis shows that in most cases the contact sensors can give more reliable results than the accelerometers because the later are considered to be too sensitive to other excitations.

7.2 BACKGROUND THEORY

According to the bit whirl kinematics described in chapter 5, the coordinates of any point on the bit body can be expressed in the absolute frame $X_hO_hY_h$ (Fig.5.2):

$$\begin{aligned} X_h &= \Delta R\cos(\Omega t) + r_c\cos(\theta_c + \omega t) \\ Y_h &= \Delta R\sin(\Omega t) + r_c\sin(\theta_c + \omega t) \end{aligned} \tag{7.1}$$

where ΔR is called whirl radius. The first part of equation (7.1) is the bit center trajectory which is a circle with ΔR as its radius and Ω as its angular frequency.

The corresponding acceleration is :

$$\begin{aligned} \ddot{X}_h &= -\Delta R\Omega^2\cos\Omega t - r_c\omega^2\cos(\theta_c + \omega t) \\ \ddot{Y}_h &= -\Delta R\Omega^2\sin\Omega t - r_c\omega^2\sin(\theta_c + \omega t) \end{aligned} \tag{7.2}$$

The bit center acceleration, or bit acceleration, is obtained by inserting $r_c = 0$ into equation (7.2):

$$\begin{aligned} \ddot{X}_{hbit} &= -\Delta R\Omega^2\cos\Omega t \\ \ddot{Y}_{hbit} &= -\Delta R\Omega^2\sin\Omega t \end{aligned} \tag{7.3}$$

Its amplitude is

$$a_{bit} = \sqrt{\ddot{X}_{hbit}^2 + \ddot{Y}_{hbit}^2} = \Delta R\Omega^2 \tag{7.4}$$

Note that equations (7.2) express the acceleration components of any point on bit body in the fixed coordinate system $X_hO_hY_h$. On the other hand, the acceleration may also be projected on the bit rotating coordinate system $X_bO_bY_b$:

$$\begin{aligned} \ddot{X}_b &= -\Delta R\Omega^2\cos(\omega - \Omega)t - r_c\omega^2\cos\theta_c \\ \ddot{Y}_b &= \Delta R\Omega^2\sin(\omega - \Omega)t - r_c\omega^2\sin\theta_c \end{aligned} \tag{7.5}$$

There is no difficulty to verify that equation (7.5) and equation (7.2) express the same absolute acceleration of the same point on the bit body. However, the acceleration projected on the bit coordinate system can be directly measured by mounting the accelerometer on the bit body.

The bit center acceleration projected on $X_bO_bY_b$ is obtained by inserting $r_c = 0$ into equation (7.5):

$$\begin{aligned} \ddot{X}_{bbit} &= -\Delta R\Omega^2\cos(\omega - \Omega)t \\ \ddot{Y}_{bbit} &= \Delta R\Omega^2\sin(\omega - \Omega)t \end{aligned} \tag{7.6}$$

Its amplitude is:

$$a_{bit} = \sqrt{\ddot{X}_{bbit}^2 + \ddot{Y}_{bbit}^2} = \Delta R\Omega^2 \tag{7.7}$$

From above equations it is noted that the bit whirl motion can be fully described by three parameters (we call them latter whirl parameters):

(a) bit rotation speed ω;

(b) bit whirl speed Ω;

(c) whirl radius ΔR.

7.3. BIT WHIRL IDENTIFICATION BY ACCELEROMETERS

7.3.1. Bit rotation speed ω

According to equation (7.5), two accelerometers at the two opposite locations ($\theta_c = 0^0$ and $\theta_c = 180^0$) on the bit body should measure the following acceleration components in the rotating bit coordinate system:

$$\begin{aligned} a_{x1} &= -\Delta R\Omega^2 \cos(\omega - \Omega)t - R_1\omega^2 \\ a_{x2} &= -\Delta R\Omega^2 \cos(\omega - \Omega)t + R_1\omega^2 \end{aligned} \tag{7.8}$$

Where R_1 is the radial position of the accelerometer in the bit coordinate system.

From equation (7.8), we obtain the bit rotation speed:

$$\omega = \sqrt{\frac{a_{x2} - a_{x1}}{2R_1}} \tag{7.9}$$

It means that only two accelerometers placed at opposite locations are sufficient to obtain the bit instantaneous rotation speed ω.

7.3.2. Bit whirl speed Ω

Method 1: Frequency domain

From equation (7.8) it is seen that the accelerometer signal should contain the angular frequency $(\omega - \Omega)$. Hence by performing the autospectrum of either a_{x1} or a_{x2}, one can obtain the frequency difference $(\omega - \Omega)$, and thus determine the whirl speed Ω.

However, this method may be difficult to apply to the case of synchronous forward whirl because $(\omega - \Omega) = 0$. In that case method 2 may be useful to overcome this difficulty.

Method 2: Time domain

The bit center acceleration in the X_b direction (in $X_bO_bY_b$ system) may be obtained from equation (7.8) as follows:

$$a_{xb} = (a_{x1} + a_{x2})/2 = -\Delta R\Omega^2 \cos(\omega - \Omega)t \tag{7.10a}$$

The bit center acceleration in the Y_b direction (in $X_bO_bY_b$ system) is obtained directly from another radial accelerometer located on the bit center ($r_c = 0$ in equation 7.5) :

$$a_{yb} = \Delta R\Omega^2 \sin(\omega - \Omega)t \tag{7.10b}$$

Finally we have the unwrapped phase angle:

$$\phi(t) = \arctan \frac{a_{yb}}{a_{xb}} + \phi_0 = (\omega - \Omega)t + \phi_0 \tag{7.11a}$$

and its derivative:

$$\frac{d\phi}{dt} = \omega - \Omega \tag{7.11b}$$

where ϕ_0 is a constant depending on initial conditions.

Hence, $(\omega - \Omega)$ can be deduced by performing a linear least square fitting on $\phi(t)$. If the bit rotation speed ω is known, Ω can be determined. Theoretically the unwrapped phase angle should be constant in the case of synchronous forward whirl.

7.3.3 Whirl radius ΔR

According to equations (7.4) or (7.7), the bit center acceleration should be:

$$a_b = \Delta R\Omega^2 \tag{7.12}$$

Hence, we have:

$$\Delta R = a_b/\Omega^2 \tag{7.13}$$

where a_b is measured by:

$$a_b = \sqrt{a_{xb}^2 + a_{yb}^2} \tag{7.14}$$

7.3.4. Bit center trajectory

The bit center acceleration components obtained by the accelerometers are described by equation (7.10). Performing twice time integration on a_{xb} and a_{yb} under the zero initial conditions we obtain:

$$x_b = \frac{\Delta R\Omega^2}{(\omega - \Omega)^2} \cos(\omega - \Omega)t \tag{7.15a}$$

$$y_b = \frac{-\Delta R\Omega^2}{(\omega - \Omega)^2} \sin(\omega - \Omega)t \tag{7.15b}$$

However, the absolute bit center trajectory is the first part of equation (7.1), i.e.:

$$\begin{aligned} X_h^b &= \Delta R \cos(\Omega t) \\ Y_h^b &= \Delta R \sin(\Omega t) \end{aligned} \tag{7.16}$$

The difference between equation (7.15) and (7.16) means that one can not directly obtain the actual bit center trajectory by twice integrating the accelerations a_{xb} and a_{yb} measured by the accelerometers mounted on the rotating bit body.

7.3.5. Practical considerations

In the drilling field, even under good controlled laboratory conditions, the outputs of accelerometers may be polluted by noise and other excitations, particularly in the case of backward whirl in which the bit shocks may be dominant.

Taking the noise and other excitations into consideration, the outputs of accelerometers should be expressed as follows:

$$\begin{aligned} a_{x1} &= -\Delta R\Omega^2 cos(\omega - \Omega)t - R_1\omega^2 + a_n \\ a_{x2} &= -\Delta R\Omega^2 \ cos(\omega - \Omega)t + R_1\omega^2 + b_n \\ a_y &= \Delta R\Omega^2 \sin(\omega - \Omega)t + c_n \end{aligned} \tag{7.17}$$

Where a_n,b_n,c_n represent the terms induced by the noises and all other excitations.

If the outputs of accelerometers are of shock type, the terms of a_n,b_n,c_n in equations (7.17) may be dominant. Without any further treatment of raw data, the results obtained by the above methods may be questionable. In practice, the following steps should be performed to treat with the raw data provided by accelerometers:

(1) For the estimation of the bit rotation speed ω, the high frequency contents of the signals delivered by the accelerometers should be filtered using a digital lowpass filter before using equation (7.9). This is because in equation (7.17) the term corresponding to the bit rotation speed ω, i.e. $R_1\omega^2$ is theoretically a constant, thus with zero frequency. In practice, it is unlikely for the bit rotation speed to vary with time at high frequency. Hence, the cutoff frequency may be taken very low for this purpose.

(2) For the estimation of frequency difference $(\omega - \Omega)$ and whirl radius ΔR, a lowpass filter should also be used to filter the high frequency caused by other excitations. In this case, however, the cutoff frequency should be taken higher than the frequency $\omega - \Omega$.

(3) Before using equation (7.13) to estimate the whirl radius ΔR, the constant terms contained in a_{xb} and in a_{yb} (equation 7.10) should be taken out as follows:

$$a_{xb} = a_{xb} - mean(a_{xb}) \tag{7.18a}$$

$$a_{yb} = a_{yb} - mean(a_{yb}) \tag{7.18b}$$

It is because that the geometry position of the accelerometers may have errors. This step is very important because any error of a_b will lead to the same order error on ΔR.

(4) Before integrating twice the bit center acceleration components a_{xb}, a_{yb} to obtain the bit center trajectory (equation 2.15) it is necessary to use the so called time domain average technique to take out the random errors (white noise) contained in the raw data.

Since the frequency of white noise cover a very wide frequency range, the lowpass filter is not able to filter it completely.

The principle of the time domain average technique is described as follows.

Let $x(t)$ be the output of the accelerometer. It consists of a periodic signal $f(t)$ and white noise $n(t)$, or:

$$x(t) = f(t) + n(t) \tag{7.19}$$

Dividing the raw data $x(t)$ into N intervals, written as $x_1(t), x_2(t), ..., x_n(t)$, the length of each interval, T, is the periodicity of $f(t)$. By summing all of the N intervals, and noting that the white noise $n(t)$ is not correlated with $x(t)$, we have:

$$x(t_i) = Nf(t_i) + \sqrt{N}n(t_i) \tag{7.20a}$$

Its average is:

$$y(t_i) = f(t_i) + n(t_i)/\sqrt{N} \tag{7.20b}$$

Equation(19b) means that after performing the time average the white noise contained in the raw data is decreased by $\sqrt{N}$ times. If we know exactly the periodicity of $f(t)$, we may track it from the raw data.

7.4. BIT WHIRL IDENTIFICATION BY CONTACT SENSORS

7.4.1. Working principle of contact sensor

The contact sensor has been recently developed by DBS and is specially used for bit whirl identification.

The contact sensor is of micro resistivity type with DC signal excitation and has the shape of a thin disk of radius 5 mm. A carbide steel cylinder with a beveled bottom is used for construction of the central contact. Zirconia serves as a rugged material to insulate the contact sensor from the bit body. The zirconia insulator is also beveled on the bottom and is pressed fit into the bit body with an "O" ring contacting the beveled portion. Then the contact sensor is pressed fit into the zirconia insulator. The bit body serves as an electrical return for the contact sensor.

The contact sensor itself may be considered as a perfect conductor and its surrounding medium (usually oil based mud in drilling practice) may have very large resistivity (may be

regarded as infinite). On the other hand, most of the formation resistivities are in the range $1 \sim 20$ Ohms.

Based on these facts, the contact sensor works as an open circuit until it contacts the formation. In other words, if no contact occurs between contact sensor and holewall, the contact sensor will theoretically have no output. In practice, because the resistivity of the mud is not infinite, the contact sensor will still have some output even in the case of no contact. The relationship between the contact sensor output and the distance is strongly nonlinear. Fig.7.1 depicts a calibration curve for the contact sensor.

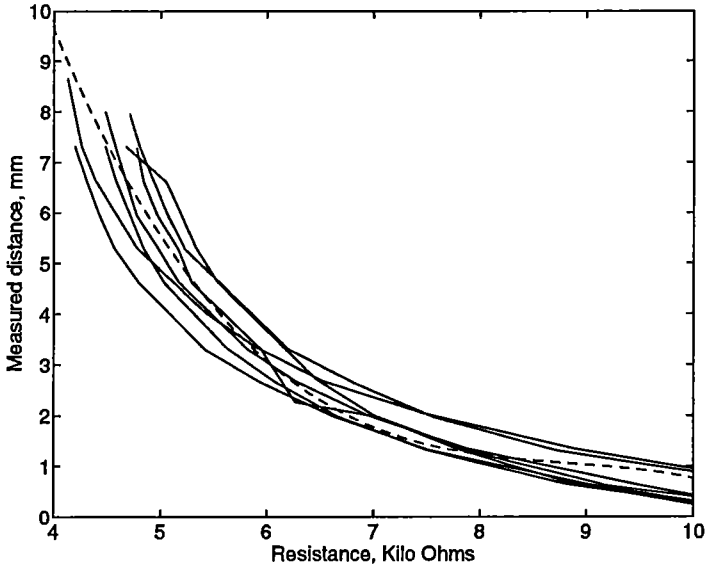

Fig.7.1: Calibration curve of contact sensor
——: Experimental data; – – –: Fitting curve

7.4.2. Bit whirl speed Ω

The number of hole lobes generated by the whirling bit is obtained in chapter 5:

$$N = abs(\Omega/\omega - 1) \tag{5.9}$$

If N_0 represents the hitting frequency, which is defined as the number of the bit gauge hitting the hole wall per second, then:

$$N = 2\pi N_0/\omega \tag{7.21}$$

In the case of backward whirl, Ω is negative compared to ω, so we finally have:

$$\omega - \Omega = 2\pi N_0 \tag{7.22}$$

Equation (7.22) tells us that the output signal of contact sensor should contain the frequency $(\omega - \Omega)$. Hence, N_0 may be estimated directly from the spectrum of output of contact sensors. If the bit rotation speed ω is known, Ω can be deduced.

7.4.3. Whirl radius ΔR and bit center trajectory

Fig.5.2 of chapter 5 is repeated here in order to show clearly the identification procedure.

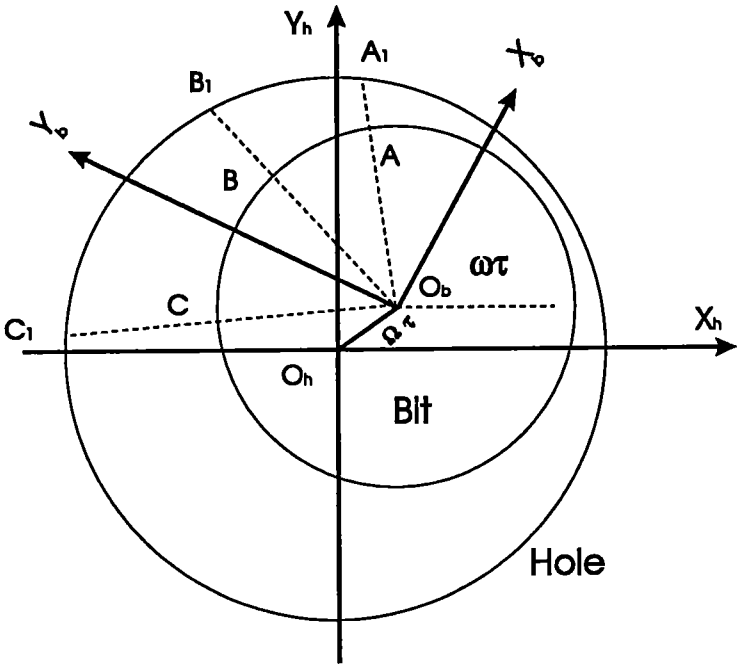

Fig.5.2: Bit whirl motion

In the above figure, A, B, C represent three contact sensors on the bit body and A_1, B_1, C_1 are three corresponding points on the hole-wall at time t. The distance of AA_1, BB_1 and CC_1 may be measured by the contact sensors. In the bit coordinate system the points A_1, B_1, C_1 have the following coordinates:

$$\begin{aligned} X_{A1} &= (R_b + AA_1)\cos\alpha_a \\ Y_{A1} &= (R_b + AA_1)\sin\alpha_a \\ X_{B1} &= (R_b + BB_1)\cos\alpha_b \\ Y_{B1} &= (R_b + BB_1)\sin\alpha_b \\ X_{C1} &= (R_b + CC_1)\cos\alpha_c \\ Y_{C1} &= (R_b + CC_1)\sin\alpha_c \end{aligned} \tag{7.23}$$

where R_b is the bit radius and α_a, α_b and α_c are the angles of contact sensors in bit coordinate system.

The three points A_1, B_1, C_1 determine a circle with the hole center O_h. Let (X_o, Y_o) be the hole center coordinate in $X_bO_bY_b$ system and R_h be the hole radius, then (X_o, Y_o) and R_h can be obtained by solving the following equations:

$$\begin{pmatrix} 2X_{A1} & 2Y_{A1} & -1 \\ 2X_{B1} & 2Y_{B1} & -1 \\ 2X_{C1} & 2Y_{C1} & -1 \end{pmatrix} \begin{pmatrix} X_o \\ Y_o \\ q \end{pmatrix} = \begin{pmatrix} X_{A1}^2 + Y_{A1}^2 \\ X_{B1}^2 + Y_{B1}^2 \\ X_{C1}^2 + Y_{C1}^2 \end{pmatrix} \tag{7.24}$$

And the hole radius R_h is obtained:

$$R_h = \sqrt{X_o^2 + Y_o^2 - q} \tag{7.25}$$

The whirl radius ΔR is

$$\Delta R = \sqrt{X_o^2 + Y_o^2} \tag{7.26}$$

It means if we could stay at the bit center we would see that the hole center rotates around bit center O_b with radius ΔR and angular frequency $(\omega - \Omega)$. The hole center trajectory seen from the bit center is described by $(X_o(t), Y_o(t))$. In the case of synchronous forward whirl, the hole center trajectory become a fixed point in bit coordinate system $X_bO_bY_b$ because its angular frequency $(\omega - \Omega)$ equals to zero. The absolute bit center trajectory will follow the same path as $(X_o(t), Y_o(t))$ but with the angular frequency Ω. Hence we should have

$$\phi(t) = (\omega - \Omega)t + \phi_0 = \arctan(Y_o/X_o) \tag{7.27}$$

It is now also possible to obtain the whirl frequency by equation (7.27).

The above analysis shows that if the hole section is a perfect circle, three contact sensors are enough to identify the whirl parameters. However, more than three contact sensors are usually recommended in order to improve the identification results.

Assuming that the number of contact sensors is m, then we have the following equation similar to equation (7.24):

$$\begin{pmatrix} 2X_{A1} & 2Y_{A1} & -1 \\ 2X_{B1} & 2Y_{B1} & -1 \\ 2X_{C1} & 2Y_{C1} & -1 \\ \cdots & \cdots & \cdots \\ 2X_{m1} & 2Y_{m1} & -1 \end{pmatrix} \begin{pmatrix} X_o \\ Y_o \\ q \end{pmatrix} = \begin{pmatrix} X_{A1}^2 + Y_{A1}^2 \\ X_{B1}^2 + Y_{B1}^2 \\ X_{C1}^2 + Y_{C1}^2 \\ \cdots \\ X_{m1}^2 + Y_{m1}^2 \end{pmatrix} \tag{7.28a}$$

Equation (7.28a) may be simply written in the form:

$$[A]_{m\times 3} X_{3\times 1} = b_{3\times 1} \tag{7.28b}$$

The least square solution of equation (7.28) is

$$X = ([A]^T[A])^{-1}[A]^T b \tag{7.29}$$

Equation (7.29) may give higher accuracy of the estimated whirl parameters than equation (7.24).

7.5. EXPERIMENTAL CONDITIONS AND IDENTIFICATION EXAMPLES

7.5.1. Experimental conditions

(a) Bit type: Antiwhirl PDC bit, PD5AW from DBS;

(b) Formation type: Belgian limestone;

(c) Sensor locations on the bit body: 8 contact sensors and 3 accelerometers are used. Their locations on the bit body are shown in Fig.7.2. The contact sensors No. 1 is located on the low friction pad. The accelerometers used can measure both DC and AC components;

(d) Operating conditions: for test 1, $RPM = 270rpm$ and $WOB = 8000$ kg; for test 2, $RPM = 470rpm$ and $WOB = 2000$ kg;

(e) Drilling machine with maximal WOB=50000 kg.

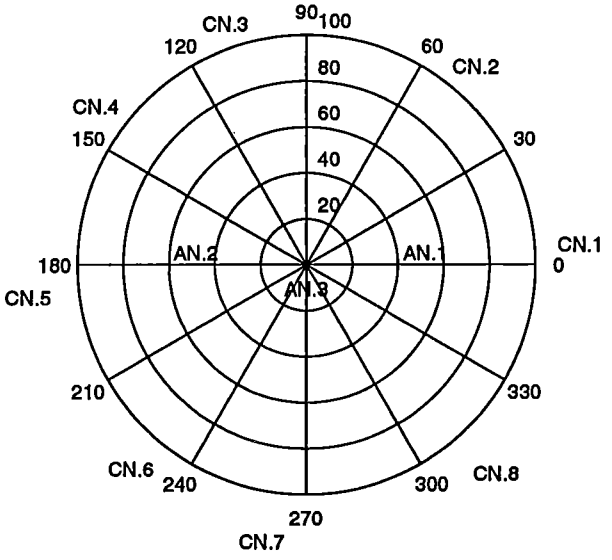

Fig.7.2: Locations of contact sensors and accelerometers

7.5.2 Identification examples

Example 1: Synchronous forward whirl (test 1)

Fig.7.3 shows the identification results using accelerometer signals. The estimated bit rotation speed is about 271.5 *rpm* which is very close to the directly measured value (270 *rpm*).

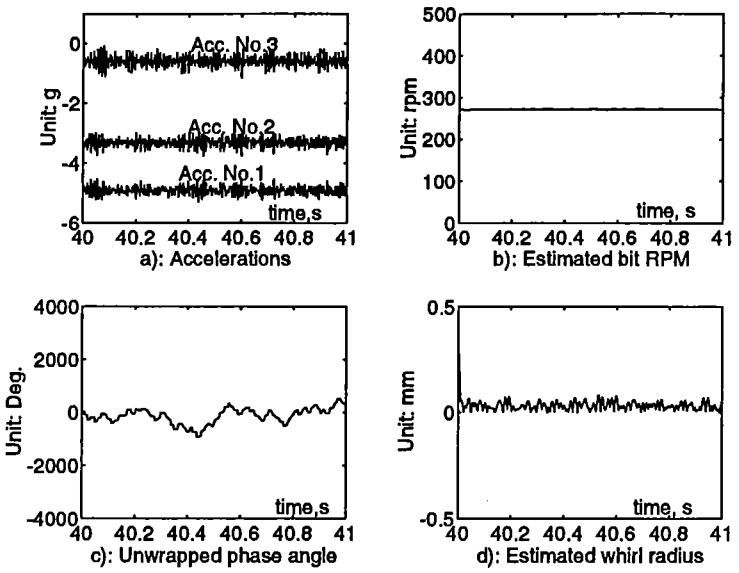

Fig.7.3: Whirl parameters estimated by accelerometers (test 1)

The unwrapped phase angle shown in Fig.7.3c is obtained using equation (11a). A lowpass filter with cutoff frequency 50 Hz is used here to filter the high frequency contents of the signal. During most of the time, this angle varies only a little.

According to equation (7.11b), we have $\omega - \Omega = 0$, or $\omega = \Omega$. It means that the bit is in synchronous forward whirl.

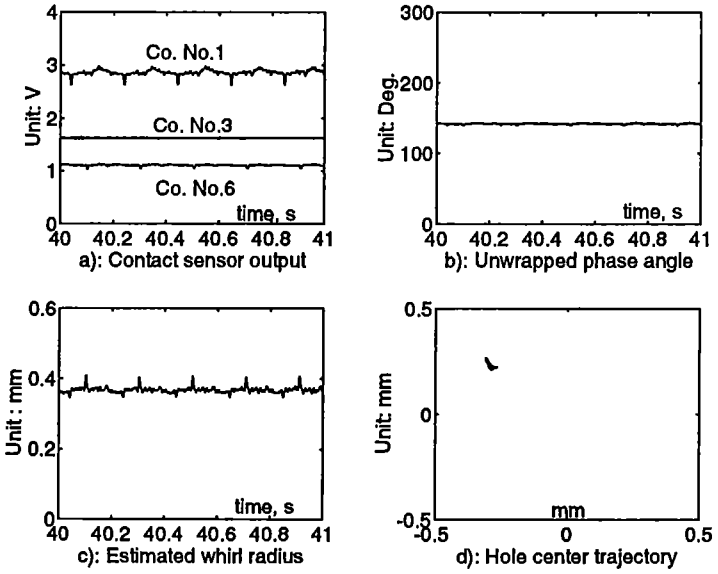

Fig.7.4: Whirl parameters estimated by contact sensors (test 1)

Fig.7.4 shows the identification results using contact sensors signals. The contact sensors No.1, No.3 and No.6 are used here. The unwrapped phase angle (Fig.7.4b) obtained by equation (7.23) remain almost constant. The hole center trajectory seen from the bit center (Fig.7.4c) is a fixed point in bit coordinate system. All these verify the above conclusions, i.e., the bit is in synchronous forward whirl.

Example 2: Backward whirl (test 2)

Fig.7.5 depicts all the results estimated by using accelerometer signals. The instantaneous bit rotation speed estimated using equation (7.9) is 473 *rpm* which is very close to reordered value (470 *rpm*). The lowpass filter with cutoff frequency 50 Hz is used here. From the unwrapped phase angle of bit acceleration (Fig.7.5c) we obtain $\omega - \Omega = 18.5Hz$, hence, we have $\Omega = -10.6Hz$. If we look at the autospectrum of bit acceleration (Fig.7.6) a very clear frequency is about 18 Hz. We also obtain $\Omega = -10.1\ Hz$. The negative value of Ω means that the bit is in backward whirl.

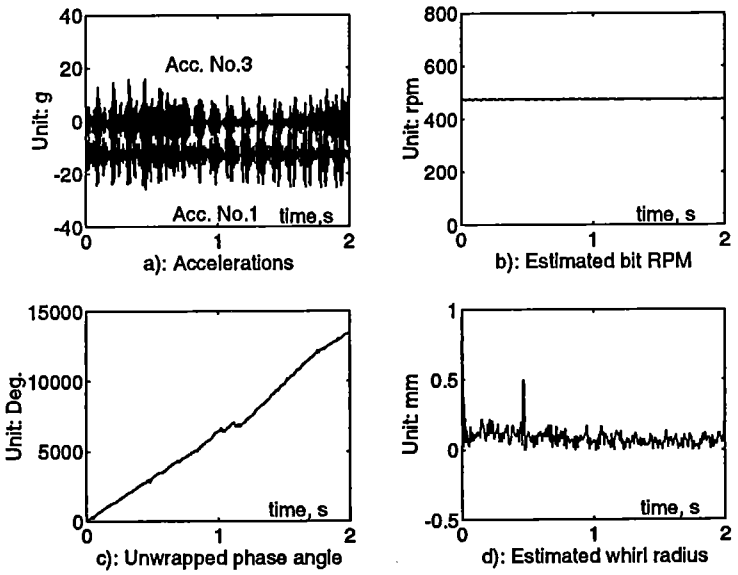

Fig. 7.5: Whirl parameters estimated by accelerometers (test 2)

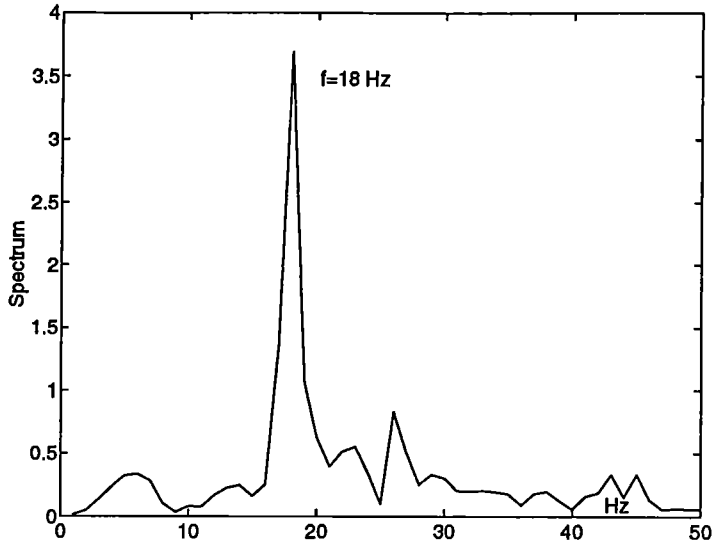

Fig.7.6: Auto spectrum of bit acceleration (test 2)

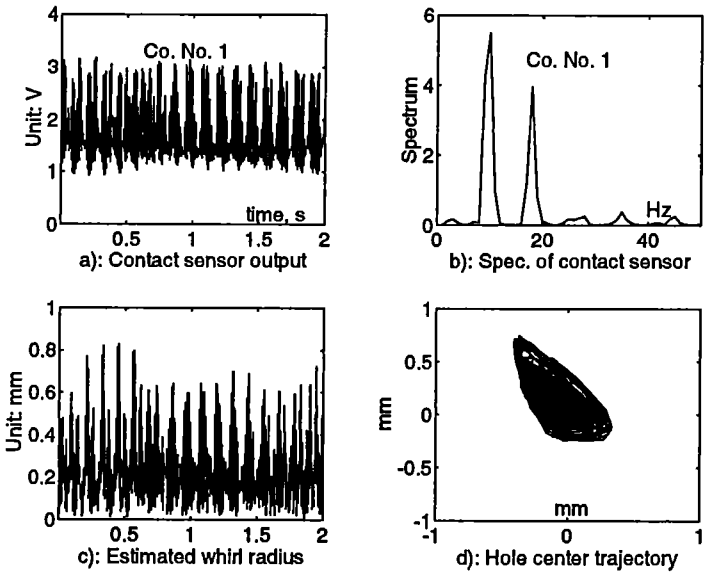

Fig. 7.7: Whirl parameters estimated by contact sensors (test 2)

On the other hand, let us examine the identification results (Fig.7.7) obtained by contact sensors. Two frequencies are very clear in the spectrum of contact sensor output. The first one is close to the bit rotation speed. The second one is about 18 Hz which is the hitting

frequency N_0 defined earlier. Hence, according to equation (7.22), we have $\omega - \Omega = 18Hz$, or $\Omega = -10.1Hz$. It is almost the same as the value obtained by above accelerometers.

The hole center trajectory seen from the bit center is shown in Fig.7d. The hole center rotates about the bit center. It is reasonable to conclude at this stage that the bit is in backward whirl with whirl frequency 10.6 Hz.

7.5.3. Results analysis

The only difference between test 1 and test 2 lies in the operating conditions, or more precisely the bit rotation speed (RPM) and the weight on bit (WOB). They are respectively:

(a) For test 1: RPM=270 rpm, WOB=8 tons;

(b) For test 2: RPM=470 rpm, WOB=2 tons;

It has been identified above that the bit is in backward whirl with $\Omega = 10Hz$ in test 2 and in synchronous forward whirl with $\Omega = \omega = 4.5Hz$ in test 1.

The above results show that the combination of WOB and RPM has a significant effect on the whirl initiation. By systematically changing the WOB and RPM, it should be possible to determine the conditions under which the bit whirl is initiated. The knowledge of the condition is helpful to the driller on drilling field.

The results also show that the antiwhirl bit may work with backward whirl under some conditions.

7.6. DISCUSSIONS AND CONCLUSIONS

It has been shown that there are two independent ways to identify downhole bit whirl while drilling. One way is to use accelerometers mounted just above the bit. Three accelerometers are enough to identify the whirl parameters. However, before the estimation can be performed, lowpass filters should be employed to filter high frequency contents because the accelerometers are very sensitive to other excitations. Furthermore, it is difficult to obtain the bit center trajectory in a straightforward manner by integrating twice the acceleration measured by the accelerometers mounted on the rotating bit body.

Another more powerful way is to use contact sensors which measure the distance between the bit gauge and the hole-wall. Three contact sensors mounted on the bit gauge are theoretically enough to estimate the bit whirl parameters. The use of more than three contact sensors may improve the estimation accuracy. No filter is needed before the estimation. The bit center trajectory may be obtained directly. Because their simplicity and reliability, the contact sensors may be used for real time analysis in drilling field. However, the sensitivity and stability problems associated with the contact sensor have to be improved before industrial applications.

CHAPTER 8:

CONCLUSIONS AND FUTURE WORK

8.1 Conclusions

On-line vibration control of drillstring systems is currently a hot research subject in the oil-well drilling industry. Establishing simple and high accuracy dynamic model of drillstrings is a critical issue in this area. This these study both the linear and nonlinear dynamics of drillstrings. Following contributions have been made in the thesis:

(1) An improved dynamic stiffness method (IDSM) is proposed and applied to different aspects of modal analysis. What makes the present approach useful for the modal analysis of beam-like structures is that (a) A one-dimensional substructure can be always reduced exactly to an equivalent element. (b) The master degrees of freedom in the model can be arbitrarly selected. It has been demonstrated through several numerical examples that the procedure proposed in this thesis benefits analysis and solution of the eigenvalues, forced response and force identification problems for beam-like structures.

It is obvious that the IDSM is different from the transfer matrix method and from the dynamic stiffness method. In transfer matrix method, the explicit equation of motion of the system is disappeared. Only the boundary conditions are related by the global transfer matrix. In the dynamic stiffness method, on the other hand, the internal degrees of freedom in a substructure have to be used which leads to high order dimension. The present method is also different from the Dokainish combination method. Firstly, the exact stiffness matrix is used in the present method while in Dokainish combination method finite element matrices are used. Secondly, the Dokainish's method was actually an improved transfer matrix method because the eigenproperties were obtained from the global transfer matrix. Only eigenfrequencies, mode shapes and harmonic responses are available in Dokainish's method. In the IDSM, however, the explicit equation of motion is obtained and all the modal parameters such as eigenfrequencies, mode shapes, modal masses, modal stiffness, and FRF matrix can be calculated.

(2) The lateral, axial and torsional vibrations of linear drillstring are exactly modeled using the IDSM which leads to much more easy and more accurate determination of modal parameters, buckling loads and dynamic responses than those available from the FEM approach. For lateral vibration, the drillstring is modeled as an equivalent two degrees of freedom system for a given frequency. The axial force (WOB) has a significant influence on the lateral vibration. Both the WOB and the curvature decrease the lateral natural frequencies of the drillstring. Exact buckling loads may be conveniently calculated based on the IDSM model. For axial and torsional vibrations, the drillstring is modeled as an equivalent single or two degrees of freedom system depending on the research purposes. The established models make it easy and accurate to predict bit forces and bit displacements during drilling using the measurement data at the surface. The IDSM model for axial vibration benefits also the design of shock absorber. A computer program (both Fortran code and Matlab code) is developed which can be run on personal computers. The numerical examples have demonstrated that the IDSM is special useful for the dynamic analysis of drillstrings in the drilling fields.

(3) Backward whirl due to bit-holewall contact has been investigated based on both lumped model and finite element model. The contact element developed in the thesis can simulate both static contact and dynamic contact between drillstring and holewall. Following common features can be found from both lumped and FEM model:

(a) The bit-holewall contact can lead to steady-state backward whirl under certain conditions. These conditions include a large bit side force and friction coefficient. However, once initiated, the backward whirl motion does not depend on the values of side force amplitude and friction coefficient.

(b) There is a critical friction force below which forward whirl occurs and above which backward whirl occurs. In other words, there is a critical friction coefficient (for a given formation stiffness) or a critical formation stiffness (for a given friction coefficient). This fact may explain why PDC bit with low friction pad can resist backward whirl and why backward whirl occurs often in the hard formations.

From the lumped model it is found that there is a maximum possible backward whirl frequency which is the eigenfrequency of joint drillstring-formation system. From the FEM model, however, the maximum backward whirl frequency seems to be the second bending natural frequency of the drillstring system. In addition, it is also found from the FEM model that the backward whirl frequency, once initiated, is greater than the lowest bending eigenfrequency of the BHA system in the case of contact. In other words, there is a lowest backward whirl speed which is near to but larger than the first bending eigenfrequency of the system. This fact is not predicted by the lumped model. These observations show that the lumped model is too simple to completely describe the behaviors of the system.

(4) In this thesis several methods have been developed to identify bit whirl motion (including whirl frequency, whirl radius, bit rotation speed, bit center trajectory) using accelerometers and contact sensors. It has been shown that there are two independent ways to identify downhole bit whirl while drilling. One way is to use accelerometers mounted just above the bit. Three accelerometers are enough to identify the whirl parameters. However, before the estimation can be performed, lowpass filters should be employed to filter high frequency contents because the accelerometers are very sensitive to other excitations. Furthermore, it is difficult to obtain the bit center trajectory in a straightforward manner by integrating twice the acceleration.

Another more powerful way is to use contact sensors which measure the distance between the bit gauge and the hole-wall. Three contact sensors mounted on the bit gauge are enough to estimate the bit whirl parameters. No filter is needed before the estimation. The bit center trajectory may be obtained directly. Because their simplicity and reliability, the contact sensors may be used for real time analysis in drilling field. However, the sensitivity and stability problems associated with the contact sensor have to be improved before industrial applications.

8.2 Future Work

It becomes obviously in recent years that dynamic analysis plays an important role in the design of drillstring systems and drilling bit. However, many dynamic problems remain to be solved. In the author's opinion, following subjects may be challenging research areas:

(1) **Dynamic modelling of bit-formation interaction.** Modeling of the PDC bit-formation interaction was initiated in 1987 in an effort to investigate the wear condition of PDC cutters (Glowka, 1987). Later, 2D (Warren and Sinor,1989a,b) and 3D (Behr and Warren, 1991, Langeveld, 1991, Chen and Géradin, 1993b) PDC bit-formation models have been developed. Most of these models are based on the bit kinematics, that is, the bit motion is predescribed. Although these models are successfully used to predict the drilling forces, the combination with a full drillstring dynamic model is not completely solved. Difficulties exist in updating the bottomhole condition and in convergence of time integration. Undoubtedly, succesfully combination of bit-formation interaction model with drillstring dynamic model will be helpful to understand more deeply the dynamic phenomena of drillstring system, including backward whirl initiation, vibration coupling and stick-slip vibration, and hence to improve the bit design.

(2) **Vibration coupling in drillstring.** Strictly speaking, the axial, torsional and lateral vibrations are coupled through drillstring large deformation and bit-formation interaction. The drillstring structure is peculiar in the sense that its diameter to length ratio is very small so that it may be subject to very large static deflections. Therefore, the structure, in general, cannot be considered as straight and planar. As a result, the axial, torsional and lateral vibrations will be coupled through geometric non-linearity. The interdependent drilling forces may induce another coupling phenomenon. The axial and lateral vibration coupling has been studied by Shyu (1989). Obviously, more detailed researches are needed.

(3) **Dynamic stabilities.** Dynamic stability problems of drillstrings cover a large number of topics. For example, the stabilities induced by fluctuations of WOB, TOB and drilling fluid, the stabilities induced by non-constant rotation speed of drillstrings, the stabilities induced by drillstring-holewall contact, and so on. Although work has been performed in recent years, for example, Dunayevsky and Judzis (1985), Jansen (1993) and Heijden (1993), the state of the art is far from perfect.

(4) **Prediction of drilling direction using dynamic models.** Great achievements have been made in the area of directional drilling through the contributions mainly made by, among others, Millheim (1978a,b, 1979 a-d) and Ho (1986,1987,1988). These works are based on static model and hence are unreliable to predict the azimuth of a well. Probably the dynamics of the drillstrings, especially the dynamics of the BHA play an important role in the undesired azimuth changes.

REFERENCES

Allen M.B., 1987, *BHA lateral vibration: Case studies and evaluation of important parameters*, SPE/IADC 16110

Alley S.D., Sutherland G.B., 1991, *The use of real-time downhole shock measurement to improve component reliability*, SPE 22537.

Apostal M.C., Haduch G.A., Williams J.B., 1990, *A study to determine the effect of damping on finite-element-based, forced-frequency-response models for bottomhole assembly vibration analysis*, SPE 20458.

Aarrestad T.V., et al, 1986, *Drillstring vibrations: comparison between theory and experiments on a full scale research drilling rig*, SPE/IADC 14760.

Banerjee J.R., and Williams F.W., 1985, *Exact Bernoulli-Euler dynamic stiffness matrix for a range of tapered beams*, Int. J. for Num. Meth. in Engrg. 21, 2289-2302.

Banerjee J.R., and Williams F.W., 1992, *An exact dynamic stiffness matrix for coupled extension-torsional vibration of structural members*, Computer and Structures, 50(2), 161-166.

Bansal P.N., Kirk R.G., 1975, *Stability and damped critical speed of rotor-bearing systems*, ASME J. of Engrg. for Industry, Vol. 97, pp 1325-1332.

Bateman V.I., Carne T.G., et al., 1991, *Force reconstruction for impact tests*, Transactions of the ASME, J. of Vibration and Acoustics, Vol.113, pp 192-200.

Behr S.M, Warren T.M,, 1991, *Three Dimensional Modeling of PDC Bits*, SPE/IADC 21928

Besaisow A.A., Payne M.L., 1986, *A study of excitation mechanisms and resonance inducing BHA vibration*, SPE 15560.

Bickford W.B.,Strom B.T., 1975, *Vibration of plane curved beams*, J. of Sound and Vibration, 39(2), 135-146.

Birades M., 1988, *Static and dynamic three dimensional bottomhole assembly computer models*, SPE drilling Engineering, June 1988, pp160-166.

Bogdanoff J.L., Goldberg J.E.,1961, *A new analytical approach to drill pipe breakage II*, Transaction of the ASME, J. of Eng. for Ind., 101-106

Book A.K., Meehan R.J., 1993, *Drillstring imaging—An interpretation of surface drilling vibrations*, SPE drilling and Completion, June 1993, p93-98.

Brakel J.D., Azar J.J., 1989, *Prediction of wellbore trajectory considering BHA and drill-bit dynamics*, SPE Drilling Engrg., pp 109-118.

Brett J.F., Warren T.M., et al, 1989,*Bit whirl: A new theory of PDC bit failure*, SPE paper 19571.

Brett J.F., 1991, *The genesis of bit induced torsional drillstring vibrations*, SPE/IADC 21943.

Cardona A., Géradin M., 1987, *SAMCEF: module d'analyse de mèanismes MECANO (manuel d'utilisation)*, LTAS report, Uni. of Liège, Belgium.

Carne T.G., Mayes R.L., Bateman V.I, 1994, *Force reconstruction using the sum of weighted accelerations technique-max-flat procedure*, 12th IMAC Proceedings, pp 1054-1062.

Chandrashekhar S., Osman M.O.M., Sankar T.S., 1984, *An experimental investigation for the stochastic modelling of the resultant force system in BTA deep hole machining*, Int. J. Prod. Res., Vol 23, No.4, p657-673

Chandrashekhar S., 1984, *An analytical and experimental stochastic modelling of the resultant force system in BTA deep hole machining and its influence on the dynamic of the machine tool workpiece system*, Ph.D thesis, Concordia University, Canada.

Chen S.L., Géradin M., 1992a, *A study of BHA dynamics using a modified transfer matrix method*, Technical report No.VA-83, LTAS, University of Liége, Belgium.

Chen S.L., Géradin M., 1992b, *Development of a random cutting force model for PDC bit*, LTAS report, VA 102, University of Liége, Belgium.

Chen S.L., Géradin M., 1993a, *Three dimensional modeling of PDC bit/formation interaction*, LTAS tech report, VA 103.

Chen S.L., Géradin M., 1993b, *Stability analysis of anti-whirl PDC bit*, LTAS tech report, VA 104, University of Liége, Belgium.

Chen S.L, Géradin M., 1993c, *An improved transfer matrix method as applied to BHA lateral vibration analysis.* Accepted for publication in Journal of Sound and Vibration.

Chen S.L, Géradin M., 1993d, *Dynamic modelling of transverse drillstring vibrations due to bit/formation interaction*, LTAS tech report, VA 114, University of Liége, Belgium.

Chen S.L., Géradin M., 1994a, *Modal parameter evaluation for beam systems using a combined method of transfer and dynamic stiffness matrices, LTAS technical report*, VA 124.

Chen S.L, Géradin M., 1994b, *An exact and direct technique for modeling of beam systems with expected degrees of freedom*, Proc. of 19th ISMA, Tools for Noise and Vibration Analysis, Vol.2, p867-878, Sep.,1994, Leuven, Belgium.

Chen S.L, Géradin M., 1994c, *An exact and direct modeling technique for rotor-bearing systems with arbitrary selected degrees of freedom*, Accepted for publication in the Journal of Shock and Vibration.

Chen S.L, Géradin M., 1994d, *Dynamic force identification for beam-like structures using an improved dynamic stiffness method*, LTAS report, VA 139, also submitted to Shock and Vibration.

Chen S.L, Géradin M., 1994e,*A direct model reduction technique for in-plane vibration of plates with arbitrary selected degrees of freedom*, LTAS report, VA 126, Uni. of Liège.

Chen S.L, Géradin M., 1994f,*Dynamic modelling of rotating drillstring by a combined method of transfer and dynamic stiffness matrices*, LTAS report, VA 129, Uni. of Liège.

Chen S.L, Géradin M., 1994g, *Buckling analysis of drillstrings by a combined stiffness-transfer matrix method*, LTAS report, VA 133, Uni. of Liège.

Chen S.L, Géradin M., 1994h,*Identification of dynamic downhole bit forces and motions during drilling by surface measurement*, LTAS report, VA 138, Uni. of Liège.

Chen S.L., Géradin M., Lamine E., 1993,*Identification of downhole bit whirl while drilling*, Proc. of 64th Shock and Vibration Symposium, pp 261-269, Oct., 1993, Florida, USA

Chen S.L., Géradin M., Lamine E., 1994a, *An improved dynamic stiffness method and modal analysis for beam-like structures*, Proc. of 65th Shock and Vibration Symposium, USA.

Chen S.L., Géradin M., Lamine E., 1994b, *An improved dynamic stiffness method with application to vibration analysis of linear drillstrings*, Accepted for publication in the Journal of Machine Vibration.

Chen S.L, Géradin M., Lamine E., 1994c, *A study of backward whirl due to bit-holewall contact by finite element method*, Submitted for publication.

Chen S.L., Golinval J.C., Géradin M., 1993, *In-plane vibration analysis and application of curved beam subject to axial load*, LTAS technical report, VA 123, Uni. of Liege.

Chen S.L., Golinval J.C., Géradin M., 1994a, *On the dry friction induced backward whirling vibration of rotating drillstring*, Proc. of 3rd Belgium National Conf. on Mechanics and Applications, p261-264.

Chen S.L., Golinval J.C., Géradin M., 1994b, *Dry friction induced steady-state backward whirling vibration of rotating drillstring*, Accepted for publication in the Euro. J. of Mechanical Engrg.

Chen S.L., Golinval J.C., Géradin M., 1994c, *A dynamic stiffness-transfer matrix method for forced response analysis of one-dimensional structures*, LTAS report, VA 137, Uni. of Liège. Also submitted to Int J. of Modal Analysis.

Chen S.L., Golinval J.C., Géradin M., 1995, *An improved dynamic stiffness method for modal analysis of branched beam-like structures*, Proc. of the 13th IMAC, USA.

Chen S.L, Rixen D., Géradin M., 1992, *Bit whirl kinematics and its simulation*, LTAS tech report, VA 84.

Chen S.L, Rixen D., Géradin M., 1994,*An analysis of lateral vibrations due to drillstring-holewall contact*, Proc. of Int. Conf. on Vibration Engrg., p377-382, published by International Academic Publishers.

Chen S.S., Wambsganss M.W., and Jendrzejczyk J.A., *Added mass and damping of a vibratiing rod in confined viscous fluids*, ASME J. of Applied Mechanics, 326-329, June 1976.

Chen Y.C., Lin Y.H., Cheatham J.B., 1990, *Tubing and casing buckling in horizontal wells*, Journal of Petroleum Technology, Feb., 140-141, 191

Chen Y.H., 1987, *General dynamic stiffness matrix of a Timoshenko beam for transverse vibrations*, Earthquake Engrg. and Structural design, 15(3), 391-402.

Chiatti G., Sestieri A., 1979, *Analysis of static and dynamic structural problems by a combined finite element-transfer matrix method*, J. of Sound and Vibration, Vol. 67, No. 1, pp35-42.

Chin W.C., 1988, *Why drill strings fail at the neutral point, Petroleum Engineer International*, May, 1988.

Choi S. H., Pierre C., Ulsoy A. G., 1992, *Consistent modeling of rotating Timoshenko shafts subject to axial loads*, ASME, J. of Vibration and Acoustics, Vol. 114, pp249-259.

Clayer F., Vandiver J.K., Lee H.Y., 1990, *The effects of surface and down hole boundary conditions on the vibration of drillstring*, SPE 20447, 65th Annual Technical Conf. of SPE.

Clegg J.M., Hycalog, 1992, *An analysis of the field performance of antiwhirl PDC bit*, IADC/SPE 23868

Close D.A., Owens S.C., 1988, *Measurement of BHA vibration using MWD* , SPE/IADC 17273.

Cooley C.H., Pastusek P.E., et al, 1992, *The design and testing of anti-whirl bits*, SPE 24586

Crandall S.H., 1987, *Nonlinearities in rotor dynamics*, Proc. ICNO-11, 44-56, Budapest.

Crandall S.H., 1990,*From whirl to whip in rotordynamics*, p 19-24, 3rd International Conf. on Rotordynamics, p 19-24, Sept.,1990, Lyon, France

Crandall S.H., Lingener A., Zhang W., 1993, *Backward whirl due to rotor-stator contact*, Nonlinear Vibration Problems, 25, p47-61.

Dareing D.W., Livesay B.J., 1968, *Longitudinal and angular drillstring vibrations with damping*, ASME J. of Engrg. for Industry, 671-679.

Dareing D.W., 1983, *Rotary speed, drill collars control drillstring bounce*, Technology Oil and Gas Journal, p63-68, June.

Dareing D.W., 1984a, *Drill collar length is a major factor in vibration control*, J. of Petroleum Technology, August 1984, p 637-644.

Dareing D.W., 1984b, *Vibrations increase available power at the bit*, Technology, Oil and Gas Journal, March, 1984.

Dareing D.W., 1987, *Applied drilling mechanics*, University of Florida, USA.

Davis R., Henshell R.D., Warburton G.B., 1972, *Constant curvature beam finite element for in-plane vibration*, J. of Sound and Vibration, 25(4), 561-576.

Dawe D.J., 1971, *The transverse vibration of shallow arches using the displacement method*, Int. J. mech. Sci., Vol. 13, 713-720.

Dawson R., Paslay P.R., 1984, *Drillpipe buckling in inclined holes*, Journal of Petroleum Technology, 1734-1738

Degen E.E., Shephard M.S., Loewy R.G., 1985, *Combined finite element transfer matrix method based on a mixed formulation*, Computers and Structures, Vol. 20, pp173-180.

Deily F.H., Dareing D.W., Paff G.H., 1968, *Download measurements of drillstring forces and motions*, Transaction of the ASME, J. of Eng. for Ind., 217-225

Dimarogonas A.D., 1975, *A general method for stability analysis of rotating shafts*, Ingenieur-Archiv, Vol. 44, pp 9-20.

Dobson B.J., Rider E., 1990, *A review of the indirect calculation of excitation forces from measured structural response data*, J. of Mechanical Engineering Science, Vol.204, pp69-75.

Dokainish M. A., 1972, *A new approach for plate vibrations: Combination of transfer matrix and finite-element technique*, ASME, J. of Engrg. for Industry, Vol. 94, pp 526-530.

Doyle J.F., Farris T.N., 1990, *A spectrally formulatated finite element for flexurl wave propagation in beams*, Modal Analysis, 5(2) p99-107.

Dufeyte M.P., Henneuse H., 1991, *Detection and monitoring of slip-stick motion: field experiments*, SPE/IADC 21945.

Dunayevsky V.A., Judzis A., 1985,*Dynamic stability of drillstring under fluctuating WOB*, SPE 14329.

Dupuis C., Rousselet J.,1985, *Application of the transfer matrix method to non-conservative systems involving fluid flow in curved pipes*, J. of Sound and Vibration, 98(3), 415-429.

Ehrich F.F., 1976,*Self-excited Vibration*, Vibration and Shock Handbook, p 5-11

Eisenberger M., 1990, *Exact static and dynamic stiffness matrices for general variable cross section members*, AIAA J., 28(6).

Elliott K.B., Juang J.N., Robinson, J., 1988, *Force prediction using singular decomposition*, 6th IMAC Proceedings, pp 1582-1588.

Ema S., Fujii H., Marui E., 1988,*Whirling vibration in drilling. part 3: Vibration analysis in drilling workpiece with a pilot hole*, ASME J. of Engrg. for Industry, Vol. 110, p315-321.

Ewins D.J., 1988, Modal Testing: *Theory and Practice*, Research Studies Press Ltd., England.

Fabunmi J.A., 1985, *Effects of structural modes on vibratory force determination by the pseudoinverse technique*, AIAA Journal, Vol.24, No.3, pp 504-509.

Farme I.W.r,1986, *Engineering Properties of Rocks*, London, E. and F. N. SPON LTD, p4-16.

Feenstra R., 1988, *Status of polycrystalline diamond compact Bit: Part 1—Development*, J. of Petr. Tech., 675-684.

Fergusson N. J., Pilkey W. D., 1991a,*The dynamic stiffness method: part 1, elements*, Shock and Vib. Tech. Rev., 1(7), pp4-13.

Fergusson N. J, Pilkey W. D., 1991b, *The dynamic stiffness method: Part 2, frequency extraction technology*, Shock and Vib. Tech. Rev., 1(8), pp14-20.

Fergusson N.J., Pilkey W.D., 1992, *Frequency-dependent element mass matrices, Journal of Applied Mechanics*, Vol.59, pp136-139.

Fergusson N.J., Pilkey W.D., 1993a,*Finite dynamic elements and modal analysis*, Shock and Vibration 1(2), 171-176.

Fergusson N. J., Pilkey W. D., 1993b, *Literature review of variants of the dynamic stiffness method, part 1: the dynamic element method*, Shock and Vib. Dig., 25(2), pp3-12.

Fergusson N. J., Pilkey W. D., 1993c, *Literature review of variants of the dynamic stiffness method, part 2: frequency-dependent matrix and other corrective methods*, Shock and Vib. Dig., 25(4), pp3-10.

Firoozian R., Zhu H., 1991, *A hybrid method for the vibration analysis of rotor-bearing systems*, Journal of Mechanical Engineering Science, Vol 205.

Freed A.M., Flanigan C.C., 1990, *A comparison of test-analysis model reduction methods*, Proc. 8th IMAC, pp1344-1351.

Fujii H., Marui E., Ema S., 1986,*Whirling vibration in drilling. Part 1 and Part 2*, ASME J. of Engrg. for Industry, Vol 108, pp157-168.

Géradin M., Rixen D., 1994, *Mechanical Vibrations, Theory and Application to Structural Dynamics*, Wiley Publishers, 1994.

Géradin M., Cardona A., 1992, *The finite element approach to kinematics and dynamics of flexible multibody system*, Comet course, University of Liege

Géradin M., Chen S. L., 1994, *An exact model reduction technique for beam structures: combination of transfer and dynamic stiffness matrices*, LTAS technical report, No. VA 125, Uni. of Liège. Accepted for publication in Journal of Sound and Vibration.

Glowka D.A., 1987, *Development of a method for predicting the performance and wear of PDC drill bit*, SANDIA report,Sand 86-1745,UC-66c

Goodwin M.J., 1992, *Dynamics of rotor-bearing systems—an overview*, Shock and Vibration Dig., Vol 24, No. 2, pp 3-14.

Gregory D.L., Priddy T.G., Smallwood D.O., 1986,*Experimental determination of the dynamic forces acting on non-rigid bodies, SAE technical paper series*, Paper No. 861791, Aerospace Technology Conf. and Expo., USA.

Hallauer W.L., Liu R.L., 1982,*Beam bending-torsion dynamic stiffness method for calculation of exact vibration modes*, J. of Sound and Vibration, 85(1), pp107-113.

Harvey P., Wassel M., 1991, *The design of steerable BHA's to minimize the adverse effets of motor imbalance and drilling forces*, SPE 22565.

Heijden V., 1993, *Bifurcation and chaos in drillstring dynamics*, Chaos, Solitons and Fractals, 3(2), 219-247.

Heisig G., 1993, *Zum statischen und dynamischen Verhalten von Tifebohr Straengen in raeumlich gekruemmten Bohrloechern*, Dr-Ing. Dissertation, Technischen Universitaet Braunschweig.

Henrych J., 1981, *The Dynamics of Arches and Frames*, Elsevier, Amsterdam.

Hillary B., Ewins D.J., 1984, *The use of strain gauges in force determination and frequency response function measurements*, Proc. of the 2nd IMAC, pp 627-634.

Ho H.S., 1986, *General formulation of drillstring under large deformation and its use in BHA analysis*, SPE 15562.

Ho H.S., 1987, *Prediction of drilling trajectory in directional wells via a new rock-bit interaction model*, SPE 16658.

Ho H.S., 1988, *An improved modeling program for computing the torque and drag in directional and deep wells*, SPE 18047.

Howson W.P., Banerjee J.R., Williams F.W., 1983, *Concise equations and program for exact eigensolutions of plane frams including member shear*, Engineering Software III, 3rd Int. Conf. proc., London.

Holzer H., 1948, *Die Berechnung der Drehschwingungen.*, Republished by J.W.Edwards Inc., Ann Arbor, MI.

Huang T. and Dareing D.W., 1968, *Buckling and lateral vibration of drill pipe*, ASME J. of Engrg for Industry, Nov., 1968.

Huang T. and Dareing D.W., 1969, *Buckling and frequencies of long vertical pipes*, J. of Engrg. Mechanics Division, ASCE, Feb., 1969.

Irie T., Yamada G.,and Takahashi I., 1979, *In-plane vibration of Timoshenko arcs with variable cross-sectio*, Ingenieur-Archiv, 48, 337-346.

Irie T., Yamada G., and Takahashi I.,1980, *The Steady State In-Plane Response of a Curved Timoshenko Beam With Internal Damping*, Ingenieur-Archiv, 49, 41-49.

Jansen J.D., 1991, *Nonlinear rotor dynamics as applied to oilwell drillstring vibrations*, J. of Sound and Vibration, 147(1), 115-135.

Jansen J.D., 1992, *Whirl and chaotic motion of stabilised drill collars*, SPE drilling Engrg., June 1992, p107-114.

Jansen J.D., 1993, *Nonlinear dynamics of oilwell drillstrings*, Ph.D thesis, Delft University, Holland.

Johnson, D.C., Bishop R.E.D., 1960, *The Mechanics of Vibrations*, University Press, Cambridge.

Kreisle L.F., Vance J.M., 1970, *Mathematical analysis of the effects of a shock sub on the longitudinal vibrations of an oilwell drillstring*, SPEJ 349-356.

Kolousek V., 1973, *Dynamics in Engineering Structures*, Butterworths.

Kronenberg M., 1966, *Machining Science and Application*, Pergamon Press Inc., 209-225

Kyllingstad A., Halsey G.W., 1989, *A study of slip/stick motion of the bit*, SPE drilling Engrg., 369-373.

Kuru W., 1987, *Dynamics drilling strategy for PDC bits*, SPE/IADC 16118.

Langeveld J.C., 1991, *PDC bit dynamics*, SPE 23867.

Lee H.G., Dobson B.J., 1991, *The direct measurement of structural mass, stiffness and damping properties*, J. of Sound and Vibration, 145(1), pp61-81.

Lee A.C., Kang Y., Liu S.L., 1991,*A modified transfer matrix method for linear rotor-bearing systems*, ASME J. of Applied Mechanics, Vol. 58, pp 776-783.

Lee A.C., Shin Y.P., Kang Y., , 1993a,*The analysis of linear rotor-bearing systems: A general transfer matrix method*, ASME, J. of Vibration and Acoustics, Vol.115, pp 490-497.

Lee A. C., Kang Y., Liu S.L., 1993b, *Steady-state analysis of a rotor mounted on nonlinear bearings by the transfer matrix method*, Int. J. Mech. Sci., Vol. 35, No. 6, pp 479-490.

Lee H.Y., 1991,*Drillstring axial vibration and wave propagation in boreholes*, Ph.D thesis, MIT, USA.

Lee S.J., Ewan K.F., Wu S.M., 1987, *An analysis of the drill wandering motion*, ASME J. of Engrg. for Industry, Vol. 109, p297-305.

Leung A.Y.T., 1978, *An accurate method of dynamic condensation in structural analysis*, Int. J. for Numerical Methods in Engrg. Vol.12 1705-1715.

Leung A.Y.T., 1979, *An accurate method of dynamic substructuring with simplified computation*, Int. J. for Numerical Methods in Engrg., Vol.14, pp1241-1256.

Leung A. Y. T., 1980, *Dynamic analysis of periodic structures*, J. of Sound and Vibration, 72(4), 451-467.

Leung A.Y.T., 1985, *Dynamic stiffness method for exponentially varying harmonic excitation of continuous systems*, J. of Sound and Vibration, 98(3), pp 337-347, 1985.

Leung A.Y.T., 1987, *Dynamic stiffness and response analysis, Dynamics and Stability of Systems*, 2(2), 125-137.

Leung A.Y.T., Fergusson N.J., 1993, *A generalization of Leung's theorem*, Proc. of Dynamics and Design Conf. JSME, Vol.B, paper No. 708, pp443-445, July 1993, Tokyo, Japan.

Leung A. Y. T, Zhou W.E., 1993, *Dynamic stiffness analysis of curved thin-walled beams*, Shock and Vibration, Vol. 1, Issue 1, pp77-88.

Lin Y.K., 1967, *Probabilistic theory of structural dynamics*, McGraw-Hill, New York.

Lin Y.K., McDaniel T.J., 1969, *Dynamics of beam-type periodic structures*, J. Engrg. Industry 91, 1133-1141.

Lin Y.Q., Wang Y.H., 1991, *Stick-slip vibration of drilling strings*, Transactions of the ASME, J. of Engrg. for Industry, Vol. 113.

Lingener A., 1990,*Experimental investigation of reverse whirl of a flexible rotor*, 3rd International Conf. on Rotordynamics, p 13-18, Sept.,1990, Lyon, France

Liu T.S., Lin J.C., 1993, *Forced vibration of flexible body systems: A dynamic stiffness method*, ASME, J. of Vib. and Acoustics, Vol 115, 468-476.

Lubinski, A., 1950, *A study of the buckling rotory drilling strings*, Drill. and Prod. Prac., API, Dallas 178.

Lundon R., and Akesson B., 1983, *Damped second order Rayleigh-Timoshenko beam vibration in space: an exact complex dynamic member stiffness matrix*, Int. J. for Num. Meth. in Engrg., 19, 431-449.

Lund J.W, Orcutt F.K., 1967, *Calculations and experiments on the unbalance response of a flexible rotor*, ASME J. Engrg. Ind. 89, 785.

Lund J.W., 1974, *Stability and damped critical speeds of a flexible rotor in fluid-film bearings*, ASME J. of Engineering for industry, Vol. 96, pp509-516.

Lutz J., et al, 1971, *Thèorie dynamique du forage et diagraphie instantanèe*, Revue de l'institut francais du pétrole 1181.

Macpherson J.D., Mason J.S., Kingman J.E.E., 1993, *Surface measurement and analysis of drillstring vibrations while drilling*, SPE/IADC 25777.

McDaniel T.J., 1971a,*Dynamics of circular periodic structures*, J. Aircraft 8, 143-149.

McDaniel T.J, Logan J.D., 1971b, *Dynamics of cylindrical shells with variable curvature*, J. of Sound and Vib., 19, 38-49.

McDaniel T.J, Eversole K.B., 1977, *A combined finite element-transfer matrix structural analysis method*, J. of Sound and vibration, 51, 157-169.

Mercer C.A., Seavey C., 1967, *Prediction of natural frequencies and normal modes of skin-stringer panel rows*, J. of Sound and Vib..

Mead D.J., *Vibration response and wave propagation in periodic structures*, J. Engrg. Industry, 93, 783-792.

Millheim K.K., Jordan S., Ritter C.J., 1978, *Bottomhole assembly analysis using the finite element method*, J. of Pet. Tech. Feb. 1978, p265-274.

Millheim K.K., 1978a,*Here are the basis of bottom-hole assembly mechanics*, Oil and Gas J., Dec. 4, 1978.

Millheim K.K., 1978b, *Single-stabilizer behavior described*, Oil and Gas J., Dec., 1978.

Millheim K.K., 1979a, *Behavior of multiple stabilizer bottom-hole-assemblies*, Oil and Gas J., Jan., 1979.

Millheim K.K., 1979b, *Controlling hole direction in very soft formations*, Oil and Gas J., Jan., 1979.

Millheim K.K., 1979c, *Contro techniques for medium-soft and medium formations*, Oil and Gas J., Jan., 1979.

Millheim K.K., 1979d, *Hard formation directional drilling calls for special care*, Oil and Gas J., Feb., 1979.

Millheim K.K., Apostal M.C., 1981a,*The effect of bottomhole assembly dynamics on the trajectory of a bit*, J. of Petroleum and Technology, p2323-2337, Dec., 1981.

Millheim K.K., Apostal M.C., 1981b,*How BHA dynamics affect bit trajectory*, World Oil, May 1981.

Mitchell R.F., Allen M.B., 1985, *Lateral Vibration: the key to BHA failure analysis*, World Oil, 101-106.

Mitchell R.F., 1986, *Simple Frictional analysis of helical buckling of tubing,* SPE drilling Engrg., December, 457-465.

Mottershead J.E., Friswell M.I., 1993,*Model updating in structural dynamics: A survey*, J. of Sound and Vibration, 167(2), 347-375.

Mucino V.H., Pavelic V., 1981, *An exact condensation procedure for chain-like structures using a finite element-transfer matrix approach,* ASME J. of Mechanical Design, Vol. 103, pp295-303.

Myklestad N.O.,1944, *A new method of calculating natural modes of uncoupled bending vibration of airplane wings and other types of beams,* J.Aero. Sci., No. 4, pp153-162

Myklestad N.O.,1945, *New method of calculating natural modes of coupled bending torsion of beams*, Trans ASME 67, 61-67.

Ohga M., Shigematsu T., Hara T., 1983, *Structural analysis by a combined finite element -transfer matrix method*, Computers and Structures, Vol. 17, No.3, pp321-326.

Ohga M., Shigematsu T., Hara T., 1984, *A combined finite elemenr-transfer matrix method*, ASCE, J. of the Engrg. Meca. Div., 110, 1335-1349.

Ohga M., Shigematsu T., Hara T., 1993, *A finite element-transfer matrix method for dynamic analysis of frame structures,* J. of Sound and Vib., 167(3), 401-411.

Parisis A., Géradin M., 1990, *BHA project (Part 2)*, Internal report to DBS.

Park H., Park Y., 1994, *Transient response of an impacted beam and indirect impact force identification using strain measurements*, Shock and Vibration, 1(3), pp 267-278.

Pastusek P.E., Cooley C.H., 1992, *Directional and stability characteristics of anti-whirl bits with non-axisymmetric loading*, SPE 24614

Pearson D., Wittrick W.H., 1986, *An exact solution for the vibration of helical springs using a Bernoulli-Euler model*, Int. J. for Mech. Sci., 28, 83-96.

Pestel E.C., Leckie F.A., 1963, *Matrix Methods in Elastomechanics*, McGraw-Hill, New York.

Pilkey W.D., Fergusson N.J., 1990, *Some characteristics of frequency-dependent structural matrices*, Computers and Structures, Vol.35, pp413-416.

Priddy T.G., Gregory D.L.,Coleman,R.G., 1988, *Strategic placement of accelerometers to measure forces by the sum weighted accelerations*, SAND87-2567.UC-38, USA.

Priddy T.G., Gregory D.L., Coleman R.G., 1989, *Measurement of time-dependent external moments by the sum weighted accelerations*, SAND88-3081.UC-38, USA.

Prohl M.A., 1945, *A genearl method for calculating critical speed of flexible rotors*, ASME J. of Applied Mechanics, Vol. 67, pp 142-148.

Raeymakers V., Géradin M., 1988, *Développement d'un logiciel d'analyse du comportement de train de tiges*, Internal report to DBS.

Richards T.H., Leung Y.T., 1977, *An accurate method in structural vibration analysis*, J. of Sound and Vibration, 55, 363-376.

Rixen D., 1991, *Analyse simplifiée des vibrations transversales d'une BHA en rotation*, LTAS tech. report, Universite de Liege.

Rixen D., 1992a, *Vibrational Behaviour of Drillstrings: An Overview*, LTAS report, VA 77, Universite de Liege.

Rixen D., 1992b, *BHA with reamer dynamic analysis, LTAS tech. report*, VA 79, Universite de Liege.

Rixen D., 1992c,*Nonlinear analysis of drillstring whirl initiation under initial large deflection*, LTAS tech. report, VA 85, Universite de Liege.

Romanelli E., Laura P.A., 1972, *Fundamental Frequencies of Non-Circular Elastic, Hinged Arcs*, J. of Sound and Vibration, 24(1), 17-22.

Rubin S., 1964, *Transmission matrices for vibration and their relation to admittance and impedance*, J. Engrg. Industry, Trans ASME 86, 9-21.

Rubin S., 1967, *Review of mechanical immittance and transmission matrix concepts*, J. Acoust. Soc. Am. 41, 1171-1179.

Samtech, 1994, *Samcef 5.0 User's guide*

Starkey J.M., Merrill G.L., 1989, *On the ill-conditioned nature of indirect force-measurement techniques*, J. of Modal Analysis, July, 1989, pp 103-108.

Sinor L.A., Warren T.W., 1989, *Drag bit wear model*, SPEDE, p128-136

Sinor L.A., Brett J.F., et al., 1990, *Field testing of low friction gauge PDC bits*, SPE paper 20416

Sinor L.A., Warren T.M., et al, 1992, *Development of an antiwhirl core bit*, SPE 24587

Simpson A., 1982, *A Newtonian procedure for the solutions of* $Ex = \lambda Ax$, J. of Sound and Vibration, 82, 161-170.

Simpson A., 1984, *On the solution of* $S(\omega)X = 0$ *by a Newtonian procedure*, J. of Sound and Vibration, 97(1), 153-164.

Skaugen E., 1987, *The effects of quasi-random drill bit vibrations upon drillstring dynamic behavior*, SPE 16660, 105-116.

Spanos P.D., Rice U., Payne M.L.,1992, *Advances in dynamic bottomhole assembly modeling and dynamic response determination*, IADC/SPE 23950

Squire W.D., Whitehouse H.J., 1979, *A new approach to drillstring acoustic telemetry*, 5th SPE fall meeting, USA.

Shultz L.A., Murthy V.R., 1992,*Direct application of the transfer matrix method to solve nonlinear autonomous boundary value problems with multiple branches*, Computer and Structures Vol.49, No.3, pp439-452.

Shyu R.J., 1989, *Bending vibration of rotating drill string*, MIT PhD Thesis

Suryanarayana P.V.R., McCann R.C., 1994, *Experimental study of buckling and post buckling of laterally constrained rods: Part 1: Friction effects*, presented at the Energy-sources Technology Conf. and Exhibition, USA.

Thomson W.T., 1950, *Matrix solution of vibration of nonuniform beams*, J. Appl. Mech.17, 337-339.

Tucker T, 1981, *Sample variance measurement of mixing*, Chemical Engrg. Science, Vol 36, No 11, p1829-1839.

Vandiver J.K., Nicholson, J.W., Shyu, R.J., 1988, *Case studies of the bending vibration and whirling motion of drill collars*, SPE paper 18652

Vandiver J.K., Ligrone A., Ferrara P., Rao R., 1993, *Drillstring axial vibration control and shock absorber positioning criteria.* Presented at the Offshore Mediterranean Conf., Italy.

Wang M.L., Kreitinger T, Luo H.L., 1987, *Force identification from structural response*, Proc. of the 1987 SEM Spring Conf. on Experimental Mechanics, Houston, TX,USA, pp 851-855.

Warren, T.M., Sinor L.A, 1989, *Drag bit performance modelling*, SPEDE, p119-127

Williams F.W., Wittrick W.H., 1970, *An automatic computational procedure for calculating natural frequencies of skeletal structures*, Int. J. of Mech. Sci., 12, pp781-791.

Williams F.W., Kennedy D., 1994, *Accelerated solutions for transcendental stiffness matrix eigenproblems*, Proc. of the Int. Conf. on Vibration Engrg., pp3-8, Peking.

Wittrick W.H., Willams F.W., 1971, *A general algorithm for computing natural frequencies of elastic structures,* The Quarterly J. of Mechanics and Applied Mathematics, 24, 263-284.

Wolf S.F., Zoukenhouse M., Arian A., 1985,*Field measurements of downhole drillstring vibrations,* SPE 14330.

Wu J., Juvkam-Wold H.C., Lu R., 1993,*Helical buckling of pipes in extended reach and horizontal wells, Part 1 and Part 2,* ASME J. of Energy Resources Technology, Vol. 115, 190-201.

Wu J., Juvkam-Wold H.C., 1994a, *Buckling and lockup of tubulars in inclined wellbores,* PD-Vol.56, Proc. of ASME Drilling Technology, pp7-15.

Wu J., Juvkam-Wold H.C., 1994b, *The effect of wellbore curvature on the tubular buckling and lockup,* PD-Vol.56, Proc. of ASME Drilling Technology, pp17-24.

Yang B.S., Pilkey W.D., 1992, *Accurate approach to free vibration analysis for a rotating shaft,* Machine Vibration, No.1, pp164-170.

Yang Y.B., Kuo S.R., 1986, *Static stability of curved thin-walled beams,* J. of Engineering Mechanics, Vol. 112, 821-841.

Zhang G.M., Kapoor S.G., 1991, *Dynamic generation of machined surfaces, part 1, part 2,* Transaction of the ASME, J. of Eng. for Ind., Vol 113, p 137-153

Zu J.W.Z., Han R.P.S., 1992, *Natural frequencies and normal modes of a spinning Timoshenko beam with general boundary conditions,* ASME J. of Applied Mechanics, Vol.59, pp197-204.

APPENDIX A: Transfer matrices of some lumped elements

A.1: For Lateral Vibration

(1) A lumped stiffness k_l with damping c_l:

$$[T^l_{kc}] = \begin{pmatrix} 1 & 0 & 0 & 0 \\ 0 & 1 & 0 & 0 \\ k_l + i\omega c_l & 0 & 1 & 0 \\ 0 & 0 & 0 & 1 \end{pmatrix} \tag{A1}$$

(2) A lumped mass m_l

$$[T^l_m] = \begin{pmatrix} 1 & 0 & 0 & 0 \\ 0 & 1 & 0 & 0 \\ -m_l\omega^2 & 0 & 1 & 0 \\ 0 & 0 & 0 & 1 \end{pmatrix} \tag{A2}$$

where ω is angular frequency.

A.2: For Axial Vibration

(1) A lumped stiffness k_a with damping c_a:

$$[T^a_{kc}] = \begin{pmatrix} 1 & \frac{1}{k_a+i\omega c_a} \\ 0 & 1 \end{pmatrix} \tag{A3}$$

(2) A lumped mass m_a

$$[T^a_m] = \begin{pmatrix} 1 & 0 \\ -m_a\omega^2 & 1 \end{pmatrix} \tag{A4}$$

A.3: For Torsional Vibration

(1) A lumped stiffness k_t with damping c_t:

$$[T^t_{kc}] = \begin{pmatrix} 1 & \frac{1}{k_t+i\omega c_t} \\ 0 & 1 \end{pmatrix} \tag{A5}$$

(2) A lumped polar mass moment J_p

$$[T^a_m] = \begin{pmatrix} 1 & 0 \\ -J_p\omega^2 & 1 \end{pmatrix} \tag{A6}$$

APPENDIX B: The matrices [A] and [N] in equation (4.8)

The non-zero elements of matrix [A] are:

$A_{11} = 1.$; $A_{23} = 1.$; $A_{27} = \frac{1}{KGA}$;

$A_{31} = \frac{\rho\Omega^2}{KG}$; $A_{35} = \frac{1}{EI}$; $A_{43} = b$;

$A_{44} = \frac{2\rho\omega\Omega}{E}$; $A_{47} = a$; $A_{52} = 1.$; $A_{64} = 1.$;

$A_{68} = \frac{1}{KGA}$; $A_{72} = \frac{\rho\Omega^2}{KG}$; $A_{76} = \frac{1}{EI}$;

$A_{83} = \frac{-2\rho\omega\Omega}{E}$; $A_{84} = b$; $A_{88} = a$;

with $a = \frac{1}{EI} - \frac{\rho\Omega^2}{KGA}(\frac{1}{E} - \frac{1}{KG})$; $b = \frac{\rho\Omega^2}{KG} - \frac{\rho\Omega^2}{E}$;

the other elements being equal to zero.

Matrix [N] is obtained as follows:

$$[N] = [H_b][M_b]^{-1} \tag{B1}$$

The matrix $[H_b]$ takes the form

$$[H_b] = \begin{pmatrix} H_1 & H_2 \\ H_1 & -H_2 \end{pmatrix} \tag{B2}$$

with the submatrices $[H_1], [H_2]$

$$[H_1] = \begin{pmatrix} C_1 & C_2 & C_3 & C_4 \\ \lambda_a C_2 & \lambda_a C_1 & -\lambda_b C_4 & \lambda_b C_3 \\ \lambda_a^2 C_1 & \lambda_a^2 C_2 & -\lambda_b^2 C_3 & -\lambda_b^2 C_4 \\ \lambda_a^3 C_2 & \lambda_a^3 C_1 & \lambda_b^3 C_4 & -\lambda_b^3 C_3 \end{pmatrix} \tag{B3}$$

$$[H_2] = \begin{pmatrix} C_5 & C_6 & C_7 & C_8 \\ \lambda_c C_6 & \lambda_c C_5 & -\lambda_d C_8 & \lambda_d C_7 \\ \lambda_c^2 C_5 & \lambda_c^2 C_6 & -\lambda_d^2 C_7 & -\lambda_d^2 C_8 \\ \lambda_c^3 C_6 & \lambda_c^3 C_5 & \lambda_d^3 C_8 & -\lambda_d^3 C_7 \end{pmatrix} \tag{B4}$$

where C_i, i=1,8, are constants

$$C_1 = \cosh \lambda_a L, C_2 = \sinh \lambda_a L, C_3 = \cos \lambda_b L, C_4 = \sin \lambda_b L$$

$$C_5 = \cosh \lambda_c L, C_6 = \sinh \lambda_c L, C_7 = \cos \lambda_d L, C_8 = \sin \lambda_d L$$

and λ_a,λ_b,λ_c,λ_d are the roots of equation (5).

The matrix $[M_b]$ is similarly given by:

$$[M_b] = \begin{pmatrix} M_1 & M_2 \\ M_1 & -M_2 \end{pmatrix} \tag{B5}$$

with the submatrices $[M_1], [M_2]$

$$[M_1] = \begin{pmatrix} 1 & 0 & 1 & 0 \\ 0 & \lambda_a & 0 & \lambda_b \\ \lambda_a^2 & 0 & -\lambda_b^2 & 0 \\ 0 & \lambda_a^3 & 0 & -\lambda_b^3 \end{pmatrix} \tag{B6}$$

$$[M_2] = \begin{pmatrix} 1 & 0 & 1 & 0 \\ 0 & \lambda_c & 0 & \lambda_d \\ \lambda_c^2 & 0 & -\lambda_d^2 & 0 \\ 0 & \lambda_c^3 & 0 & -\lambda_d^3 \end{pmatrix} \tag{B7}$$

As a by product, the exact dynamic stiffness matrix [D] for a rotating shaft subject to axial force can be obtained by rearranging the transfer matrix [T] using equation (2.15) of chapter 2.

Appendix C: Transfer Matrix for a Curved Beam

Following the procedure used in section 4.2.2 of Chapter 4, the transfer matrix for the curved beam may be obtained:

$$[T] = [B]^{-1}[L][B] \tag{C1}$$

The matrix [B] is:

$$[B] = \begin{pmatrix} 1 & 0 & 0 & 0 \\ 0 & 1 & 0 & 0 \\ a & 0 & b & 0 \\ 0 & c & 0 & d \end{pmatrix}$$

with

$$a = \frac{\rho\Omega^2}{KG} - \frac{1}{R^2}; \quad b = \frac{1}{EI}; \quad c = \frac{\rho\Omega^2}{KG} - \frac{\rho\Omega^2}{E} - \frac{1}{R^2};$$

$$d = \frac{1}{EI} - \frac{\rho}{KGA}\left(\frac{1}{E} - \frac{1}{KG}\right)\Omega^2$$

and R being the radius of the curvature.

The matrix [L] is given by:

$$[L] = [H][M]^{-1} \tag{C2}$$

with matrices [H] and [M]:

$$[H] = \begin{pmatrix} C_1 & C_2 & C_3 & C_4 \\ \lambda_a C_2 & \lambda_a C_1 & -\lambda_b C_4 & \lambda_b C_3 \\ \lambda_a^2 C_1 & \lambda_a^2 C_2 & -\lambda_b^2 C_3 & -\lambda_b^2 C_4 \\ \lambda_a^3 C_2 & \lambda_a^3 C_1 & \lambda_b^3 C_4 & -\lambda_b^3 C_3 \end{pmatrix}$$

$$[M] = \begin{pmatrix} 1 & 0 & 1 & 0 \\ 0 & \lambda_a & 0 & \lambda_b \\ \lambda_a^2 & 0 & -\lambda_b^2 & 0 \\ 0 & \lambda_a^3 & 0 & -\lambda_b^3 \end{pmatrix}$$

The four constants C_i, i=1,4, are written in terms of

$$C_1 = cosh\lambda_a L, \quad C_2 = sinh\lambda_a L, \quad C_3 = cos\lambda_b L, \quad C_4 = sin\lambda_b L$$

where λ_a, λ_b are the roots of equation:

$$\lambda^4 - f\lambda^2 + g = 0 \qquad (C3)$$

Appendix D: Stiffness matrix for buckling analysis

$$[K] = \frac{EI}{L^3} \begin{pmatrix} \gamma & \nu L & -\eta & \delta L \\ \nu L & \alpha L^2 & -\delta L & \beta L^2 \\ -\eta & -\delta L & \gamma & -\nu L \\ \delta L & \beta L^2 & -\nu L & \alpha L^2 \end{pmatrix} \qquad (D1)$$

where $\alpha = \chi(S - ZC)$, $\beta = \chi(Z - S)$, $\nu = \alpha + \beta$, $\gamma = \chi SZ^2$, $\delta = \nu$ and $\eta = \gamma$.

with $\chi = p^2/(2Z(1-C) - Z^2S)$, $Z = t\phi$, $C = \cos\phi$, $S = \sin\phi$, $\phi = \sqrt{2\sigma}$,

$\sigma = p^2/(2t)$, $t = 1 - s^2p^2$, $s = \sqrt{EI/KAGL^2}$, $p = \sqrt{PL^2/EI}$.

The other parameters have the same meaning as in Appendix A and B and C.